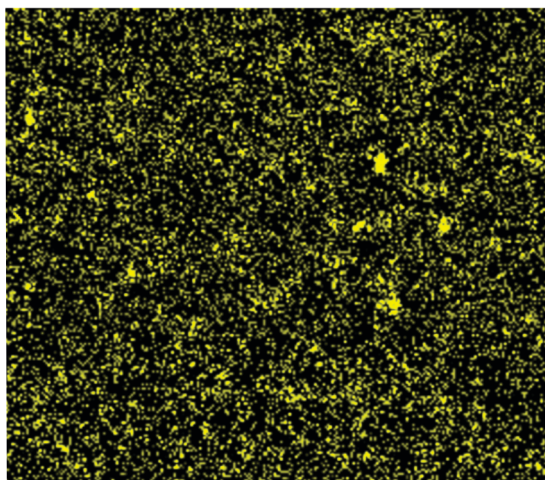
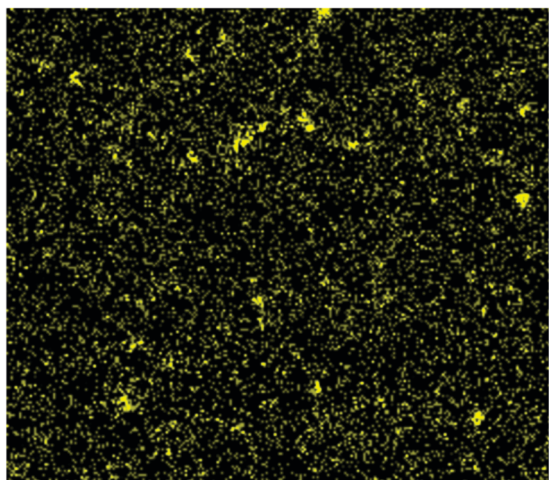
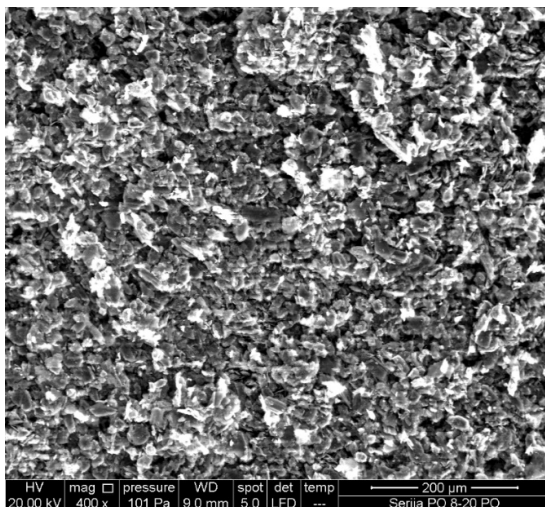
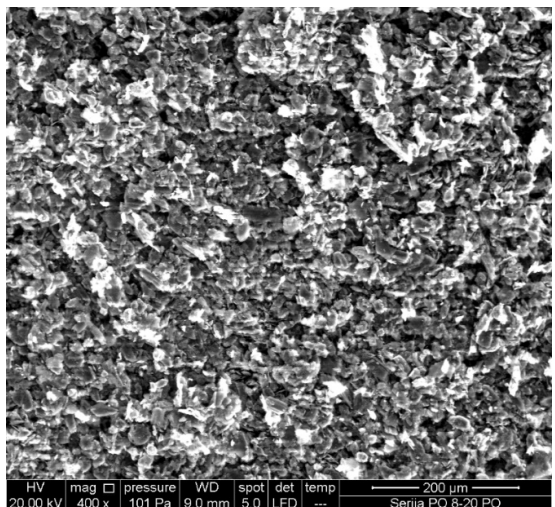


3

Hemijiska industrija

Vol. 76

Časopis Saveza hemijskih inženjera Srbije

Chemical Industry

Aktivnosti Saveza hemijskih inženjera Srbije pomažu:



MINISTARSTVO PROSVETE,
NAUKE I TEHNOLOŠKOG RAZVOJA
REPUBLIKE SRBIJE



Tehnološko-metallurški fakultet
Univerziteta u Beogradu, Beograd



Hemijski fakultet Univerziteta u
Beogradu, Beograd



Institut za tehnologiju nuklearnih i
drugih mineralnih sirovina, Beograd



Institut za opštu i fizičku hemiju,
Beograd



Tehnološki fakultet
Univerziteta u Novom Sadu, Novi Sad



Prirodno-matematički fakultet
Univerziteta u Novom Sadu, Novi Sad



NU Institut za hemiju, tehnologiju i metalurgiju
Univerziteta u Beogradu, Beograd



Institut IMS, Beograd



Tehnološki fakultet
Univerziteta u Nišu, Leskovac



Fakultet tehničkih nauka,
Kosovska Mitrovica



Chemical Industry

Химическая промышленность

Hemijska industrija

Časopis Saveza hemijskih inženjera Srbije

Journal of the Association of Chemical Engineers of Serbia

Журнал Союза химических инженеров Сербии

VOL. 76

Beograd, maj-juni 2022.

Broj 3

Izdavač

Savez hemijskih inženjera Srbije
Beograd, Kneza Miloša 9/1

Glavni urednik

Bojana Obradović

Zamenica glavnog i odgovornog urednika

Emila Živković

Pomoćnik glavnog i odgovornog urednika

Ivana Drvenica

Urednici

Enis Džunuzović, Ivana Banković-Ilić, Maja Obradović,
Dušan Mijin, Marija Nikolić, Tatjana Volkov-Husović,
Đorđe Veljović,

Članovi uredništva

Nikolaj Ostrovska, Milorad Cakić, Željko Čupić, Miodrag Lazić, Slobodan Petrović, Milovan Purenović, Aleksandar Spasić, Dragoslav Stojiljković, Radmila Šećerov-Sokolović, Slobodan Šerbanović, Nikola Nikćević, Svetomir Milojević

Članovi uredništva iz inostranstva

Dragomir Bukur (SAD), Jiri Hanika (Češka Republika), Valerij Meshalkin (Rusija), Ljubiša Radović (SAD), Constantinos Vayenas (Grčka)

Likovno-grafičko rešenje naslovne strane

Milan Jovanović

Redakcija

11000 Beograd, Kneza Miloša 9/1

Tel/fax: 011/3240-018

E-pošta: shi@ache.org.rs

www.ache.org.rs

Izlazi dvomesečno, rukopisi se ne vraćaju

Za izdavača: Ivana T. Drvenica

Sekretar redakcije: Slavica Desnica

Izdavanje časopisa pomaže

Republika Srbija, Ministarstvo prosvete, nauke i tehnološkog razvoja

Upłata preplate u oglasnog prostora vrši se na tekući račun Saveza hemijskih inženjera Srbije, Beograd, broj 205-2172-71, Komercijalna banka a.d., Beograd

Menadžer časopisa i Kompjuterska priprema

Aleksandar Dekanski

Štampa

Razvojno-istraživački centar grafičkog inženjerstva, Tehnološko-metalurški fakultet, Univerzitet u Beogradu, Karnegijeva 4, 11000 Beograd

Indeksiranje

Radovi koji se publikuju u časopisu *Hemijska Industrija* indeksiraju se preko Thompson Reuters Scietific® servisa *Science Citation Index - Expanded™* i *Journal Citation Report (JCR)*

SADRŽAJ/CONTENTS

Reactor Engineering / Reaktorsko inženjerstvo

- Dragana Prokić-Vidojević, Sandra B. Glišić, Radojica Pešić, Aleksandar M. Orlović, **Desulfurizacija dibenzotiofena i 4,6 – dimetildibenzotiofena procesom hidrogenovanja uz korišćenje RePd-TiO₂/SiO₂ aerogel katalizatora: proračun kinetičkih parametara i simulacijaprocesa / Desulfurizacija dibenzotiofena i 4,6 – dimetildibenzotiofena procesom hidrogenovanja uz korišćenje RePd-TiO₂/SiO₂ aerogel katalizatora: proračun kinetičkih parametara i simulacijaprocesa 135**

Elektrohemski inženjerstvo / Electrochemical Engineering

- Saša Mićin, Borislav N. Malinović, Tijana Đuričić, **Razvoj i karakterizacija elektrohemiskog senzora na bazi ugljenika modifikovanog nanočesticama TiO₂ / Ispitivanje korozije bakarne trake u hidrokrekovanom baznom ulju u prisustvu različitih inhibitora s 147**

- Borislav N. Malinović, Aleksandra Borković, Tijana Đuričić, **Copper strip corrosion testing in hydrocracked base oil in the presence of different inhibitors / Korelacija uslova dobijanja i kvaliteta briketa krečnjaka za upotrebu u kalcicaciji kiselih zemljišta 159**

Metalni materijali / Metal materials

- Aleksandar Sedmak, Radzeya Zaidi, Borivoje Vujičić, Živče Šarkočević, Snežana Kirin, Zoran Stamenić, Miloš Đukić, Gordana Bakić, **Corrosion effects on structural integrity and life of oil rig drill pipes / Efekti korozije na integritet konstrukcije i životni vek cevi za bušenje izvora nafte 167**

Prikaz knjiga i događaja / Book & Event Review

- Slavko Mentus, Milica Vujković, **Overview of the conference COIN2022 - Contemporary batteries and Supercapacitors, International Symposium, Belgrade 2022 / Osvrt na simpozijum COIN2022 – Savremene baterije i superkonenzatori, međunarodni simpozijum, Beograd 2022 179**

Desulphurisation of dibenzothiophene and 4,6 – dimethyl dibenzothiophene via enhanced hydrogenation reaction route using RePd–TiO₂/SiO₂ aerogel catalysts: Kinetic parameters estimation and modelling

Dragana Prokić-Vidojević¹, Sandra B. Glišić², Radojica Pešić² and Aleksandar M. Orlović²

¹Military Technical Institute (VTI), Ratka Resanovića 1, 11132 Belgrade, Serbia

²University of Belgrade, Faculty of Technology and Metallurgy, Karnegijeva 4, 11000 Belgrade, Serbia

Abstract

Re/Pd-TiO₂/SiO₂ aerogel catalysts were synthesized by using a sol-gel method and supercritical drying in excess solvent and investigated in the reaction of hydrodesulphurisation (HDS) of dibenzothiophene (DBT) and 4,6-dimethyl dibenzothiophene (4,6-DMDBT). Both Re/Pd catalysts, obtained with and without the use of mesitylene in the synthesis step, have shown increased conversions of up to 70 % in the desulphurization of 4,6-DMDBT, when compared to conventional Co/Mo hydroprocessing catalysts. This observation is of importance for conversion of highly refractory 4,6-DMDBT and hydroprocessing to produce ultra-low sulphur diesel fuels, ULSD. In order to quantify the extent of desulphurisation, which proceeds via a hydrogenation route, conversions of DBT and 4,6-DMDBT along with evolution of reaction products characteristic for the direct desulphurisation route and the hydrogenation route were monitored by using a gas chromatography-mass spectrometry (GC-MS) analytical technique. The reaction was performed at 630 K and 6 MPa in a batch catalytic reactor. The experimental results were used in the Hougen-Watson kinetic model describing DBT and 4,6-DMDBT desulphurisation on σ and τ active sites. Kinetic parameters of this complex catalytic kinetics were determined by using a Genetic Algorithm method and minimum deviation function. Values of calculated kinetic parameters and values of the ratio of 3-methylcyclohexyltoluene (MCHT) and dimethyl biphenyl (DMBPH) expressed as the MCHT/(MCHT+DMBPH) ratio ranging between 0.66 and 0.94, have confirmed that the hydrogenation route is the dominant route for desulphurisation of 4,6-DMDBT.

Keywords: Aerogel hydrodesulphurisation catalysts; hydrodesulphurisation; 4,6-DMDBT; Hougen-Watson kinetic model; kinetic and adsorption parameters.

Available on-line at the Journal web address: <http://www.ache.org.rs/HI/>

1. INTRODUCTION

Production of clean transportation fuels is becoming considerable challenge due to increased availability of heavier feedstock and depleted supply of light feedstock, which results in the continuous increase in molecular weight of available petroleum. Thus, the development of highly active hydrotreating catalysts for upgrading the heavy and sulphur-rich feedstock became inevitably important. This need was even more compelling in the view of recent environmental regulations, placing the current limit for sulphur content in diesel fuel down to below 10 ppm [1]. Decreasing the sulphur content to these levels is very difficult since sulphur compounds that remain after the conventional hydrodesulphurization (HDS) process are highly refractory [1]. Difficulties are encountered with dibenzotiphenes, especially its substituted derivative 4,6-dimethylbenzotriophene (4,6-DMDBT) [2,3]. Substitute methyl groups cause considerable steric hindrance thereby making sulphur atom inaccessible to the active catalyst surface and hydrogen reactant. Deep HDS could be improved by the development of new state-of-the-art catalysts, capable of achieving efficient clean fuel production [3,4].

Corresponding authors: Sandra B. Glišić, University of Belgrade, Faculty of Technology and Metallurgy, Karnegijeva 4, 11000 Belgrade, Serbia,
Tel: +381 113303707; fax: +381 113370378

E-mail: : s.glisic@tmf.bg.ac.rs

Paper received: 14 January 2022; Paper accepted: 10 April 2022; Paper published: 17 July 2022.

<https://doi.org/10.2298/HEMIND220114008P>

ORIGINAL SCIENTIFIC PAPER

UDC: 666.762.12:549.514.5:54.062

Hem. Ind. **76(3)** 135-145 (2022)



Deep HDS requires supports with high surface areas, enhanced pore sizes, higher fraction of mesopores and small macropores, larger pore volumes allowing increased exposure of active sites and better dispersion of active components and their availability to large sulphur molecules. Due to these reasons, the conventionally used γ -alumina ($\gamma\text{-Al}_2\text{O}_3$) support is a far less efficient option compared to other supports like highly porous silicas, which are increasingly attractive [5-10]. Their main advantages for use as catalyst supports are: high surface areas of about 600-1300 m²/g and huge pore volumes; uniform topology providing high dispersion of metal nanoparticles and easy access of the reactants to the active sites; excellent mechanical properties and hydrothermal stability for demanding reaction conditions. Further HDS improvement was reported with the incorporation of heteroatoms: Al, Ti and Zr ions, into frameworks of highly porous silica materials [3,11-14] which increased pore diameters and facilitated hydrogenation of benzene ring. A Ti-containing catalyst was found to be 30 % more active than the conventional industrial catalyst and 50% more active than the Ti-free catalyst [15]. In order to achieve desired catalytic and textural characteristics of HDS catalysts the choice of the preparation method is very important [16-19]. Improvements in specific surface area [18,19], pore volume, homogenous formation of hetero-linkages and development of appropriate surface acid sites [16,17] was reported by using a sol-gel method whereas higher acidity in the sol-gel samples was attributed to higher density of hetero-linkages formed [18,19]. To overcome the problem of deteriorated textural properties caused by conventional drying methods (collapse of the formed gel structure and reduction of mesoporosity by the increasing fraction of micropores leading to decreased surface areas) [20,21], a supercritical drying method (SCD) can be applied to obtain aerogels [22-24]. SCD can be performed for solvent removal by solvent phase change to supercritical (SC) fluid, followed by solvent evacuation from the gel network by applying transition from supercritical fluid to gas. Aerogels produced by supercritical drying typically have high porosities (50-99 vol%), lower microporosity, higher surface areas and can yield highly porous amorphous mixed oxide aerogels [22-24]. Besides advantageous textural properties, the choice of active phase is equally important in order to design a highly active catalyst for "deep HDS". Numerous studies have confirmed high activity of nonconventional sulphides, such as Re, Rh or Ru [25-28]. The way to further enhance activity of ReS₂ can be achieved through understanding of the HDS reaction mechanism of 4,6-DMDBT and potential for the use of noble metals as promoters. This potential is based on the exceptional properties of Pd, Pt and Ru, suitable for hydrogen spillover in aromatics hydrogenation, necessary for deep HDS [29-33].

The sol-gel synthesis method and supercritical drying of the obtained gels, for RePd supported on Ti-HMS (Ti incorporated in highly mesoporous silica), were previously investigated as HDS catalysts [34]. The sol-gel method and supercritical drying were found to result in amorphous aerogels with a relatively high degree of uniformity of both supports and active phases [34,35]. Catalytic activities of the obtained aerogels and a commercial Co/Mo catalyst in HDS of DBT were not significantly different [34]. However, large differences were observed in HDS of 4,6-DMDBT since all Re/Pd-TiO₂/SiO₂ aerogel catalysts were considerably more active than Co/Mo-Al₂O₃/SiO₂ aerogel catalysts and a Co/Mo on γ -alumina commercial HDS catalyst, alike [34]. Conversion of 4,6-DMDBT was found to be 70 % higher for RePd aerogel catalysts obtained by using mesitylene addition (RePd MA) and 64 % higher for RePd aerogel catalysts obtained without mesitylene addition (RePd A), when compared to conversion achieved by using a commercial Co/Mo catalyst [34].

Kinetic modelling of HDS reactions has been carried out by several researchers [36-47]. The Langmuir-Hinshelwood, also well known as the Hougen-Watson mechanism, has been reported to suitably describe the HDS reactions [20-22]. Hougen-Watson rate equations for hydrogenolysis and hydrogenation of dibenzothiophenes to bicyclohexyl through several steps, were developed by Froment and co-workers [36-38]. Two different types of active sites were considered: σ sites for hydrogenolysis and τ sites for hydrogenation. The surface reaction between adsorbed reactants and two competitively adsorbed hydrogen atoms was found to be the rate-determining step for both types of reaction. Actually, the HDS mechanism of substituted aromatic sulphur compounds involves a pre-hydrogenation step (HYD) before desulphurization [29,30]. This is the key step in order to remove the steric hindrance of the substituents, contrary to the non-sterically hindered compounds that are straightforwardly desulphurised *via* a direct desulphurization (DDS) pathway [33]. Consequently, for well-established catalytic formulations (*e.g.* CoMo, NiMo) even with excellent DBT HDS properties, HYD efficiency becomes an obstacle for substituted DBTs like 4,6-DMDBT. The present research is focused on investigating the kinetics of the simultaneous HDS of two sulphur containing model compounds (DBT and

4,6-DMDBT), using RePd MA and RePd A catalysts. The novelty of this study is the approach which includes DDS and HYD pathways for all reacting species in the kinetic model.

Thus, the objective of the study is to investigate the hydrodesulphurisation (HDS) of dibenzothiophene (DBT) and 4,6-dimethyl dibenzothiophene (4,6-DMDBT) for Re/Pd-TiO₂/SiO₂ aerogel catalysts, obtained with and without the use of mesitylene in the synthesis step. Gas chromatography–mass spectrometry (GC-MS) was used to quantify concentrations of reactants and emerging reaction products over time, at 630 K and 60 bar in a batch catalytic reactor. Based on the experimental data, the Hougen-Watson kinetic model for desulphurisation of DBT and 4,6-DMDBT on σ and τ active sites was developed. Kinetic parameters of the model were determined in a procedure based on the use of the Genetic Algorithm (GA) method and minimum deviation function.

2. EXPERIMENTAL

2. 1. Catalysts used in catalytic HDS tests

Re/Pd-TiO₂/SiO₂ aerogel catalysts were synthesized by using a sol-gel method and supercritical drying in excess solvent as described in previously published work [34,35]. The Re/Pd-TiO₂/SiO₂ catalysts were obtained by using two different pathways of the sol-gel method, the pathway which applies mesitylene in the sol phase as the additional template for enhancement of the mesopore region (RePd MA catalyst) and the pathway without mesitylene (RePd A catalyst), while in both pathways supercritical drying with excess solvent was applied. Structural and textural properties of the obtained aerogel HDS catalysts and TiO₂/SiO₂ supports were investigated and reported previously [34].

2. 2. Hydrodesulphurisation (HDS) reaction tests of dibenzothiophene (DBT) and 4,6-dimethylbenzothiophene (4,6-DMDBT) - catalytic activity of the RePd A and RePd MA catalysts

Re/Pd-TiO₂/SiO₂ aerogel catalyst (RePd A) and Re/Pd-TiO₂/SiO₂ aerogel catalyst obtained by using mesitylene during sol-gel synthesis (RePd MA) were investigated by performing HDS of DBT and 4,6-DMDBT in a high pressure stirred-batch reactor (Autoclave Engineers BTRS Jr, Division of Snap-title, Inc., Erie, PA, USA). Prior to the reaction, each catalyst (0.84 g) was activated by sulphidation with carbon disulphide (7 cm³, grade, producer, country) at 603 K and 35 bar of H₂ during 4 h. The DBT and 4,6-DMDBT HDS activity tests were performed in a 300 cm³ stirred-batch reactor at 603 K and 6 MPa total pressure, for 6 h. All reaction tests were performed with the 100 ml solution of DBT (0.8 g) and 4,6-DMDBT (0.10 g) in the (1:1 v/v) mixture of n-hexadecane (grade, producer, country) and n-dodecane (grade, producer, country) leading to the total elemental sulphur concentration of 2000 ppm weight based. The reaction was monitored by withdrawing samples (2 ml) at 0.25, 0.5, 1, 1.5, 2, 3, 4, 5 and 6 h of reaction time. All experiments were done in 2 repetitions.

2. 3. Product analysis

Quantitative analysis of the reactants (DBT and 4,6-DMDBT) and products was carried out using Shimadzu GC-2010 Plus, MS QP 2020 instrument (Shimadzu, Japan), equipped with a capillary column sh-rtx-5 (30 m × 0.25 μm × 0.25 mm) using a temperature program starting from 333 to 503 K (heating rate of 6 K/min). GC-MS quantification was applied on samples withdrawn from the liquid phase using calibration lines obtained with DBT and 4,6-DMDBT. Identification of mass spectra peaks was performed using the scientific library NIST11s. Quantities and concentrations of hydrogen sulphide in both phases (vapour and liquid) were calculated from the material balance of sulphur containing reactants (DBT and 4,6-DMDBT) and vapour-liquid equilibrium calculation using the Peng-Robinson equation of state. Hydrogen sulphide concentration in the liquid phase is relevant for the kinetic model and phase distribution is given by K_{eq} values in Eq. 19.

3. KINETIC MODEL AND DETERMINATION OF KINETIC PARAMETERS

Kinetic model describing HDS of DBT and 4,6-DMDBT, shown in Figure 1, was employed to develop the kinetic model equations, experimental reactor material balance equations and optimisation technique for determination of kinetic parameters.



The removal of sulphur from organic sulphur compounds can occur through two pathways: direct desulphurization (DDS) by C-S bond cleavage without affecting the aromatic ring and hydrogenation of the aromatic ring (HYD) prior to the cleavage of C-S bond [36-41]. Both reaction pathways are generally believed to occur at separate catalytic sites. The DDS pathway is economical because this route consumes lower amounts of hydrogen. Both routes, the HYD of DBT and DDS of DBT yield biphenyl (BPH), while the HYD route produces intermediates such as tetrahydrodibenzothiophene (THDBT) and hexahydrodibenzothiophene (HHDBT), that rapidly convert to cyclohexyl benzene (CHB) and further to bicyclic hexyl (BCH). Similarly, the DDS of 4,6-DMDBT produces 3,3'-dimethyl biphenyl (DMBPH), whereas the HYD pathway results in 3-methylcyclohexyltoluene (MCHT) and furthermore to 3,3-dimethyl bicyclic hexyl (DMBCH). Figure 1 shows simple schemes for the reaction pathways of the DBT and 4,6-DMDBT. The transitional compounds produced through HDS of DBT and 4,6-DMDBT via the HYD routes were observed in negligible amounts whereas the major products were CHB and MCHT from the HDS of DBT and 4,6-DMDBT, respectively.

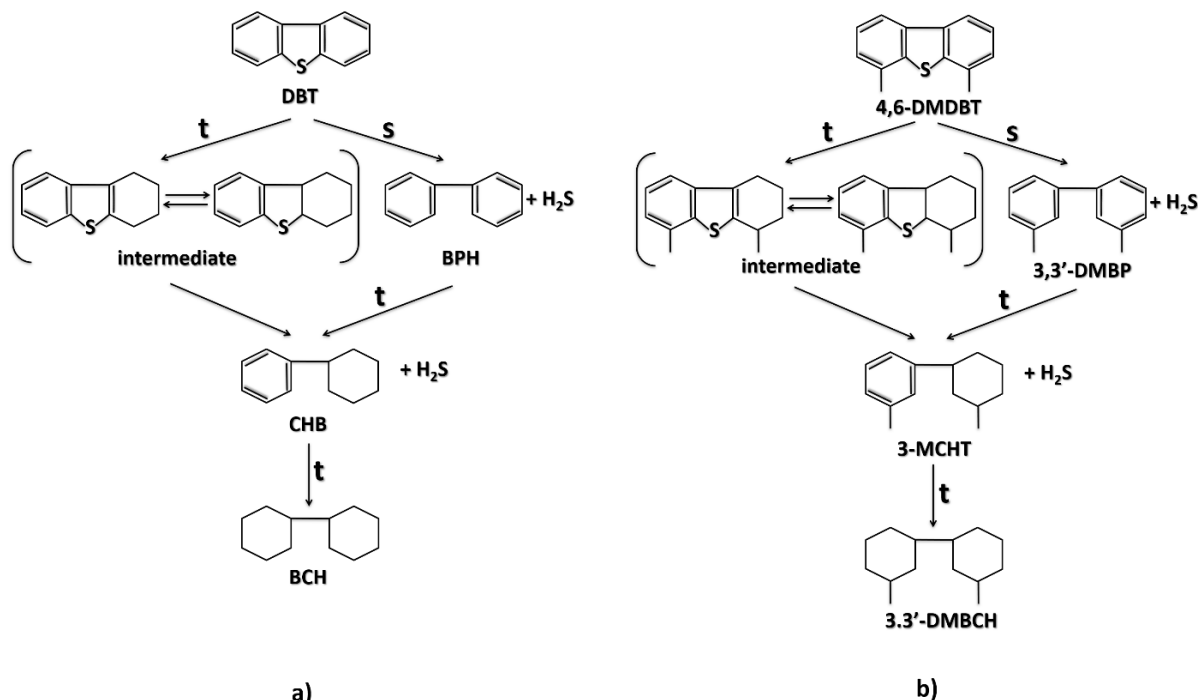


Figure 1. Kinetic model describing HDS of a) DBT and b) 4,6-DMDBT on σ and τ active sites

A Hougen-Watson based kinetic model was developed based on the reaction network presented in Figure 1 that included the simultaneous HDS reactions supported by the experimental results. Based on the kinetic model scheme the set of differential equations representing material balances for each compound involved in the reaction was developed and shown in Eq. 1-19:

DBT:

$$-r_{\text{DBT}}^{\sigma} = \frac{k_{\text{DBT}}^{\sigma} K_{\text{H}}^{\sigma} K_{\text{DBT}}^{\sigma} C_{\text{DBT}} C_{\text{H}_2}}{\left(1 + K_{\text{DBT}}^{\sigma} + C_{\text{DBT}} \sqrt{K_{\text{H}}^{\sigma} C_{\text{H}_2}} + K_{\text{BPH}}^{\sigma} C_{\text{BPH}} + K_{\text{H}_2S}^{\sigma} C_{\text{H}_2S} + K_{\text{DMDBT}}^{\sigma} C_{\text{DMDBT}} + K_{\text{DMBP}}^{\sigma} C_{\text{DMBP}}\right)^3} \quad (1)$$

$$-r_{\text{DBT}}^{\tau} = \frac{k_{\text{DBT}}^{\tau} K_{\text{H}_2}^{\tau} C_{\text{DBT}} C_{\text{H}_2}}{\left(1 + K_{\text{DBT}}^{\tau} C_{\text{DBT}} + \sqrt{K_{\text{H}_2}^{\tau} C_{\text{H}_2}} + K_{\text{BPH}}^{\tau} C_{\text{BPH}} + K_{\text{CHB}}^{\tau} C_{\text{CHB}} + K_{\text{BCH}}^{\tau} C_{\text{BCH}} + K_{\text{DMDBT}}^{\tau} C_{\text{DMDBT}} + K_{\text{DMBP}}^{\tau} C_{\text{DMBP}} + K_{\text{MCHT}}^{\tau} C_{\text{MCHT}} + K_{\text{DMBCH}}^{\tau} C_{\text{DMBCH}}\right)^3} \quad (2)$$

$$-r_{\text{BPH}}^{\tau} = \frac{k_{\text{BPH}}^{\tau} K_{\text{H}}^{\tau} K_{\text{BPH}}^{\tau} C_{\text{BPH}} C_{\text{H}_2}}{\left(1 + K_{\text{DBT}}^{\tau} C_{\text{DBT}} + \sqrt{K_{\text{H}}^{\tau} C_{\text{H}_2}} + K_{\text{BPH}}^{\tau} C_{\text{BPH}} + K_{\text{CHB}}^{\tau} C_{\text{CHB}} + K_{\text{BCH}}^{\tau} C_{\text{BCH}} + K_{\text{DMDBT}}^{\tau} C_{\text{DMDBT}} + K_{\text{DMBP}}^{\tau} C_{\text{DMBP}} + K_{\text{MCHT}}^{\tau} C_{\text{MCHT}} + K_{\text{DMBCH}}^{\tau} C_{\text{DMBCH}}\right)^3} \quad (3)$$

$$r_{\text{CHB}}^{\tau} = -r_{\text{DBT}}^{\tau} - r_{\text{BPH}}^{\tau} - \frac{k_{\text{CHB}}^{\tau} K_{\text{H}}^{\tau} K_{\text{CHB}}^{\tau} C_{\text{CHB}} C_{\text{H}_2}}{\left(1 + K_{\text{DBT}}^{\tau} C_{\text{DBT}} + \sqrt{K_{\text{H}}^{\tau} C_{\text{H}_2}} + K_{\text{BPH}}^{\tau} C_{\text{BPH}} + K_{\text{CHB}}^{\tau} C_{\text{CHB}} + K_{\text{BCH}}^{\tau} C_{\text{BCH}} + K_{\text{DMDBT}}^{\tau} C_{\text{DMDBT}} + K_{\text{DMBP}}^{\tau} C_{\text{DMBP}} + K_{\text{MCHT}}^{\tau} C_{\text{MCHT}} + K_{\text{DMBCH}}^{\tau} C_{\text{DMBCH}}\right)^3} \quad (4)$$

$$r_{\text{BCH}}^{\tau} = -\frac{k_{\text{CHB}}^{\tau} K_{\text{H}}^{\tau} K_{\text{CHB}}^{\tau} C_{\text{CHB}} C_{\text{H}_2}}{\left(1 + K_{\text{DBT}}^{\tau} C_{\text{DBT}} + \sqrt{K_{\text{H}}^{\tau} C_{\text{H}_2}} + K_{\text{BPH}}^{\tau} C_{\text{BPH}} + K_{\text{CHB}}^{\tau} C_{\text{CHB}} + K_{\text{BCH}}^{\tau} C_{\text{BCH}} + K_{\text{DMDBT}}^{\tau} C_{\text{DMDBT}} + K_{\text{DMBP}}^{\tau} C_{\text{DMBP}} + K_{\text{MCHT}}^{\tau} C_{\text{MCHT}} + K_{\text{DMBCH}}^{\tau} C_{\text{DMBCH}}\right)^3} \quad (5)$$

DMDBT:

$$-r_{\text{DMDBT}}^{\sigma} = \frac{k_{\text{DMDBT}}^{\sigma} K_{\text{H}}^{\sigma} K_{\text{DMDBT}}^{\sigma} C_{\text{DMDBT}} C_{\text{H}_2}}{\left(1 + K_{\text{DBT}}^{\sigma} C_{\text{DBT}} + \sqrt{K_{\text{H}}^{\sigma} C_{\text{H}_2}} + K_{\text{BPH}}^{\sigma} C_{\text{BPH}} + K_{\text{H}_2S}^{\sigma} C_{\text{H}_2S} + K_{\text{DMDBT}}^{\sigma} C_{\text{DMDBT}} + K_{\text{DMBP}}^{\sigma} C_{\text{DMBP}}\right)^3} \quad (6)$$

$$-r_{\text{DMDBT}}^{\tau} = \frac{k_{\text{DMDBT}}^{\tau} K_{\text{H}}^{\tau} K_{\text{DMDBT}}^{\tau} C_{\text{DMDBT}} C_{\text{H}_2}}{\left(1 + K_{\text{DBT}}^{\tau} C_{\text{DBT}} + \sqrt{K_{\text{H}}^{\tau} C_{\text{H}_2}} + K_{\text{BPH}}^{\tau} C_{\text{BPH}} + K_{\text{CHB}}^{\tau} C_{\text{CHB}} + K_{\text{BCH}}^{\tau} C_{\text{BCH}} + K_{\text{DMDBT}}^{\tau} C_{\text{DMDBT}} + K_{\text{DMBP}}^{\tau} C_{\text{DMBP}} + K_{\text{MCHT}}^{\tau} C_{\text{MCHT}} + K_{\text{DMBCH}}^{\tau} C_{\text{DMBCH}}\right)^3} \quad (7)$$

$$-r_{\text{DMBP}}^{\tau} = \frac{k_{\text{DMBP}}^{\tau} K_{\text{H}}^{\tau} K_{\text{DMBP}}^{\tau} C_{\text{DMBP}} C_{\text{H}_2}}{\left(1 + K_{\text{DBT}}^{\tau} C_{\text{DBT}} + \sqrt{K_{\text{H}}^{\tau} C_{\text{H}_2}} + K_{\text{BPH}}^{\tau} C_{\text{BPH}} + K_{\text{CHB}}^{\tau} C_{\text{CHB}} + K_{\text{BCH}}^{\tau} C_{\text{BCH}} + K_{\text{DMDBT}}^{\tau} C_{\text{DMDBT}} + K_{\text{DMBP}}^{\tau} C_{\text{DMBP}} + K_{\text{MCHT}}^{\tau} C_{\text{MCHT}} + K_{\text{DMBCH}}^{\tau} C_{\text{DMBCH}}\right)^3} \quad (8)$$

$$r_{\text{MCHT}}^{\tau} = -r_{\text{DMDBT}}^{\tau} - r_{\text{DMBP}}^{\tau} - \frac{k_{\text{MCHT}}^{\tau} K_{\text{H}}^{\tau} K_{\text{MCHT}}^{\tau} C_{\text{MCHT}} C_{\text{H}_2}}{\left(1 + K_{\text{DBT}}^{\tau} C_{\text{DBT}} + \sqrt{K_{\text{H}}^{\tau} C_{\text{H}_2}} + K_{\text{BPH}}^{\tau} C_{\text{BPH}} + K_{\text{CHB}}^{\tau} C_{\text{CHB}} + K_{\text{BCH}}^{\tau} C_{\text{BCH}} + K_{\text{DMDBT}}^{\tau} C_{\text{DMDBT}} + K_{\text{DMBP}}^{\tau} C_{\text{DMBP}} + K_{\text{MCHT}}^{\tau} C_{\text{MCHT}} + K_{\text{DMBCH}}^{\tau} C_{\text{DMBCH}}\right)^3} \quad (9)$$

$$r_{\text{DMBCH}}^{\tau} = -\frac{k_{\text{MCHT}}^{\tau} K_{\text{H}}^{\tau} K_{\text{MCHT}}^{\tau} C_{\text{MCHT}} C_{\text{H}_2}}{\left(1 + K_{\text{DBT}}^{\tau} C_{\text{DBT}} + \sqrt{K_{\text{H}}^{\tau} C_{\text{H}_2}} + K_{\text{BPH}}^{\tau} C_{\text{BPH}} + K_{\text{CHB}}^{\tau} C_{\text{CHB}} + K_{\text{BCH}}^{\tau} C_{\text{BCH}} + K_{\text{DMDBT}}^{\tau} C_{\text{DMDBT}} + K_{\text{DMBP}}^{\tau} C_{\text{DMBP}} + K_{\text{MCHT}}^{\tau} C_{\text{MCHT}} + K_{\text{DMBCH}}^{\tau} C_{\text{DMBCH}}\right)^3} \quad (10)$$

Material balance equations:

$$\text{DBT: } \frac{dC_{\text{DBT}}}{dt} = -r_{\text{DBT}}^{\sigma} - r_{\text{DBT}}^{\tau} \quad (11)$$

$$\text{BPH: } \frac{dC_{\text{BPH}}}{dt} = -r_{\text{DBT}}^{\sigma} - r_{\text{BPH}}^{\tau} \quad (12)$$

$$\text{CHB: } \frac{dC_{\text{CHB}}}{dt} = -r_{\text{DBT}}^{\tau} - r_{\text{BPH}}^{\tau} - \frac{k_{\text{CHB}}^{\tau} K_{\text{H}}^{\tau} K_{\text{CHB}}^{\tau} C_{\text{CHB}} C_{\text{H}_2}}{\left(1 + K_{\text{DBT}}^{\tau} C_{\text{DBT}} + \sqrt{K_{\text{H}}^{\tau} C_{\text{H}_2}} + K_{\text{BPH}}^{\tau} C_{\text{BPH}} + K_{\text{CHB}}^{\tau} C_{\text{CHB}} + K_{\text{BCH}}^{\tau} C_{\text{BCH}} + K_{\text{DMDBT}}^{\tau} C_{\text{DMDBT}} + K_{\text{DMBP}}^{\tau} C_{\text{DMBP}} + K_{\text{MCHT}}^{\tau} C_{\text{MCHT}} + K_{\text{DMBCH}}^{\tau} C_{\text{DMBCH}}\right)^3} \quad (13)$$

$$\text{BCH: } \frac{dC_{\text{BCH}}}{dt} = r_{\text{BCH}}^{\tau} \quad (14)$$

$$\text{DMDBT: } \frac{dC_{\text{DMDBT}}}{dt} = -r_{\text{DMDBT}}^{\sigma} - r_{\text{DMDBT}}^{\tau} \quad (15)$$

$$\text{DMBP: } \frac{dC_{\text{DMBP}}}{dt} = -r_{\text{DMBP}}^{\sigma} - r_{\text{DMBP}}^{\tau} \quad (16)$$

$$\text{MCHT: } \frac{dC_{\text{MCHT}}}{dt} = -r_{\text{DMDBT}}^{\tau} - r_{\text{DMBP}}^{\tau} - \frac{k_{\text{MCHT}}^{\tau} K_{\text{H}}^{\tau} K_{\text{MCHT}}^{\tau} C_{\text{MCHT}} C_{\text{H}_2}}{\left(1 + K_{\text{DBT}}^{\tau} C_{\text{DBT}} + \sqrt{K_{\text{H}}^{\tau} C_{\text{H}_2}} + K_{\text{BPH}}^{\tau} C_{\text{BPH}} + K_{\text{CHB}}^{\tau} C_{\text{CHB}} + K_{\text{BCH}}^{\tau} C_{\text{BCH}} + K_{\text{DMDBT}}^{\tau} C_{\text{DMDBT}} + K_{\text{DMBP}}^{\tau} C_{\text{DMBP}} + K_{\text{MCHT}}^{\tau} C_{\text{MCHT}} + K_{\text{DMBCH}}^{\tau} C_{\text{DMBCH}}\right)^3} \quad (17)$$

$$\text{DMBCH: } \frac{dC_{\text{DMBCH}}}{dt} = \frac{k_{\text{MCHT}}^{\tau} K_{\text{H}}^{\tau} K_{\text{MCHT}}^{\tau} C_{\text{MCHT}} C_{\text{H}_2}}{\left(1 + K_{\text{DBT}}^{\tau} C_{\text{DBT}} + \sqrt{K_{\text{H}}^{\tau} C_{\text{H}_2}} + K_{\text{BPH}}^{\tau} C_{\text{BPH}} + K_{\text{CHB}}^{\tau} C_{\text{CHB}} + K_{\text{BCH}}^{\tau} C_{\text{BCH}} + K_{\text{DMDBT}}^{\tau} C_{\text{DMDBT}} + K_{\text{DMBP}}^{\tau} C_{\text{DMBP}} + K_{\text{MCHT}}^{\tau} C_{\text{MCHT}} + K_{\text{DMBCH}}^{\tau} C_{\text{DMBCH}}\right)^3} \quad (18)$$

$$\text{H}_2\text{S: } \frac{dC_{\text{H}_2S}}{dt} = \frac{1}{K_{\text{eq}}} (-r_{\text{DBT}}^{\sigma} - r_{\text{DBT}}^{\tau} - r_{\text{DMDBT}}^{\sigma} - r_{\text{DMDBT}}^{\tau}) \quad (19)$$

The total of 23 parameters contained in the Hougen-Watson kinetic model (k_i – kinetic constants and K_i – adsorption coefficients, listed in Eqs. (1)–(19)) were determined using an optimization technique in the MATLAB software (MathWorks, USA). The technique used is a combination of Genetic Algorithm GA and Fminsearch methods as a hybrid optimization technique (GA-Fminsearch) that determines parameters in a way to minimize the deviation (Error) between the model and experimental data, Eq. (20):

$$\text{Error} = \sum_i \frac{\sum_j |C_{ij}^{\text{Exp}} - C_{ij}^{\text{Model}}|}{C_{ij}^{\text{Exp}}} \quad (20)$$

Genetic Algorithm (GA) is an optimization method which is using operators Selection, Crossover, Mutation, and Sampling, and finds the global minimum at the end [48-50]. One of the superiorities of GA over classical optimization techniques is that it does not need any additional information, such as derivatives, about the target function [49], searching from population of points, handling coded values of the problem parameters, and using probabilistic transition operators [50,51]. By combining GA with a local search method, such as Fminsearch, finding the exact optimum point becomes the less time-consuming process. Fminsearch is an optimization technique that determines the minimum of an unconstrained multivariable function by using a derivative-free method starting from an initial guess, employing the Nelder-Mead simplex algorithm [52], and finding the local minimum corresponding to the initial guess. Fminsearch converges faster to a solution than GA does, but it needs a suitable initial guess to obtain the global minimum without being trapped in the local minimum. The role of GA in the hybrid GA-Fminsearch technique is finding the initial guess of the reactions' constants.

4. RESULTS AND DISCUSSION

Testing of catalytic activity of RePd A and RePd MA catalysts on TiO₂/SiO₂ supports was performed at 630 K and 60 bar in a batch catalytic reactor. Concentrations of all relevant species were determined in order to quantify species evolving through DDS and HYD reaction pathways, so to generate sufficient experimental data, which can be used in determination of kinetic parameters. Values of concentrations for reactants and all reaction products are shown in Table 1 (average absolute deviations of two runs are: 0.124 for RePd A and 0.107 for RePd MA).

Table 1. Experimental data of concentration profiles along the reaction time for reactants and reaction products

Time, h	RePd A catalyst								
	Concentration, mol dm ⁻³								
	DBT	BPH	CHB	BCH	DMDBT	DMBPH	MCHT	DMBCH	H ₂ S*
0	0.0339	0	0	0	0.00368	0	0	0	0
0.25	0.02702	0.00625	0.00063	0	0.00342	0.00004	0.0002	0.00002	0.00293
0.5	0.02649	0.00621	0.00075	0.00045	0.00298	0.00008	0.00031	0.0003	0.00332
1	0.02299	0.0092	0.00115	0.00057	0.00287	0.00014	0.00047	0.00019	0.0048
1.5	0.02132	0.01062	0.00138	0.00058	0.00265	0.00022	0.00061	0.00021	0.00557
2	0.0144	0.01599	0.00256	0.00095	0.0025	0.00025	0.00063	0.0003	0.00847
3	0.01111	0.0185	0.00333	0.00095	0.0021	0.00029	0.0006	0.00069	0.00998
4	0.00898	0.02016	0.00383	0.00093	0.00184	0.00026	0.00044	0.00114	0.01095
5	0.00608	0.02182	0.0048	0.0012	0.00125	0.00022	0.00028	0.00193	0.01238
6	0.00521	0.02212	0.00531	0.00127	0.00099	0.00013	0.00016	0.0024	0.01285
RePd MA catalyst									
Time, h	Concentration, mol dm ⁻³								
	DBT	BPH	CHB	BCH	DMDBT	DMBPH	MCHT	DMBCH	H ₂ S
0	0.0339	0	0	0	0.00368	0	0	0	0
0.25	0.0339	0	0	0	0.00305	0.00009	0.00016	0.00038	0.00026
0.5	0.03083	0.00188	0	0.00119	0.00261	0.0002	0.00031	0.00056	0.0017
1	0.02799	0.00286	0.00021	0.00284	0.00239	0.00025	0.0004	0.00064	0.00295
1.5	0.02417	0.00522	0.0005	0.00401	0.00236	0.00026	0.00047	0.0006	0.00453
2	0.01854	0.00918	0.00138	0.0048	0.00195	0.00025	0.00057	0.00091	0.007
3	0.01598	0.00974	0.00455	0.00363	0.00173	0.00022	0.00074	0.00099	0.00814
4	0.0148	0.00983	0.00593	0.00334	0.00151	0.00027	0.00084	0.00106	0.00871
5	0.00845	0.01098	0.01012	0.00435	0.0011	0.0004	0.00111	0.00106	0.01147

*Concentration of H₂S is in the liquid phase. Values were obtained by molar balance calculation and vapour – liquid equilibrium calculation using the Peng – Robinson Equation of State



The obtained experimental results, concentration profiles, were applied in the widely used Hougen-Watson kinetic model describing DBT and 4,6-DMDBT desulphurisation on σ and τ active sites, as shown above. Kinetic parameters of this complex catalytic kinetics were determined in a procedure using GA-Fminsearch method and minimum deviation function. The results of parameter estimation are reported in Table 2 and comparison of simulated and experimental data obtained with optimized constants are shown in Figure 2.

Table 2. Values of determined and optimized kinetic parameters and comparison with the same constants obtained by Froment and co-workers for a Co/Mo catalyst [36-38]

Kinetic and adsorption constants on σ and τ active sites	RePd A	RePd MA	Co/Mo catalyst recalculated constants for 603 K [36-38]
Adsorption equilibrium constant, $m^3 \text{ kmol}^{-1}$			
K^σ_{BPH}	12.68	0.00	5.78
K^τ_{DMPP}	7.51	329.32	0
K^τ_{DMDBT}	9.08	2.12	1.09
K^τ_{MCHT}	25.72	40.14	NA
K^σ_{DBT}	2.74	0.82	75.69 constant value for all temperatures
K^τ_{DBT}	3.13	0.00	2.14
K^τ_{BPH}	3.20	13.51	0.95
K^τ_{CHB}	4.02	10.15	$K^\tau_{\text{CHB}} k^\tau_{\text{CHB}} (573 \text{ K}) = 0.000339$
K^τ_{DMBP}	14.33	25.17	0
K^σ_{DMDBT}	2.19	0.36	18.04
K^τ_{DMBCH}	0.19	24.05	NA
K^τ_{BCH}	0.00	2470.34	NA
$K^\sigma_{\text{H}_2\text{S}}$	12.75	1.89	20.92
K^σ_{H}	0.13	3.17	0.216
K^τ_{H}	0.00	2.42	0.00321
K_{eq} for H_2S	2.48	2.25	NA
Kinetic constant, $\text{kmol kg}_{\text{cat}}^{-1} \text{ h}^{-1}$			
k^σ_{DBT}	1.11	0.33	0.57
k^τ_{DBT}	2.15	0.33	2.14
k^σ_{DMDBT}	0.23	0.66	0.041
k^τ_{DMDBT}	3.07	0.63	46.12
k^τ_{BPH}	1.33	3.08	24.19
k^τ_{DMBP}	2.96	6.23	Not in the kinetic model
k^τ_{CHB}	2.96	2.83	$K^\tau_{\text{CHB}} k^\tau_{\text{CHB}} (573 \text{ K}) = 0.000339$
k^τ_{MCHT}	4.19	0.66	Not in the kinetic model
Error	0.1312	0.1435	Not known

The Figure 2 confirms that the concentrations of different species predicted by the Hougen-Watson based kinetic model closely match the experimentally determined values.

Results of test reactions for conversion of DBT and 4,6-DMDBT are shown in Figure 3, obtained by using the estimated kinetic parameters for RePd A and RePd MA catalyst. The Figure 3 also shows conversion of DBT and 4,6-DMDBT obtained by using kinetic parameters developed by the Froment group for a commercial Co/Mo catalyst [36-38] and recalculated for the same temperature of reaction (603 K). It is obvious that the calculated Co/Mo catalyst activity is quite high and comparable to those of aerogel catalysts. However, it should be noted that the kinetic parameters determined by the Froment group [36-38] were obtained in the different temperature interval (temperature range 513 – 593 K) and different pressure (7 MPa) than the one used in this work. The experimental hydrogen/hydrocarbon ratio (2.3 and 3.5) and catalyst/feed ratio (4.6 times more catalyst than in this research) were also different. The commercial Co/Mo catalyst activity in HDS of 4,6-DMDBT (conversion 62.4 mol.% after 6 h) is lower than activities



of the investigated aerogels (conversion 73.6 and 76.6 mol.% after 6 h respectively for RePd MA and RePd A) (Figure 3b), which is of significance for HDS of diesel oil fractions.

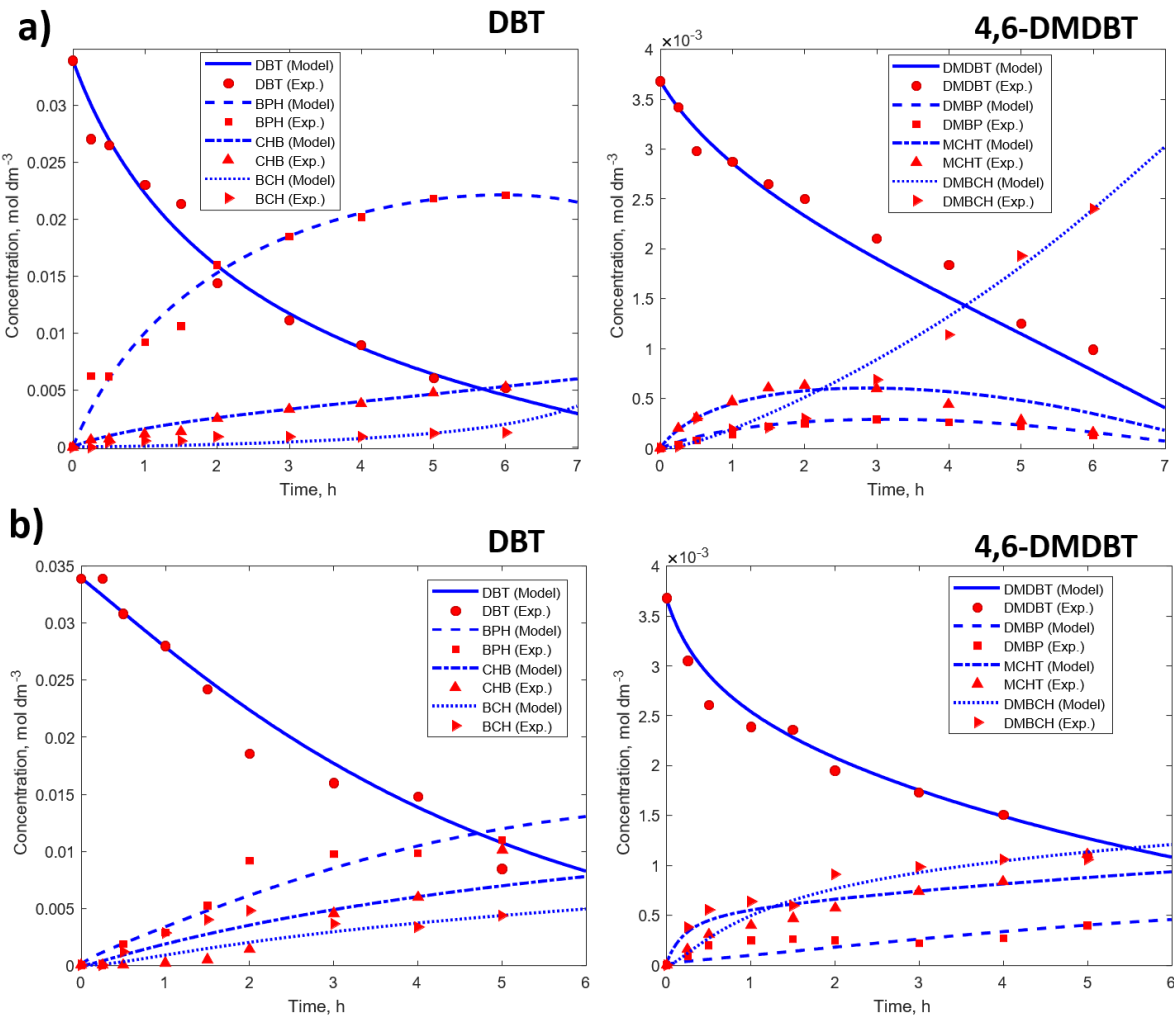


Figure 2. The experimental and simulated data obtained for hydrodesulphurization of DBT and 4,6-DMDBT using a) RePd A and b) RePd MA catalyst

High activity of RePd aerogels can be explained by, and attributed to, their unique properties. These advantageous properties are high surface area ($848 \text{ m}^2 \text{ g}^{-1}$ for RePd A and $643 \text{ m}^2 \text{ g}^{-1}$ for RePd MA) and very high mesoporosity (volume of mesopores $0.466 \text{ cm}^3 \text{ g}^{-1}$ for RePd A and $1.618 \text{ cm}^3 \text{ g}^{-1}$ for RePd MA) as determined previously [34]. Also, mesopore fractions of 0.71 for RePd A and 0.55 for RePd MA [34] indicate high proportion of catalytically active surfaces. Texture was also characterized by the presence of large mesopores and small macropores (overall porosities are $0.656 \text{ cm}^3 \text{ g}^{-1}$ for RePd A and $2.956 \text{ cm}^3 \text{ g}^{-1}$ for RePd MA [34]) which are both expected to eliminate diffusional limitations and thus increase reaction rates. Good dispersion of RePd within the catalyst structure was evidenced resulting in higher concentrations of surface active sites [34]. Finally, the increased acidity of the titania-silica support which is the result of good Ti dispersion within the silica matrix [34] and high activity of the catalytically active Re/Pd phase [53] are contributing to the overall high activity of these aerogel catalysts.

Further insights into possible explanations for high activity of RePd aerogels could be found in the modification of the overall reaction pathway. As indicated in the introductory part of this study, an explanation could be associated with the exceptional properties of Pd which were found to be suitable for hydrogen spillover in hydrogenation of aromatics [29-32]. This is the critical step for deep HDS *via* a HYD route. As a result, highly active catalytic formulations with excellent DBT HDS activity (like CoMo with depleted HYD efficiency) can become relatively inactive for desulphurisation of 4,6-DMDBT.

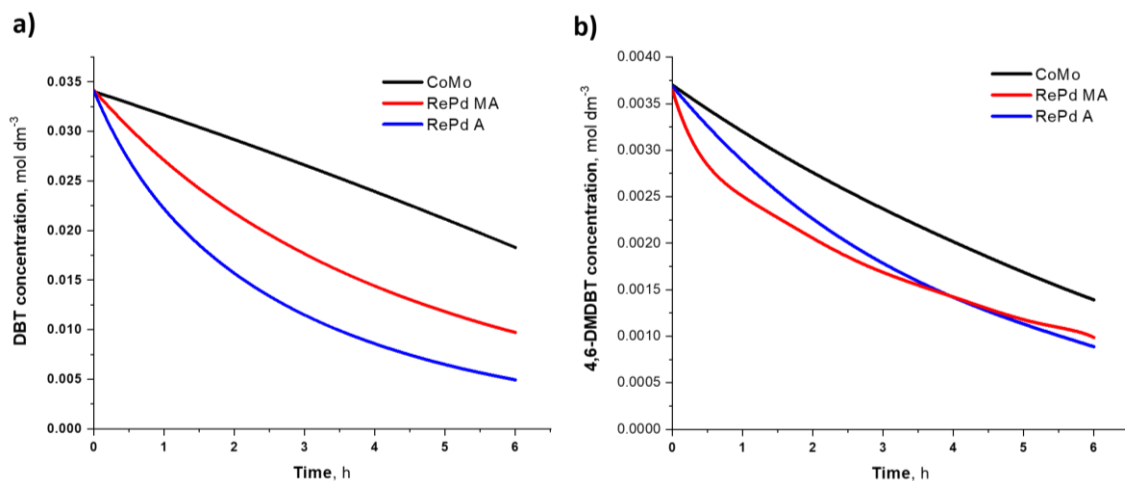


Figure 3. Predicted concentrations of a) DBT and b) 4,6-DMDBT over time in HDS for the investigated catalysts and a commercial catalyst Co/Mo based on the kinetic parameters in Table 2

Indication of the dominant reaction pathway for RePd catalysts was examined by GC-MS analysis of reaction products obtained in HDS of DBT. The selectivity towards CHB, expressed as $\text{CHB}/(\text{CHB}+\text{BP})$ ratio and MCHT expressed as $\text{MCHT}/(\text{MCHT}+\text{DMBPH})$, obtained by simulation based on using the obtained kinetic and adsorption constants during reaction (Table 2) are shown in Figure 4. It is interesting to observe that the CHB selectivity is considerably higher for RePd MA catalyst obtained with mesitylene addition than for the other two types of catalyst, RePd A without mesitylene addition and CoMo catalysts. Values of $\text{MCHT}/(\text{MCHT}+\text{DMBPH})$ ratio are significantly higher than the values of $\text{CHB}/(\text{CHB}+\text{BP})$ ratio, indicating overwhelming HYD activity in HDS of 4,6-DMDBT. A possible explanation might be found in a combination of RePd MA characteristics such as: large volume of mesopores, the shift of pore size distribution (PSD) to larger mesopores, slightly higher overall Pd/Re ratio and higher local Pd/Re ratios as compared to RePd A [34]. Some of these characteristics have been found to influence activity of RePd catalysts considerably [53] and could represent an opportunity for potential improvement of catalysts dedicated to various hydrogenation reactions, in particular hydrogenation of large molecules which are found in heavier petroleum fractions.

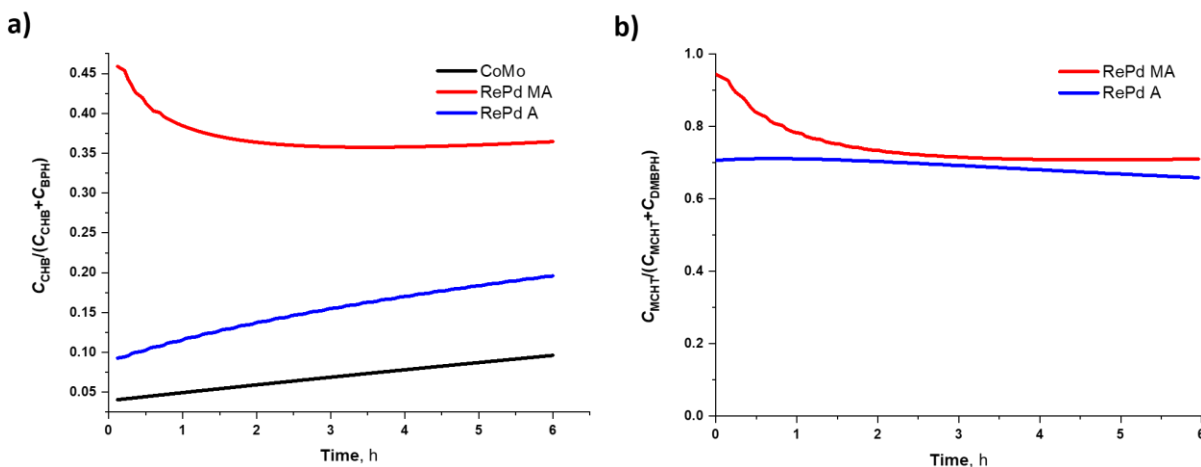


Figure 4. Predicted selectivity towards a) CHB expressed as $\text{CHB}/(\text{CHB}+\text{BP})$ and b) MCHT expressed as $\text{MCHT}/(\text{MCHT}+\text{DMBPH})$ in the HDS of DBT and 4,6-DMDBT for the investigated catalysts and a commercial catalyst Co/Mo based on the kinetic parameters in Table 2

5. CONCLUSION

Hydrodesulphurisation (HDS) of dibenzothiophene (DBT) and 4,6-dimethyl dibenzothiophene (4,6-DMDBT) by using Re/Pd catalysts (obtained with and without the use of mesitylene in the synthesis step) at 630 K and 6 MPa in a batch catalytic reactor was investigated in the present study. The Hougen-Watson kinetic model was applied to describe

desulphurisation of DBT and 4,6-DMDBT on σ and τ active sites and kinetic parameters were determined in a procedure based on using Genetic Algorithm (GA) method and minimum deviation function. Values of calculated kinetic parameters have shown that the hydrogenation route is the dominant route for desulphurisation of 4,6-DMDBT in the case of newly developed catalysts based on Re/Pd and highly mesoporous silica support with incorporated Ti. The obtained results were compared with predicted commercial Co/Mo catalyst activity in HDS of 4,6-DMDBT based on literature data indicating higher catalytic activities of the investigated Re/Pd aerogels. These findings are of potential significance for deep hydrodesulphurisation of diesel oil fractions. The most significant conclusion is that values of MCHT/(MCHT+DMBPH) ratio are significantly higher than the values of CHB/(CHB+BP) ratio, indicating overwhelming HYD activity in HDS of 4,6-DMDBT. Newly developed RePd aerogel catalysts used in this work exhibit outstanding catalytic activity and could represent an interesting opportunity for improvement of hydrogenation of large molecules, which normally occur in heavy petroleum fractions.

Acknowledgements: Financial support by the Ministry of Education and Science of the Republic of Serbia (Contract No. 451-03-68/2022-14/200135) and Institutional funding of the Faculty of Technology and Metallurgy, University of Belgrade is gratefully acknowledged.

REFERENCES

- [1] McGuiness L, Nunes MD, Kroes F, Chai I. Automated analysis of bauxite exploration drill hole samples by diffuse reflectance Fourier transform infrared (FTIR) spectroscopy. In: *Proceedings of the 7th International Alumina Quality Workshop*. Australia, 2005; 187–192.
- [2] Authier-Martin M, Forte G, Ostap S, See J. The mineralogy of bauxite for producing smelter-grade alumina. *JOM* 2001; 53(12): 36–40. <https://doi.org/10.1007/s11837-001-0011-1>
- [3] Nechitailov A P, Suss AG, Zhilina TI, Belanova E A. New method of analyzing bauxites to determine their main components and impurities. *Metallurgist* 2008; 52(11): 625–632. <https://doi.org/10.1007/s11015-009-9104-9>
- [4] Blagojević D, Lazic D, Keselj D, Skundrić B, Dugic P, Ostožić G. Determining the content of silicon dioxide in bauxites using X-ray fluorescence spectrometry. *Iran. J. Chem. Chem. Eng.* 2019; 38(4). <https://doi.org/10.30492/IJCCE.2019.34231>
- [5] Ostožić G, Lazic D, Zeljkovic S. Determination of the iron oxide content in bauxite: comparing ICP-OES with UV-VIS and volumetric analysis. *Chem. Pap.* 2020; 75(1): 389–396. <https://doi.org/10.1007/s11696-020-01305-z>
- [6] Idris N, Lahna K, Syamsuddin F, Ramli M. Study on Emission Spectral Lines of Iron, Fe in LaserInduced Breakdown Spectroscopy (LIBS) on Soil Samples. *J. Phys. Conf. Ser.* 2017; 846(012020). <https://doi.org/10.1088/1742-6596/846/1/012020>
- [7] Carvalho AAC, Alves VC, Silvestre DM, Leme FO, Oliveira PV, Nomura CS. Comparison of FusedGlass Beads and Pressed Powder Pellets for the Quantitative Measurement of Al, Fe, Si and Ti in Bauxite by Laser Induced Breakdown Spectrometry (LIBS). *Geostand. Geoanal. Res.* 2017; 41(4): 585–592. <https://doi.org/https://doi.org/10.1111/ggr.12173>
- [8] Fahad M, Sajjad A, Shah KH, Shahzad A, Abrar M. Quantitative elemental analysis of high silica bauxite using calibration-free laser-induced breakdown spectroscopy. *Appl. Opt.* 2019; 58(27): 7588–7596. <https://doi.org/https://doi.org/10.1364/AO.58.007588>
- [9] Upendra S, Mishra RS. Simultaneous multielemental analysis of alumina process samples using inductively coupled plasma spectrometry (ICP-AES). *Anal. Chem.: Indian J.* 2012; 11(1). <https://www.tsijournals.com/articles/simultanious-multielemental-analysis-of-alumina-process-samples-using-inductively-coupled-plasma-spectrometry.pdf>
- [10] Murray RW, Miller DJ, Krys KA. Analysis of major and trace elements in rocks, sediments, and interstitial waters by inductively coupled plasma-atomic emission spectrometry (ICP-AES). *ODP Tech. Note*, 2000; 29. <https://doi.org/10.2973/ODP.TN.29.2000>
- [11] SPECTRO - Smart Analyzer Vision Software, Online-Help vers. 5.01.09XX. Spectro Analytical Instruments GmbH. 2012
- [12] Giavarina D. Understanding Bland Altman analysis. *Biochem. Medica* 2015; 25(2), 141–151. <https://doi.org/10.11613/BM.2015.015>
- [13] Bilić-Zulle L. Comparison of methods: Passing and Bablok regression. *Biochem. Medica* 2011; 21 (1): 49–52. <https://doi.org/10.11613/bm.2011.010>
- [14] Medcalc manual, <https://www.medcalc.org/manual/mountain-plot.php>, Accessed May 23rd 2020
- [15] Linsinger T. Comparison of a measurement result with the certified value. Application Note 1, European Reference Materials. 2010; 1–2.
- [16] Certificate of Analysis, Standard Reference Material 697, bauxite Dominican, National Institute of Standards and Technology. 1991
- [17] Liberatore PA. Determination of Majors in Geological Samples by ICP-OES: Vol. ICP-AES Inst. 1993; 12 <https://www.colby.edu/chemistry/CH332/laboratory/Geo-ICP-protocol2.pdf>
- [18] Hauptkorn S, Pavel J, Seltner H. Determination of silicon in biological samples by ICP-OES after non-oxidative decomposition under alkaline conditions. *Fresenius. J. Anal. Chem.* 2001; 370: 246–250. <https://doi.org/10.1007/s002160100759>



- [19] US. EPA Method 6010D (SW-846): Inductively coupled plasma-atomic emission spectrometry. Washington, DC, USA, 2014. <https://www.epa.gov/esam/epa-method-6010d-sw-846-inductively-coupled-plasma-atomic-emission-spectrometry>
- [20] Simundic AM. Statistical analysis in method comparison studies-Part one. 2016; www.acutecaretesting.org
- [21] AOAC (American Association Of Official Analytical Chemists), *Appendix F: Guidelines for Standard Method Performance Requirements*. 2016. <https://www.aoac.org/resources/guidelines-for-standard-method-performance-requirements/>
- [22] Taftazani A, Roto R, Ananda NR, Murniasih S. Comparison of NAA XRF and ICP-OES Methods on Analysis of Heavy Metals in Coals and Combustion Residues. *Indones. J. Chem.* 2017; 17(2): 228–237. <https://doi.org/10.22146/ijc.17686>
- [23] Rüdel H, Kösters J, Schörmann J. *Determination of the Elemental Content of Environment Sample using ICP-OES, Guidelines for Chemical Analysis*, Fraunhofer Institute for Molecular Biology and Applied Ecology, Schmallenberg, 2007. https://www.ime.fra-unhofer.de/content/dam/ime/en/documents/AE/SOP_ICP-OES_en.pdf
- [24] Amorin A, *Determination of major and minor elements in HF-digested soil samples using an Agilent 5110 ICP-OES*, application note, Agilent Technologies.Inc. 2019. https://www.agilent.com/cs/library/applications/application_inert_sample_chamber_icp-oes_5110_5994-1213en_us_agilent.pdf
- [25] Krishna AK, Murthy NN, Govil PK. Multielement Analysis of Soils by Wavelength-Dispersive X-ray Fluorescence Spectrometry. *At. Spectrosc* 2007; 28(6): 202–214. https://www.researchgate.net/profile/Keshav-Krishna/publication/233786687_Multielement_Analysis_of_Soils_by_Wavelength-Dispersive_X-ray_Fluorescence_Spectrometry/links/57ecd91a08aebb1961ffc510/Multielement-Analysis-of-Soils-by-Wavelength-Dispersive-X-ray-Fluorescence-Spectrometry.pdf

Desulfurizacija dibenzotiofena i 4,6 – dimetildibenzotiofena procesom hidrogenovanja uz korišćenje RePd–TiO₂/SiO₂ aerogel katalizatora: proračun kinetičkih parametara i simulacija procesa

Dragana Prokić-Vidojević¹, Sandra B. Glišić², Radojica Pešić² i Aleksandar M. Orlović²

¹Vojno tehnički institut (VTI), Ratka Resanovića 1, 11132 Beograd, Srbija

²Univerzitet u Beogradu, Tehnološko-metalurški fakultet, Karnegijeva 4, 11000 Beograd, Srbija

(Naučni rad)

Izvod

Re/Pd-TiO₂/SiO₂ aerogel katalizatori su sintetizovani korišćenjem sol-gel metode i natkritičnog sušenja u višku rastvarača, i njihova katalitička aktivnost je ispitana u reakcijama hidrodesulfurizacije (HDS) dibenzotiofena (DBT) i 4,6-dimetildibenzotiofena (4,6-DMDBT). Oba Re/Pd katalizatora, dobijena sa ili bez meziklena u procesu sinteze, su pokazala povećan stepen konverzije, za 70 %, u reakciji hidrodesulfurizacije 4,6-DMDBT u poređenju sa konvencionalnim Co/Mo katalizatorom koji se koristi u procesima hidroobrade. Ova zapažanja, veći stepen konverzije teško reagujućih 4,6-DMDBT u procesu hidroobrade, su značajna za dobijanje nisko-sumpornih dizel goriva (engl. ultra-low sulphur diesel fuels, ULSD). Kvantitativna analiza produkata hidrogenovanja DBT i 4,6-DMDBT, uključujući međuproizvode, izvedena je tehnikom gasne hromatografije – masene spektrometrije (engl. gas chromatography–mass spectrometry, GC-MS). Eksperimentalna reakcija je izvedena na 630 K i 60 bar u šaržnom katalitičkom reaktoru. Eksperimentalni podaci su korišćeni u okviru Hagen-Vatson (Hougen-Watson) kinetičkog modela koji opisuje proces hidrodesulfurizacije DBT i 4,6-DMDBT na σ i τ aktivnim centrima. Kinetički parametri su određeni korišćenjem numeričkih optimizacionih metoda, genetski algoritam simultano sa funkcijom minimuma odstupanja, i dobijeni rezultati pokazuju dobro slaganje sa eksperimentalnim podacima. Vrednosti izračunatih kinetičkih parametara kao i vrednosti selektivnosti (tj. odnosa metilcikloheksiltoluena i dimetilbifenila kao MCHT/(MCHT+DMBPH)) su potvrđene da je hidrogenovanje dominantni reakcioni put za hidrodesulfurizaciju 4,6-DMDBT. Potencijalne prednosti korišćenja Re/Pd aerogel katalizatora za konverziju 4,6-DMDBT potvrđene su i rezultatima uporednih simulacija ovog i konvencionalnog Co/Mo katalizatora.

Ključne reči: Aerogel katalizator; hidrodesulfurizacija; 4,6-DMDBT; Hagen-Vatson kinetički model; kinetički parametri



Razvoj i karakterizacija elektrohemiskog senzora na bazi ugljenika modifikovanog nanočesticama TiO₂

Saša Mićin¹, Borislav N. Malinović² i Tijana Đuričić²

¹Fakultet bezbjednosnih nauka, Univerzitet u Banjoj Luci, Banja Luka, Bosna i Hercegovina

²Tehnološki fakultet, Univerzitet u Banjoj Luci, Banja Luka, Bosna i Hercegovina

Izvod

Cilj ove studije je razvoj i karakterizacija elektrohemiskog senzora na bazi ugljenika, modifikovanog nanočesticama TiO₂ za potencijalnu primjenu u elektroanalitičkim tehnikama. Vršena su ispitivanja uticaja udjela vezivnog sredstva i modifikatora na morfološke, fizičko-hemiske i elektrohemische karakteristike elektrodnog materijala radi određivanja optimalnog odnosa ugljenični materijal/vezivo/modifikator. Ugljenične paste su pripremljene od grafitnog praha modifikovanog nanočesticama TiO₂ i tečnih ugljovodonika. Skenirajuća elektronska mikroskopija pokazala je da elektrodnji materijal postaje kompaktniji sa dodatkom vezivnog materijala i povećanjem njegovog udjela, te da nema značajnih morfoloških razlika s porastom udjela nanočestica TiO₂ koje su prilično homogeno raspodjeljene u grafitnom elektrodnom materijalu. Rezultati ispitivanja ukazuju da modifikovanu ugljeničnu pastu sa sadržajem 40 vol.% parafinskog ulja (PU) i 6-8 mas.% nanočestica TiO₂ karakteriše najmanja vrijednost specifičnog otpora. Primjenom ciklične voltametrije dobijen je najizraženiji stepen reverzibilnosti u odnosu na standardni reverzibilni redoks sistem ($[Fe(CN)]^{3-/4-}$) kod elektrodnog materijala sa sadržajem 30–40 vol.% PU i 8-10 mas.% nanočestica TiO₂. Karakterizacijom elektrodnog materijala na bazi ugljenika modifikovanih nanočesticama TiO₂ utvrđeno je da optimalan sastav sadrži 40 vol.% PU i 6-8 mas.% nanočestica TiO₂, što je od važnosti za primjenu u elektroanalitičkim tehnikama.

Ključne reči: elektroanalitičke tehnike, modifikovane ugljenične elektrode; parafinsko ulje; trikrezol fosfat; elektrodnji materijal.

Dostupno na Internetu sa adresu časopisa: <http://www.ache.org.rs/HI/>

1. UVOD

Elektrohemische metode koje primenjuju nemodifikovane i modifikovane elektrode od ugljenične paste su široko korišćene u elektroanalitičkim tehnikama koje su našle primjenu u različitim oblastima kao što su karakterizacija biosenzora na bazi ugljenične paste, neorganske elektroanalize, elektroanalize organskih sintetičkih jedinjenja i prirodnih polutanata, kao i analize važnih bioloških molekula i jedinjenja nastalih interakcijom organskih i bioloških makromolekula [1,2]. Elektrohemische senzore izrađene od ugljenične paste u odnosu na druge vrste elektrodnih materijala karakteriše mogućnost korišćenja u širokom rasponu potencijala, niska vrijednost rezidualne struje, specifične površinske karakteristike, ekonomičnost, jednostavnost pripreme, minimalna toksičnost i široke mogućnosti hemijskih i bioloških modifikacija [3]. Sa ciljem poboljšanja prenosa mase ili smanjenja ograničenja prenosa elektrona na površini elektrode [3,4] vršene su modifikacije ugljenične paste različitim dodacima čija uloga može biti specifična (modifikator, stabilizator, katalizator, posrednik, itd.). Pokazana je prednost modifikovanih elektroda u odnosu na makroelektrode koja se ogleda u značajno većoj specifičnoj površini, izraženoj adsorpcionoj sposobnosti, hemijskoj inertnosti, termičkoj stabilnosti, uticaju na povećanje transporta mase, uticaju na mehanizam prenosa elektrona te elektrokatalizi [5-9]. U dosadašnjim istraživanjima korišćene su različite forme ugljeničnog materijala, različita vezivna sredstva i veći broj različitih modifikatora sa različitim postupcima modifikacije [10-12]. Najčešće korišćeno vezivno

NAUČNI RAD

UDK: 544.6.076.32-039.61:
(546.26-162+549.514.6)

Hem. Ind. 76(3) 147-158 (2022)

Korespondencija: Borislav N. Malinović, Tehnološki fakultet, Univerzitet u Banjoj Luci, Banja Luka, Bosna i Hercegovina

E-mail: borislav.malinovic@tf.unibl.org

Rad primljen: 5. januara 2022; Rad prihvaćen: 16. juna 2022; Rad objavljen 18. jula 2022

<https://doi.org/10.2298/HEMIND220105013M>



sredstvo u elektrohemiskim senzorima na bazi ugljeničnih materijala je smješa tečnih alifatskih ugljovodonika (parafinsko ulje, PU) [1]. Karakteriše ga velika hemijska stabilnost, elektroneaktivnost, a interakcija sa elektroaktivnim materijama prisutnim u elektrolitu na elektrohemiski aktivnoj površini elektrode i u masi elektrode je pretežno fizičke prirode. S obzirom na električnu neprovodljivost vezivnog sredstva kinetika prenosa elektrona je usporena, a pozadinske struje se javljaju uslijed prisustva adsorbovanog kiseonika u ugljeničnoj pasti ili rastvorenog u elektrolitu [12]. Reakcionala smjesa 3-metilfenil bis(4-metilfenil) fosfata, bis(3-metilfenil) 4-metilfenil fosfata i tris(3-metilfenil) fosfata (trikrezol-fosfat, TCP) je tipični predstavnik elektroaktivnih vezivnih sredstava [3]. Pokazuje sposobnost protoniranja molekula organofosfata u kiselim sredinama pri čemu nastaju katjoni izraženih lipofilnih karakteristika. U takvom obliku učestvuje u procesima izmjene jona odnosno uparivanja jona i formira relativno stabilne elektroaktivne jonske parove [12]. Vršena su ispitivanja elektrohemiskih senzora modifikovanih različitim nanomaterijalima poput nanočestica različitih metala, metalnih oksida i nanomaterijala baziranih na ugljeniku. Nanočestice TiO₂ predstavljaju veoma atraktivan modifikator s obzirom na specifična svojstva. Posjeduju hemijsku, fotohemiju i netoksičnu stabilnost, veliku inertnost, biokompatibilnost, nisku cijenu, veliku provodljivost, veliku specifičnu površinu i optičku transparentnost. Sa stanovišta elektroanalitičkih osobina, TiO₂ predstavlja poluprovodnik *n*-tipa koji pokazuje dobru optičku transmitancu u području infracrvenog zračenja. Posjeduje jednostavnu elektronsku strukturu sa popunjrenom valentnom zonom i praznom provodnom zonom [13-16]. Ugljenične elektrode modifikovane nanočesticama TiO₂ su našle veoma široku primjenu u elektroanalitičkim metodama određivanja različitih neorganskih, organskih i bioloških supstanci [17-23]. Mogućnost praktične primjene modifikovanih ugljeničnih elektroda u elektroanalitičke svrhe u značajnoj mjeri zavisi od fizičko-hemijskih i elektrohemiskih karakteristika elektrodne paste. S obzirom na heterogen sastav ugljenične paste, karakteristike elektrodnog materijala zavise od vrste i veličine čestica ugljeničnog materijala [24-30], vrste veziva [31], modifikatora, načina pripreme [32,33], kao i od odnosa udjela ugljeničnog materijala/vezivo/modifikatora [34]. Pokazano je da vezivno sredstvo osim vezivne uloge ima i uticaj na elektrohemiske procese koji se odigravaju na površini elektrode [10]. Takođe je uočeno da odnos udjela grafit/PU/nanočestice TiO₂ u elektrodnom materijalu utiče na karakteristične parametre voltametrijskog signala odziva ispitivanog sistema [35]. Još uvjek nisu definisane opšteprihvaćene metode karakterizacije nemodifikovanih i modifikovanih ugljeničnih elektroda sa ciljem određivanja optimalnog sastava modifikovanog elektrodnog materijala. U literaturi je predložena opšta procedura karakterizacije nemodifikovanih elektroda od ugljeničnog materijala [36]. Noviji pristup optimizaciji postupka pripreme i karakterizaciji ugljične paste se zasniva na mjerenu omske otpornosti i kvalitativnog indeksa ugljenične paste [37].

Cilj ovog rada je razvoj i karakterizacija modifikovane ugljenične elektrode izvedene sa različitim vezivnim materijama i različitim odnosima udjela vezivo/nanočestica TiO₂. Izvršeno je ispitivanje uticaja kvalitativnog i kvantitativnog sastava elektrodnog materijala na morfološke, fizičko-hemijske i elektrohemiske karakteristike modifikovane elektrode primjenom skenirajuće elektronske mikroskopije (SEM), energetske disperzivne analize (EDS), određivanjem specifične provodljivosti i ciklične voltametrije (CV). Ispitivane su modifikovane ugljenične paste načinjene od grafitnog praha i tečnog veziva: i) parafinsko ulje (PU), ii) reakcionala smjesa 3-metilfenil bis(4-metilfenil) fosfata, bis(3-metilfenil) 4-metilfenil fosfata i tris(3-metilfenil) fosfata (trikrezol fosfat, TCP) i iii) smjesa parafinskog ulja i trikrezol fosfata (PUTCP) u omjeru 1:1 (v/v), modifikovane nanočesticama TiO₂. Elektrodne paste su sadržavale vezivnu materiju u rasponu od 10 do 60 vol.% i nanočestice TiO₂ u rasponu od 4-12 mas.%. Dobijeni rezultati će doprinijeti razvoju senzora za široku primjenu u elektroanalitičkim metodama.

2. MATERIJALI I METODE

2.1. Hemikalije

Korišćene hemikalije su kalijum heksacijanoferat(II) K₄[Fe(CN)]₆·3H₂O *p.a.*, Kemika, Hrvatska, kalijum hlorid, KCl *p.a.*, Kemika, Hrvatska, grafitni prah ekstra čistoće, veličine čestica <50 µm, CAS broj 7782-42-5, Merck, Njemačka, dietil eter *p.a.*, Lachner, Češka, parafinsko ulje, CAS broj 8042-47-5, Merck, Njemačka, reakcionala smjesa 3-metilfenil bis(4-metilfenil) fosfata, bis(3-metilfenil) 4-metilfenil fosfata i tris(3-metilfenil) fosfata (trikrezol fosfat), CAS broj 1330-78-5, Merck, Njemačka i nanočestice TiO₂, komercijalnog naziva AEROXIDE®TiO2P, Evonik Industries AG, Njemačka. Veličina

nanočestica iznosi 10-50 nm pretežno distribuisanih u rasponu od 15 do 25 nm [38]. Za pripremu rastvora korišćena je destilovana voda, provodljivosti 4 $\mu\text{S m}^{-1}$.

2. 2. Priprema modifikovane ugljenične paste

Serije modifikovanih ugljeničnih pasti su pripremljene na način da se smjesa grafitnog praha i nanočestica TiO₂ (5 g, pojedinačnog sadržaja nanočestica TiO₂ 4, 6, 8, 10, 12 mas.%) disperguje u 50 cm³ dietil etera uz neprekidno mješanje i zagrijavanje na temperaturi od 40°C. Nakon isparavanja dietil etera, (za svaki uzorak različitog sadržaja nanočestica TiO₂) vršeno je dodavanje 10, 20, 30, 40, 50, 60 vol.% (u odnosu na zapreminu modifikovanog ugljenikovog praha) tečne vezivne materije i) PU, ii) TCP i iii) PUTCP (zapreminske omjer 1:1). Vrijednosti gustine komponenti modifikovanih ugljeničnih elektroda, korišćenih za izračunavanje zapremine su prikazane u Dodatnom materijalu (Tabela D-1). Homogenizacija modifikovanih ugljeničnih pasti je izvedena ručnim mješanjem grafitnog praha i tečne vezivne materije u keramičkom tarioniku prema opisanoj proceduri [4]. Pripremljene modifikovane ugljenične paste su čuvane u zatvorenoj plastičnoj kutiji na sobnoj temperaturi i korišćene 24 sata nakon pripreme [32].

2. 3. Priprema elektrode

Pripremljena modifikovana pasta je utiskivana u tijelo elektrode (teflonska tuba, dužine 200 mm, prečnika 20 mm) sa šupljinom na kraju tijela elektrode (dužine 10 mm i prečnika 2,4 mm). Električni kontakt je ostvaren pomoću Cu žice (prečnika 1 mm) fiksirane u tijelu elektrode. Aktivna površina elektrode je polirana u cilju dobijanja glatke elektrodne površine. Postupak utiskivanja nove količine paste i poliranja elektrodne površine je vršeno neposredno prije svakog eksperimentalnog mjerenja [39].

2. 4. Morfološka karakterizacija

Za morfološku karakterizaciju površina ispitivanih elektrodnih pasti korišćen je skenirajući elektronski mikroskop (Quanta 250 FEG, FEI, SAD) sa nisko vakuumskim detektorom sekundarnih elektrona (LFD) i detektorom povratno raspršenih elektrona (BSED). Hemijska analiza i mapiranje elemenata prisutnih na površini ispitivanih materijala provedene su skenirajućom elektronskom mikroskopijom i energetskom disperzivnom analizom (SEM i EDS, detektor Pentafet, Oksford, UK).

2. 5. Specifična otpornost

Mjerenje omske otpornosti je provedeno pomoću digitalnog multimetra (DÜWI 07976, Njemačka). Ispitivane ugljenične paste su utisnute u horizontalno učvršćenu plastičnu tubu (prečnika 5 mm, dužine 10 mm) postavljenom između fiksiranih testnih kablova. Vrijednost specifične otpornosti (R_{CP}) je izračunata pomoću izraza (1):

$$R_{CP} = R_{CP,exp} A_{CPE} / l_{CP} \quad (1)$$

pri čemu je $R_{CP,exp}$ - eksperimentalno izmjerena vrijednost otpora; A_{CPE} - površina poprečnog presjeka elektrodnog materijala; l_{cp} - dužina nosača elektrodnog materijala. Sva eksperimentalna mjerenja su ponavljana tri puta.

2. 6. Elektrohemiska karakterizacija

Elektrohemiska karakterizacija ispitivanog modifikovanog ugljeničnog elektrodnog materijala vršena je cikličnom voltametrijom. Mjerenja su provedena korišćenjem potencijostata/galvanostata (PAR 273A, Princeton Applied Research, SAD), elektrohemiske ćelije zapremine 50 cm³, sastavljene od radne elektrode (elektroda od modifikovane ugljenične paste), referentne elektrode (Ag/AgCl 3,5 M), kontra elektrode (platinska pločica, površine 2,4 cm²) i radnog elektrolita 0,01 M K₄[Fe(CN)₆]₆×3H₂O (standardni elektrolit koji ima reverzibilnu jednoelektronsku reakciju). Kao pomoćni elektrolit korišćen je 0,1 M KCl. Mjerenja su vršena u području potencijala od 0,0 V do 1,0 V i pri brzini promjene potencijala od 50 mV s⁻¹. Eksperimenti su provedeni bez mješanja na sobnoj temperaturi 23±1 °C sa tri uzastopna mjerenja. Analiza cikličnih voltamograma je vršena pomoću softvera Powersuite 2.40 (Informer Technologies, Inc.). Svi potencijali su navedeni u odnosu na referentnu elektrodu. Analizirana je razlika potencijala (χ faktor) i odnos anodnog i



katodnog strujnog vrha voltametrijskog talasa [40]. Vrijednosti kvalitativnog indeksa modifikovane ugljenične paste (χ) su izračunate prema izrazu (2):

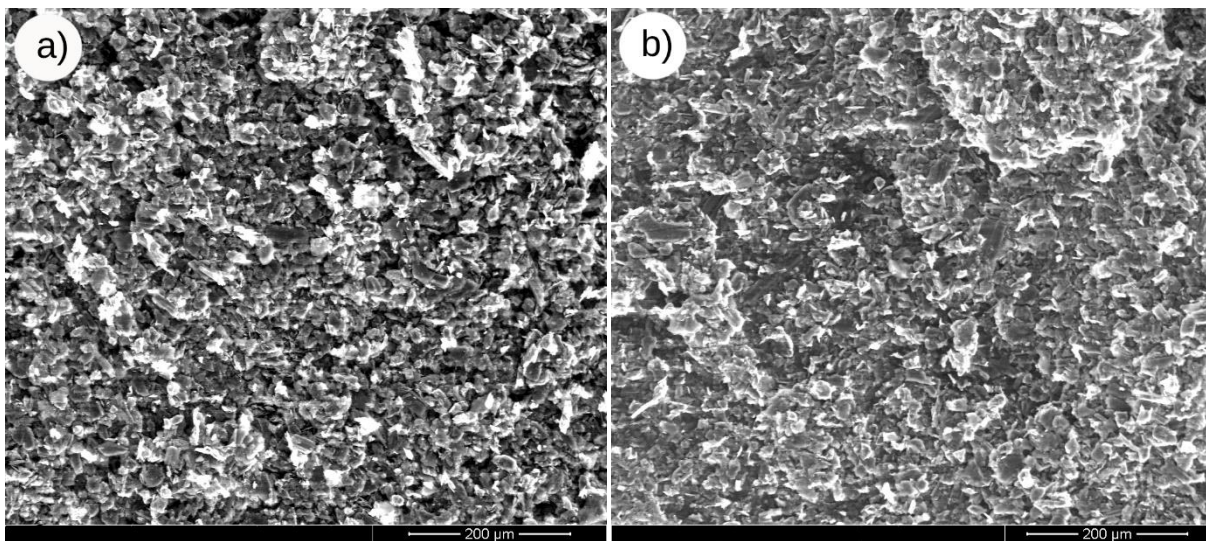
$$\chi = \frac{\Delta E_p \left([Fe(CN)]^{3/4} \right)}{\Delta E_{p,\text{theor}}} \quad (2)$$

što odgovara stepenu reverzibilnosti ispitivanog elektrohemijskog sistema. Teoretska vrijednost razlike potencijala za redoks sistem ($[Fe(CN)]^{3/4}$) iznosi 59 mV [37]. Za reverzibilne elektrohemijiske sisteme anodni i katodni strujni vrh voltametrijskog talasa pokazuju iste vrijednosti jačine struje ($I_{p,a} / I_{p,k} = 1$) [40].

3. REZULTATI I DISKUSIJA

3. 1. Morfološke karakteristike modifikovane ugljenične elektrode

Slika 1 prikazuje morfološke karakteristike površina modifikovane ugljenične paste zavisno o udjelu PU dobijene pomoću skenirajućeg elektronskog mikroskopa u LFD modu rada. Rezultati pokazuju da sa povećanjem udjela veziva, površina modifikovane ugljenične paste poprima homogeniji izgled sa slabije izraženom geometrijskom formom čestica grafita (slika 1). Homogeniji izgled površine nastaje uslijed većeg stepena popunjenoosti međuprostora između grafitnih struktura. Modifikovane paste izrađene sa TCP i PUTCP pokazuju slične morfološke karakteristike (slika D-1 prikazana u Dodatnom materijalu). Ispitivanja morfoloških karakteristika nemodifikovanog elektrodnog materijala sačinjenog od 0,17 g grafitnog praha i 35 mas.% PU pokazuju da površinsku strukturu karakteriše slojevita specifična forma karakteristična za kristalnu strukturu čestica grafita koje su međusobno izolovane. Dodane nanočestice TiO_2 popunjavaju slobodan prostor između čestica grafitnog praha [41].



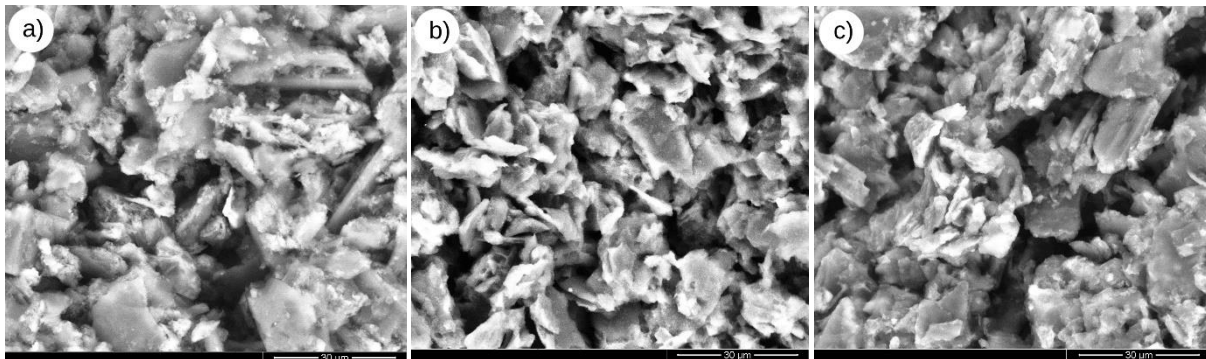
Slika 1. SEM mikrografije površine modifikovane ugljenične paste sa sadržajem 8 mas.% (m/m) nanočestica TiO_2 i a) 20 vol.% PU, b) 60 vol.% PU. Slike su snimljene u LFD modu

Figure 1. SEM images of the surfaces of modified carbon pastes with 8 wt.% TiO_2 nanoparticles and a) 20 vol.% paraffin oil (PO), b) 60 vol.% PO. The images were taken in LFD mode

U prethodnim istraživanjima uočeno je da površinu nemodifikovane ugljenične elektrode karakteriše manje izražena kristalna struktura dok je površina modifikovane ugljenične elektrode pokazala veći stepen uniformnosti. Ti rezultati su dobijeni za modifikovanu ugljeničnu elektrodu sastava 500 mg grafitnog praha, 80 mg PU i 20 mg nanočestica TiO_2 [42].

Slika 2 prikazuje morfološke karakteristike površina modifikovane ugljenične paste dobijene pomoću skenirajućeg elektronskog mikroskopa u BSED modu rada. Analiza SEM slika površine elektrodnog materijala upućuje na zaključak da povećanje udjela nanočestica TiO_2 u pastama, od 4 do 12 mas.%, ne uzrokuje značajnije promjene morfoloških karakteristika ispitivanih površina. S obzirom na veličinu korištenih nanočestica, za izradu elektrodnog materijala, kao i

preciznije definisanje veličine nastalih aglomerata potrebno je izvršiti dodatna istraživanja pomoću odgovarajućih tehnika (npr. transmisiona elektronska mikroskopija). SEM slike površine elektrodnog materijala sa 4, 8, 12 mas.% nanočestica TiO_2 i veziva PU, TCP i PUTCP, su prikazane u Dodatnom materijalu (slike D-2, D-3 i D-4).

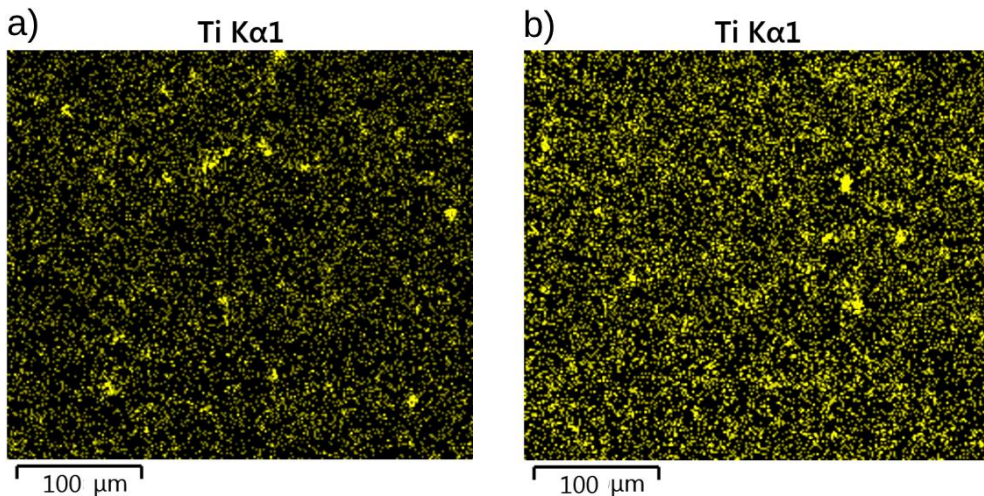


Slika 2. SEM mikrografije površine modifikovane ugljenične paste sa sadržajem 12 mas.% nanočestica TiO_2 i a) 40 vol.% PU, b) 40 vol.% TCP, c) 40 vol.% PUTCP (1:1). Slike su snimljene u BSED modu

Figure 2. SEM images of the surfaces of modified carbon pastes with 12 wt.% TiO_2 nanoparticles and a) 40 vol.% PO, b) 40 vol.% TCP, c) 40 vol.% POTCP (1: 1). The images were taken in BSED mode

U literaturi je uočena tendencija homogene adsorpcije nanočestica TiO_2 na ugljeničnim površinama, za razliku od nanočestica PdO koje su imale veći udio u pasti u odnosu na nanočestice TiO_2 i manji stepen homogenosti, a što je prouzrokovalo narušavanje nanostrukturne modifikacije elektrodne površine [43].

Energetska disperzivna analiza (EDS), vršena na četiri različita mesta na površini ispitivanih pasti, pokazuje neujednačenost udjela nanočestica TiO_2 , a koja je prouzrokovana načinom pripreme elektrodnog materijala (tabela D-2, D-3 i D-4 u Dodatnom materijalu). Ovi rezultati ukazuju da dobijeni elektrodnji materijali nisu homogeni odnosno da primjenjena tehnika disperzije nanočestica TiO_2 u matrici nije odgovarajuća. Mapiranjem prisutnih elemenata na površini elektrodnog materijala je uočeno da povećanjem udjela nanočestica TiO_2 dolazi do povećane ravnomjerne prostorne raspodjele nanočestica po površini ispitivanih pasta te prisustvo nekoliko aglomeracija nanočestica TiO_2 različitih veličina (slika 3).

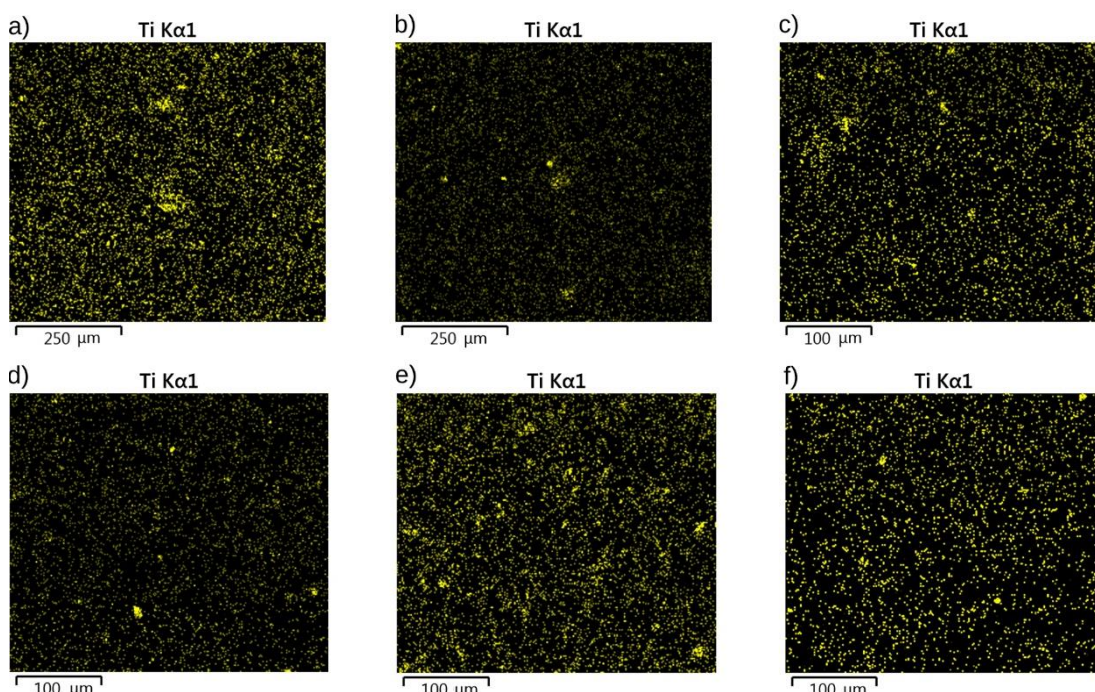


Slika 3. Prostorne mape raspodjele Ti na površini modifikovane ugljenične paste sa sadržajem 40 vol.% PU i a) 4 mas.% nanočestica TiO_2 , b) 12 mas.% nanočestica TiO_2

Figure 3. Spatial maps of Ti on the surfaces of modified carbon pastes containing 40 vol.% PO and a) 4 wt.% TiO_2 nanoparticles, b) 12 wt.% TiO_2 nanoparticles

Sa povećanjem udjela veziva dolazi do smanjenja uniformnosti nanočestica modifikatora (slika 4). Izražen stepen neuniformnosti prostorne distribucije je uočen ispitivanjem modifikovane ugljenične paste urađene sa PU (slika 4b).

Najveći uticaj na uniformnost nanočestica na ugljeničnoj pasti uočeno je kod veziva TCP (slika 4d), dok je najmanji uticaj veziva na uniformnost prostornog rasporeda nanočestica uočen kod veziva PUTCP (slika 4f). Može se prepostaviti da povećanje udjela veziva u elektrodnim pastama dovodi do povećanja stepena aglomeracije nanočestica TiO_2 odnosno do smanjenja uniformnosti prostornog rasporeda na površini elektrodnog materijala. Broj i veličina aglomerata zavise od intenziteta interakcija čestica TiO_2 i grafita sa vezivom te fizičko-hemijskih karakteristika vezivnog sredstva. Radoman i saradnici su pokazali da povećanjem udjela nanočestica TiO_2 dispergovanih u alkidnoj smoli dolazi do aglomeracije nanočestica TiO_2 uslijed povećanja specifične površine modifikatora, a samim tim i intenziteta reakcija između čestica [44].



Slika 4. Prostorne mape raspodjele Ti na površini modifikovane ugljenične paste sa: 8 mas. % nanočestica TiO_2 i a) 20 vol.% PU, b) 60 vol.% PU, c) 20 vol.% TCP, d) 60 vol.% TCP, e) 20 vol.% PUTCP (1:1), f) 60 vol. % PUTCP

Figure 4. Spatial maps of Ti distribution on the surfaces of modified carbon pastes containing 8 wt. % TiO_2 nanoparticles and a) 20 vol.% PO, b) 60 vol.% PO, c) 20 vol.% TCP, d) 60 vol.% TCP, e) 20 vol.% POTCP (1: 1), f) 60 vol. % POTCP

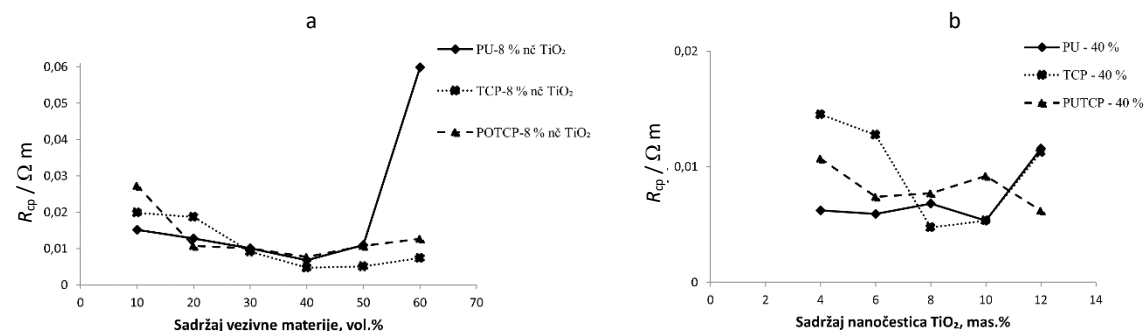
3. 2. Specifična otpornost modifikovane ugljenične elektrode

Analiziran je uticaj udjela veziva i nanočestica TiO_2 na specifičnu otpornost ispitivanih materijala. Ispitivani elektrodni materijali pokazuju tendenciju smanjenja specifične otpornosti sa povećanjem količine vezivne materije do 40 vol.%. Daljim povećanjem udjela vezivne materije do 50 vol.% zadržavaju se približno konstantne vrijednosti. Za vrijednosti udjela vezivne materije veće od 50 vol.% dolazi do povećanja specifične otpornosti, naročito izraženo za elektrodni materijal sa PU (slika 5a). Elektrodne paste sa TCP i PUTCP čiji je udio veći od 50 vol.% ne pokazuju značajno povećanje vrijednosti specifične otpornosti.

Na osnovu predloženog modela „bliskog pakovanja sfernih čestica“ povećanjem udjela veziva povećava se stepen popunjenoštvo međuprostora između aglomerata grafita i nanočestica TiO_2 . Manji udjeli veziva uzrokuju nedovoljan kontakt između čestica grafita i nanočestica TiO_2 što uzrokuje veći električni otpor. Elektrodne paste sa 40 vol.% vezivne materije pokazuju najmanji otpor što ukazuje na optimalan odnos udjela vezivnog sredstva koje se raspodjeljuje po površini čestica grafita i nanočestica TiO_2 . Dalje povećanje udjela veziva dovodi do povećanja otpornosti, a što je prouzrokovano dielektričnim karakteristikama korišćenih vezivnih materija. Slično ponašanje zavisnosti specifične otpornosti od udjela vezivne materije su pokazana ispitivanjem nemodifikovanih ugljeničnih pasti izvedenih od različitih ugljeničnih materijala i veziva (parafinsko, silikonsko ulje) [37].

Zavisnost specifične otpornosti elektrodnog materijala od udjela nanočestica TiO_2 (slika 5b) pokazuje slično ponašanje kao i zavisnost specifične otpornosti od udjela vezivne materije (slika 5a). Udio nanočestica TiO_2 do 6 mas.%

karakteriše nedovoljna kontaktna površina u odnosu na udio vezivne materije odnosno prisutno se vezivo nalazi u „višku“. Povećanje udjela nanočestica TiO_2 uzrokuje povećanje kontaktne površine, odnosno daje optimalni odnos vezivo/kontaktna površina, a koji odgovara udjelu 6-8% (m/m) nanočestica TiO_2 i 40 % (v/v) vezivnog sredstva. Dalje povećanje udjela nanočestica TiO_2 dovodi do povećanja kontaktne površine, odnosno nedovoljnog udjela vezivne materije što uzrokuje nedovoljan kontakt između čestica grafita i nanočestica TiO_2 .



Slika 5. Zavisnost specifične otpornosti (R_{Cp}) modifikovanog elektrodnog materijala od a) sadržaja vezivne materije sa 8 mas.% nanočestica (nč) TiO_2 , b) sadržaj nanočestica TiO_2 sa 40 vol.% vezivne materije

Figure 5. Specific resistance (R_{Cp}) of modified electrode materials as a function of a) amount of binder with 8 wt.% TiO_2 nanoparticles, b) amount of TiO_2 nanoparticles with 40 vol.% binder

Numeričke vrijednosti omskog otpora i specifične otpornosti ispitivanih elektrodnih pasti prikazane su u Dodatnom materijalu (Tabela D-5).

3.3. Elektrohemisika karakterizacija modifikovane ugljenične elektrode

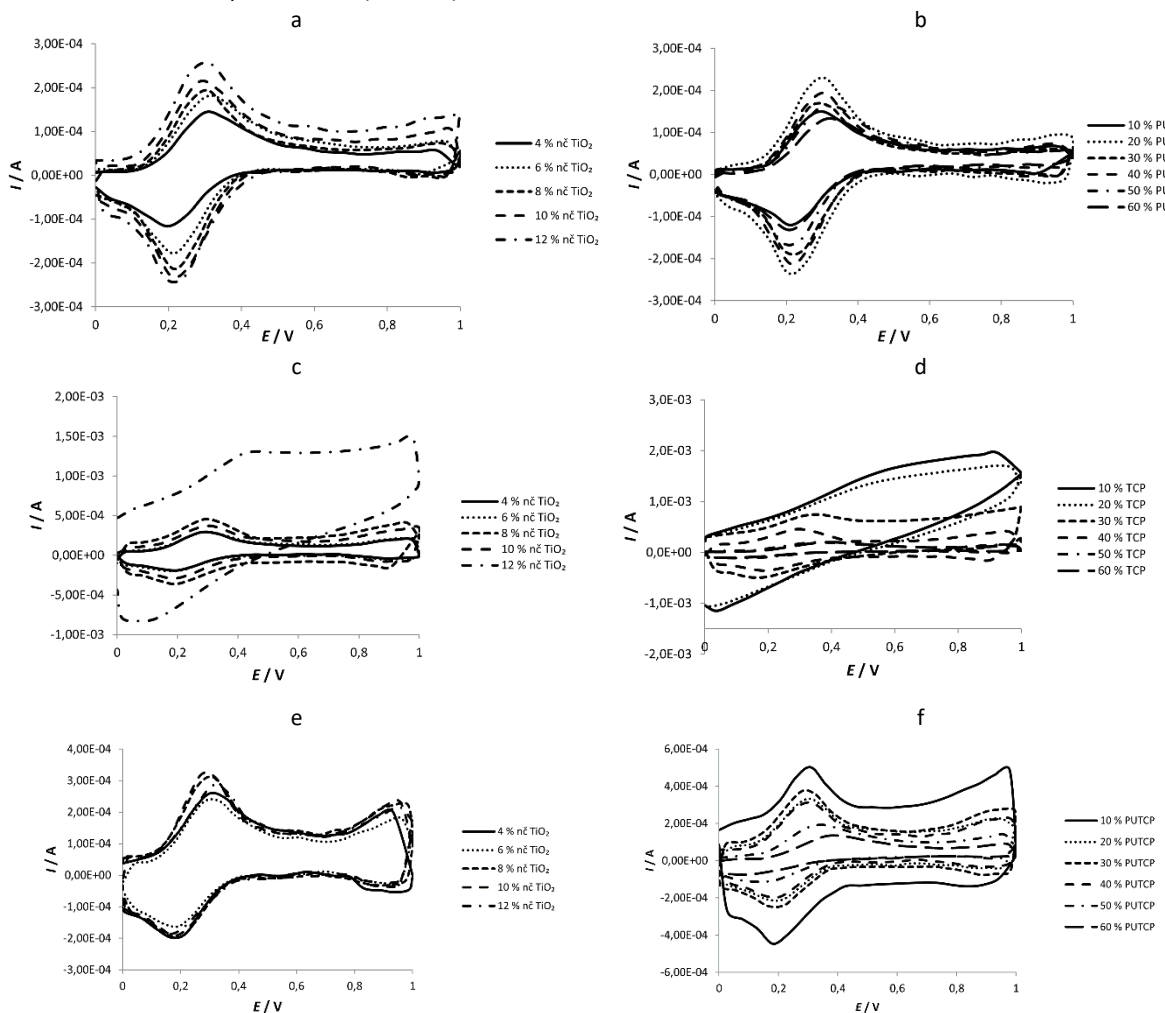
Slika 6 pokazuje ciklične voltamograme snimljene u 0,01 M rastvoru $K_4[Fe(CN)]_6 \times 3H_2O$ i 0,1 M KCl primjenom modifikovane ugljenične elektrode sastava 10–60 vol.% veziva i 4–12 mas.% nanočestica TiO_2 . Na osnovu prikazanih cikličnih voltamograma definisani su karakteristični elektrohemiski parametri (potencijal anodnog, $E_{p,a}$, i katodnog vrha strujnog talasa, $E_{p,k}$, visina strujnog talasa na potencijalu anodnog, $I_{p,a}$, i katodnog vrha strujnog talasa, $I_{p,k}$). Numeričke vrijednosti eksperimentalnih rezultata kao i izračunate vrijednosti (χ faktor, odnos $I_{p,a}/I_{p,k}$) prikazane su u Dodatnom materijalu (tabele D-6 i D-7).

Na cikličkim voltamogramima snimljenim pomoću modifikovanih ugljeničnih elektroda sa PU i PUTCP uočavaju se jasno definisani anodni i katodni strujni pikovi za razliku od voltamograma snimljenih pomoću modifikovanih ugljeničnih elektroda sa TCP na kojima se uočava izraženo prisustvo kapacitivne strujne komponente (slika 6c, 6d). Izraženo prisustvo kapacitivne struje u elektrodnom materijalu sa TCP značajno ograničava mogućnost definisanja karakterističnih elektrohemiskih parametara.

Vrijednosti χ faktora pokazuju povećanje stepena reverzibilnosti elektrohemiskog sistema sa povećanjem udjela PU do 40 vol.% nakon čega vrijednosti χ faktora za dalje povećanje udjela veziva upućuju na smanjenje stepena reverzibilnosti (slika 7a). Pasta sa PU pokazuje najveći stepen reverzibilnosti sa sadržajem nanočestica TiO_2 8–10 mas.% (slika 7b). Ovi rezultati su u saglasnosti sa rezultatima ispitivanja specifične otpornosti istog elektrodnog materijala.

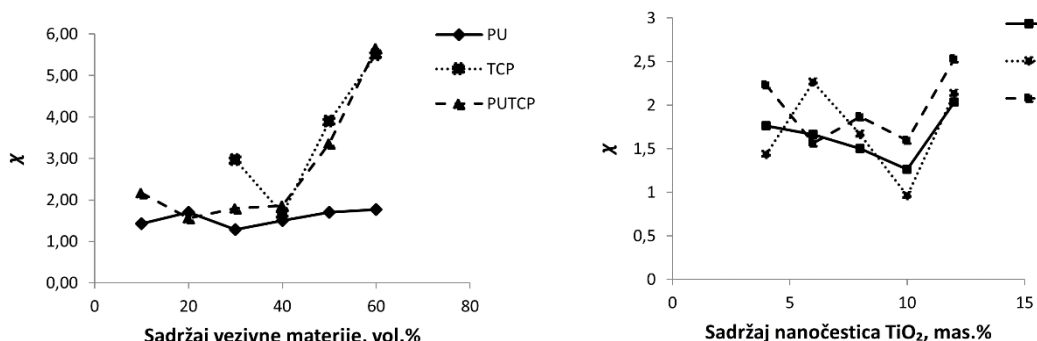
Modifikovane ugljenične paste sa trikrezol fosfatom (TCP) i smjesom parafinskog ulja i trikrezol fosfata (PUTCP) pokazuju porast stepena reverzibilnosti sa porastom udjela veziva do 40 vol.% i 10 mas.% nanočestica TiO_2 i modifikatora. Elektrode sa većim udjelom veziva (>40 vol.%) i modifikatora (>10 mas.% nanočestica TiO_2) karakteriše izraženo smanjenje stepena reverzibilnosti. Ovakvo ponašanje elektrodnog materijala sa TCP i PUTCP može se objasniti pomoću elektrohemiske aktivnosti TCP [9]. Drugi kriterijum reverzibilnosti elektrodnog procesa predstavlja vrijednost odnosa anodnog ($I_{p,a}$) i katodnog ($I_{p,k}$) strujnog vrha voltametrijskog talasa (za reverzibilni elektrodnji proces $I_{p,a}/I_{p,k} = 1$). Procjena reverzibilnosti modifikovanih elektroda, na osnovu odnosa anodnog i katodnog strujnog vrha pokazuje slične rezultate stepena reverzibilnosti procjenjene pomoću χ faktora (slika 8). Udjeli PU od 30 do 40 vol.% i 8 do 10 mas.% nanočestica TiO_2 (slika 8a) pokazuju najveći stepen reverzibilnosti pri čemu rezultati odnosa anodnog i katodnog

strujnog vrha voltamograma za elektrodne paste sa TCP i PUTCP pokazuju manje izraženiji stepen reverzibilnosti u odnosu na elektrodnu pastu sa PU (slika 8b).



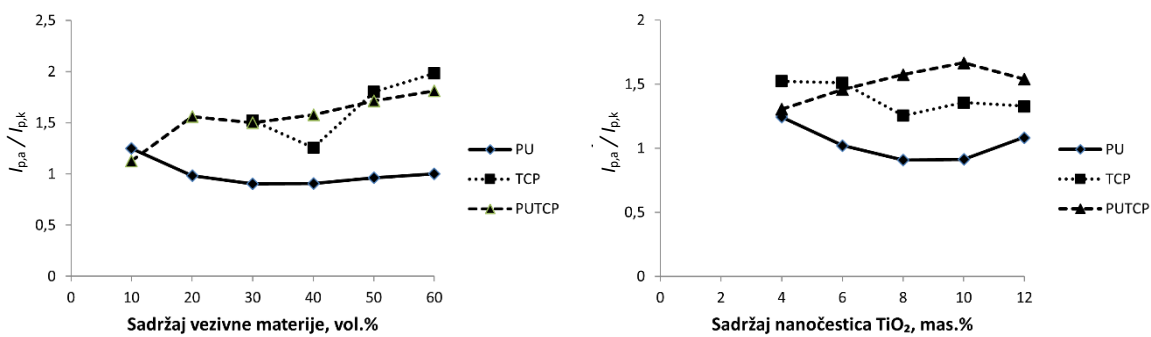
Slika 6. Ciklični voltamografi snimljeni radnom elektrodom sa sadržajem a) 40 vol.% PU, c) 40 vol.% TCP, e) 40 vol.% PUTCP i 4, 6, 8, 10, 12 mas.% nanočestica TiO_2 ; sa sadržajem 10, 20, 30, 40, 50, 60 vol.% b) PU, d) TCP, f) PUTCP i 8 mas.% nanočestica TiO_2 .

Figure 6. Cyclic voltammograms recorded with a working electrode with a) 40 vol.% PO, c) 40 vol.% TCP, e) 40 vol.% POTCP and 4, 6, 8, 10, 12 wt.% TiO_2 nanoparticles; with 10, 20, 30, 40, 50, 60 vol.% b) PO, e) TCP, f) POTCP and 8 wt.% TiO_2 nanoparticles



Slika 7. Zavisnost vrijednosti χ faktora od a) količine veziva sa 8 mas.% nanočestica TiO_2 , b) količine nanočestica TiO_2 sa 40 vol.% vezivne materije

Figure 7. Dependence of χ factor values on a) the amount of binder with 8 wt.% TiO_2 nanoparticles; b) the amount of TiO_2 nanoparticles with 40 vol.% binder



Slika 8. Zavisnost vrijednosti $I_{p,a}/I_{p,k}$ od a) količine veziva sa 8 mas. % nanočestica TiO_2 , b) količine nanočestica TiO_2 sa 40 vol.% vezivne materije

Figure 8. Dependence of the value $I_{p,a}/I_{p,k}$ on a) the amount of binder with 8 wt.% (w/w) TiO_2 nanoparticles b) the amount of TiO_2 nanoparticles with 40 vol.% binder

Rezultati ispitivanja uticaja udjela veziva i nanočestica TiO_2 na elektrohemiske karakteristike modifikovane ugljenične elektrode su u skladu sa objavljenim rezultatima prethodnih istraživanja drugih autora [34,35,45-48]. Određivanje optimalne količine modifikatora (nanočestice TiO_2) u elektrodnom materijalu izrađenom od grafitnog praha i silikonskog ulja (70:30 mas.%) vršeno je pomoću ciklične voltametrije. Posmatrane su vrijednosti katodnog strujnog pika u zavisnosti od količine modifikatora. Povećanje količine nanočestica TiO_2 do 6 mas.% pratilo je i povećanje katodnog strujnog pika. Za vrijednosti veće od 8 mas.% nanočestica TiO_2 vrijednost katodnog strujnog pika je stagnirala, a zatim i blago opadala [45]. Na osnovu istog kriterijuma slični rezultati (optimalna količina nanočestica TiO_2 6-8 mas.% su dobijeni ispitivanjem modifikovanih ugljikovih pasti sa sadržajem 60-65 mas.% grafitnog praha i 33-35 mas.% parafinskog ulja. Povećanje strujnog odgovora sa povećanjem sadržaja nanočestica TiO_2 u elektrodnom materijalu je bilo uzrokovano povećanjem broja mesta za adsorpciju na elektroaktivnoj površini modifikovane ugljenične elektrode [34,35,46]. Analiza elektrokatalitičkog odgovora ugljenične paste modifikovane nanočesticama TiO_2 -Fe je korišćena za određivanje optimalne količine modifikatora u elektrodnom materijalu. Maksimalni anodni strujni odgovor je uočen korišćenjem elektrode sa 10 mas.% nanočestica TiO_2 -Fe. Dalje povećanje sadržaja modifikatora je uzrokovalo značajno povećanje pozadinske struje koje je pripisano povećanju kapacitivnosti elektrohemiskog dvosloja na granici elektroda/elektrolit [47]. Slično ponašanje je uočeno karakterizacijom modifikovane ugljenične elektrode nanočesticama TiO_2 -Mo [48].

4. ZAKLJUČAK

U ovom radu priređene su modifikovane ugljenične elektrode različitog sastava veziva (PU, TCP, PUTCP) i modifikatora, TiO_2 nanočestica. Karakterizacijom modifikovanih ugljeničnih elektroda različitog sastava u pogledu morfoloških, fizičko-hemijskih i elektrohemiskih karakteristika ispitivanih elektrodnih materijala određen je optimalan sastav sa. Rezultati pokazuju da povećanje količine nanočestica TiO_2 od 4 mas.% do 12 mas.% ne utiče značajno na morfološke karakteristike ispitivanih elektrodnih pasti. S druge strane, povećanje količine veziva dovodi do većeg stepena popunjenoosti prostora između čestica grafita, a površina elektrodne paste poprima homogeniji izgled. Uočena je tendencija pogoršanja prostorne distribucije nanočestica TiO_2 sa povećanjem količine vezivne materije koja je naročito izražena kod elektrodnih pasti pripremljenih sa PU. Modifikovane ugljenične elektrode pripremljene sa 8 mas.% nanočestica TiO_2 i 40 vol.% PU imaju najmanje vrijednosti specifične otpornosti što bi se moglo objasniti modelom bliskog pakovanja sfernih čestica i promjene kontaktne površine između vezivne materije i čestica grafita odnosno nanočestica TiO_2 . Ciklični voltamogrami snimljeni primjenom modifikovane grafitne elektrode sa 10-20 vol.% TCP upućuju na izraženo prisustvo kapacitivne struje u odnosu na elektrode sa PU i PUTCP. Elektrohemiska karakterizacija modifikovanih ugljikovih elektroda pokazuje da modifikovane elektrode sa 40 vol.% PU i 8 mas.% TiO_2 pokazuju najveći stepen reverzibilnosti korišćenog elektrohemiskog sistema. Rezultati ovih istraživanja predstavljaju polaznu osnovu za razvoj jednostavnog i ekonomičnog elektrohemiskog senzora na bazi modifikovane ugljenične elektrode s mogućnošću

šire industrijske primjene. Zbog nehomogenosti dobijenih uzoraka, rezultati predstavljaju i smjernice za buduća istraživanja koja će uključiti primjenu na konkretnom primjeru radi potvrde navedenih tvrdnji.

LITERATURA

- [1] Švancara I, Walcarius A, Kalcher K, Vytrás K. Carbon paste electrodes in the new Millennium. *Cent Eur J Chem.* 2009; 7(4): 598-656 <https://doi.org/10.2478/s11532-009-0097-9>
- [2] Švancara I, Metelka R, Mikysek T, Vytrás K. 30 years with carbon paste electrodes at the University of Pardubice. *SciPap.* 2017; Series A 23: 5-50. <https://hdl.handle.net/10195/75317>
- [3] Guzsvány V, Papp Z, Švancara I, Vytrás K. Insecticides - Advances in Integrated pest management. In: *Insecticides – Advances in Integrated Pest Management*. Rijeka, Hrvatska, 2012, pp. 541-578 <https://doi.org/10.5772/2447>
- [4] Švancara I, Kalcher K, Walcarius A, Vytrás K. *Electroanalysis with Carbon Paste Electrodes*. Boca Raton, CRC Press, Taylor&FrancisGroup; 2012 <https://doi.org/10.1201/b11478>
- [5] Luo X, Morrin A, Killard AJ, Smyth MR. Application of Nanoparticles in Electrochemical Sensors and Biosensors. *Electroanalysis.* 2006; 18(4): 319-326 <https://doi.org/10.1002/elan.200503415>
- [6] Wongkaew N, Simsek M, Griesche Ch, Baeumner AJ. Functional Nanomaterials and Nanostructures Enhancing Electrochemical Biosensors and Lab-on-a-Chip Performances: Recent Progress, Applications, and Future Perspective. *Chem Rev.* 2019; 119(1): 120–194 <https://doi.org/10.1021/acs.chemrev.8b00172>
- [7] Brainina Kh, Stozhko N, Bukharinova M, Vikulova E. Nanomaterials: Electrochemical Properties and Application in Sensor *Phys Sci Rev.* 2018; 3(9): 201880050 <https://doi.org/10.1515/psr-2018-8050>
- [8] Katz E, Willner I, Wang J. Electroanalytical and Bioelectroanalytical Systems Based on Metal and Semiconductor Nanoparticles. *Electroanalysis.* 2004; 16(1-2): 19-44 <https://doi.org/10.1002/elan.200302930>
- [9] Welch CM, Compton RG. The use of nanoparticles in electroanalysis: a review. *Anal Bioanal Chem.* 2006; 384(3): 601–619 <https://doi.org/10.1007/s00216-005-0230-3>
- [10] Zima J, Švancara I, Barek J, Vytrás K. Recent advances in electroanalysis of organic and biological compounds at carbon paste electrodes. *Crit Rev Anal Chem.* 2009; 39: 204-227 <https://doi.org/10.1080/10408340903011853>
- [11] Kalcher K, Švancara I, Buzuk M, Vytrás K, Walcarius A. Electrochemical sensors and biosensors based on heterogeneous carbon materials. *MonatshChem.* 2009; 140: 861-889 <https://doi.org/10.1007/s00706-009-0131-9>
- [12] Švancara I, Konvalina J, Schachl K, Kalcher K, Vytrás K. Stripping voltammetric determination of iodide with synergistic accumulation at a carbon paste electrode. *Electroanalysis.* 1998; 10: 435-441 [https://doi.org/10.1002/\(SICI\)1521-4109\(199805\)10:6%3C435::AID-ELAN435%3E3.0.CO;2-J](https://doi.org/10.1002/(SICI)1521-4109(199805)10:6%3C435::AID-ELAN435%3E3.0.CO;2-J)
- [13] Bai J, Zhou B. Titanium Dioxide Nanomaterials for Sensor Applications. *Chem Rev.* 2014; 114(19): 10131-10176 <https://doi.org/10.1021/cr400625j>
- [14] Xiaobo Chen, Samuel S Mao. Titanium Dioxide Nanomaterials: Synthesis, Properties, Modifications, and Applications. *Chem Rev.* 2007; 107: 2891-2959 <https://doi.org/10.1021/cr0500535>
- [15] Ziental D, Czarczynska-Goslinska B, Mlynarczyk DT, Glowacka-Sobotta A, Stanisz B, Goslinski T, Sobotta L. Titanium Dioxide Nanoparticles: Prospects and Applications in Medicine. *Nanomaterials.* 2020; 10(2): 387 <https://doi.org/10.3390/nano10020387>
- [16] Mo SD, Ching WY. Electrical and optical properties of three phases of titanium dioxide: Rutile, anatase and brookite. *Phys Rev B.* 1995; 51(19): 13023-13032 <https://doi.org/10.1103/PhysRevB.51.13023>
- [17] Ansari SA, Khan MM, Ansari MO, Cho MH. Nitrogen-doped titanium dioxide (N-doped TiO₂) for visible light photocatalysis. *New J Chem.* 2016; 40(4): 3000-3009 <https://doi.org/10.1039/C5NJ03478G>
- [18] Babaei A, Moradi M , Sohrabi M, Feshki S, Marandi M. Fabrication of TiO₂ Hollow Spheres and its Application in Modification of Carbon Paste Electrode For Simultaneous Determination of Dopamine and Piroxicam in the Presence of Ascorbic acid. *J Nanostruct.* 2018; 8(1):119-130. <https://dx.doi.org/10.22052/JNS.2018.02.002>
- [19] Ha TJ, Hong MH, Park CS, Park HH. Gas sensing properties of ordered mesoporous TiO₂ film enhanced by thermal shock induced cracking. *Sens Actuator B Chem.* 2013; 181: 874-879 <https://doi.org/10.1016/j.snb.2013.02.093>
- [20] Fadillah G, Ariani F. A novel electrochemical synthesis of TiO₂ nanoparticles and its application as bisphenol-B sensor. AIP Conference Proceedings 2021; 2370, 050001 <https://doi.org/10.1063/5.0062211>
- [21] Zarei E, Jamali MR, Bagheri J. Application of TiO₂ Nanoparticles Modified Carbon Paste Electrode for the Determination of Vitamin B2. *J Anal Chem.* 2019; 74: 1213–1222 <https://doi.org/10.1134/S1061934819120049>
- [22] Narouei FH, Kirk KA, Andreescu S. Electrochemical Quantification of Lead Adsorption on TiO₂ Nanoparticles. *Electroanalysis.* 2020; 33(1): 188-196 <https://doi.org/10.1002/elan.202060152>
- [23] Sarma M, Valle M. Improved Sensing of Capsaicin with TiO₂ Nanoparticle Modified Epoxy Graphite Electrode. *Electroanalysis.* 2020; 32(2): 230-237 <https://doi.org/10.1002/elan.201900400>
- [24] OliveiraLuciana S, Alba Juan FG, SilvaValdinete L, RibeiroRogério T, FalcãoEduardo HL, Navarro M. The effect of surface functional groups on the performance of Graphite powders used as electrodes. *J Electroanalytical Chem.* 2018; 818: 106-113 <https://doi.org/10.1016/j.jelechem.2018.04.022>



- [25] Mikysek T, Stočes M, Švancara I, Ludvík J. Relation between the composition and properties of carbon nanotubes paste electrodes (CNTPEs). In: Vytřas K, Kalcher K, Švancara I. Sensing in Electroanalysis, Pardubice, Czech: University of Pardubice; 2010: 69-75 <http://hdl.handle.net/10195/38243>
- [26] Mikysek T, Stočes M, Švancara I, Ludvík J. The ohmic resistance effect for characterisation of carbon nanotube paste electrodes (CNTPEs). *RSC Adv.* 2012; 2: 3684-3690 <https://doi.org/10.1039/C2RA20202F>
- [27] Rabie Malha SI, Lahcen AA, Arduini F, Ourari A, Amine A. Electrochemical Characterization of Carbon Solid_like Paste Electrode Assembled Using Different Carbon Nanoparticles. *Electroanalysis*. 2015; 27: 1-9 <https://doi.org/10.1002/elan.201500637>
- [28] Ashrafi AM, Richtera L. Preparation and Characterization of Carbon Paste Electrode Bulk-Modified with Multiwalled Carbon Nanotubes and Its Application in a Sensitive Assay of Antihyperlipidemic Simvastatin in Biological Samples. *Molecules*. 2019; 24: 2215 <https://doi.org/10.3390/molecules24122215>
- [29] Čović JS, Zarubica AR, Bojić AL, Troter TM, Randelović MS. Electrochemical study of novel composite electrodes based on glassy carbon bulk-modified with Pt and MoO₂ nanoparticles supported onto multi-walled carbon nanotubes. *J Serb Chem Soc.* 2020; 85(9): 1185-1196 <https://doi.org/10.2298/JSC20021043C>
- [30] Andi Wang D, Chung DL. Dielectric and electrical conduction behavior of carbon paste electrochemical electrodes, with decoupling of carbon, electrolyte and interface contributions. *Carbons*. 2014; 72: 135-151 <https://doi.org/10.1016/j.carbon.2014.01.066>
- [31] Khodari M, Mersal GAM, Rabie EM, Assaf HF. Electrochemical Sensor based on Carbon Paste Electrode Modified by TiO₂ nano-particles for the Voltammetric Determination of Resorcinol. *Int J Electrochem Sci.* 2018; 13: 3460-3474 <http://dx.doi.org/10.20964/2018.04.04>
- [32] Lobón GS, Yepez A, Garcia LF, Morais RL, Vaz BG, Carvalho VV, Rodrigues de Oliveira GA, Luque R, Gil E. Efficient electrochemical remediation of microcystin-LR in tap water using designer TiO₂@carbon electrodes. *Sci Rep.* 2017; 7: 41326 <https://dx.doi.org/10.1038%2Fsrep41326>
- [33] Khursheed A, Akbar M, Richa R, Shaikh MM. Construction of TiO₂ nanosheets modified glassy carbon electrode (GCE/TiO₂) for the detection of hydrazine. *Mater Res Express*. 2016; 3: 074005 <http://dx.doi.org/10.1088/2053-1591/3/7/074005>
- [34] Mashhadizadeh MH, Rasouli F. Design of a New Carbon Paste Electrode Modified with TiO₂ Nanoparticles to Use in an Electrochemical Study of Codeine and Simultaneous Determination of Codeine and Acetaminophen in Human Plasma Serum Samples. *Electroanalysis*. 2014; 26: 2033–2042 <https://doi.org/10.1002/elan.201400141>
- [35] Mashhadizadeh MH, Afshar E. Electrochemical investigation of clozapine at TiO₂ nanoparticles modified carbon paste electrode and simultaneous adsorptive voltammetric determination of two antipsychotic drugs. *Electrochimica Acta*. 2013; 87: 816-823 <https://doi.org/10.1016/j.electacta.2012.09.004>
- [36] Švancara I, Schachl. Testing of unmodified carbon paste electrodes. *Chem Listy*. 1999; 93: 490-499 http://www.chemicke-listy.cz/docs/full/1999_08_490-499.pdf
- [37] Mikysek T, Švancara I, Kalcher K, Bartoš M, Vytras K, Ludvík J. New approaches to the characterization of carbon paste electrodes using the ohmic resistance effect and qualitative carbon paste indexes. *Anal Chem.* 2009; 81(15): 6327-6333 <http://dx.doi.org/10.1021/ac9004937>
- [38] Jiang X, Manawan M, Feng T, Qian R, Zhao T, Zhou G, Kong F, Wang Q, Dai S, Pan JH. Anatase and rutile in evonik aerioxide P25: Heterojunctioned or individual nanoparticles. *Catalysis Today*. 2017; 300: 12-17 <http://dx.doi.org/10.1016/j.cattod.2017.06.010>
- [39] d Kiran Kumar RS, Mamatha GP, Muralidhara HB, Kumar KY, Prashanth MK, Electrochemical Studies of Dopamine Using Titanium Dioxide Nanoparticle Modified Carbon Paste Electrode, *Anal Bioanal Electrochem*. 2015; 7(2): 175-185 [http://abechem.ir/No.%202-2015/2015,7\(2\)175-185.pdf](http://abechem.ir/No.%202-2015/2015,7(2)175-185.pdf)
- [40] Piljac I. *Senzori fizikalnih veličina i elektroanalitičke metode*. Zagreb, Hrvatska: Mediaprint-Tiskara Hrastić d.o.o.; 2010 ISBN 978-953-95404-1-6
- [41] Hassaninejad-Darzi SK, Shajie F. A Sensitive Voltammetric Determination of Anti-Parkinson Drug Pramipexole Using Titanium Dioxide Nanoparticles Modified Carbon Paste Electrode. *J Braz Chem Soc.* 2016; 28(4): 529-539 <http://dx.doi.org/10.5935/0103-5053.20160192>
- [42] Tashkhourian J, Nami Ana SF, Hashemnia S, Hormozi-Nezhad MR. Construction of modified carbon paste electrode based on TiO₂ nanoparticles for the determination of gallic acid. *J Solid State Electrochem.* 2013; 17: 157–165 <https://doi.org/10.1007/s10008-012-1860-y>
- [43] Garcia LF, Cunha CEPd, Moreno EKG, Thomaz DV, Sanz Lobón G, Luque R, Somerset V, De Souza Gil E. Nanostructured TiO₂ Carbon Paste Based Sensor for Determination of Methyldopa. *Pharmaceuticals*. 2018; 11(4):99. <http://dx.doi.org/10.3390/ph11040099>
- [44] Radoman T, Džunuzović J, Jeremić K, Marinković A, Spasojević P, Popović I, Džunuzović E. Uticaj veličine nanočestica TIO₂ i njihove površinske modifikacije na reološka svojstva alkidne smole. *Hem Ind.* 2013; 67(6): 923-932 <https://doi.org/10.2298/HEMIND131106081R>
- [45] Manjunatha KG, Kumara Swamy BE, Madhuchandra HD, Vishnumurthy KA. Synthesis, characterization and electrochemical studies of titanium oxide nanoparticle modified carbon paste electrode for the determination of paracetamol in presence of adrenaline. *Chem Data Collec.* 2021; 31: 100604 <https://doi.org/10.1016/j.cdc.2020.100604>



- [46] Tashkhourian J, Nami Ana SF, Hashemnia S, Hormozi-Nezhad MR. Construction of modified carbon paste electrode based on TiO₂ nanoparticles for the determination of gallic acid. *J Solid State Electrochem.* 2013; 17: 157–165
<https://doi.org/10.1007/s10008-012-1860-y>
- [47] Akhond M, Absalan G, Tafakori A, Ershadifar H. Simultaneous Determination of Thiocyanate and Oxalate in Urine using a Carbon Ionic Liquid Electrode Modified with TiO₂-Fe Nanoparticles. *Anal Bioanal Chem.* 2016; 3(1): 73-86
<https://dx.doi.org/10.22036/abcr.2016.14554>
- [48] Ardakani MM, Beitollahi H, Taleat Z, Niasari MS. Fabrication and characterization of molybdenum(VI) complex-TiO₂ nanoparticles modified electrode for the electrocatalytic determination of L-cysteine. *J Serb Chem Soc.* 2011; 76(4): 575–589
<http://dx.doi.org/10.2298/JSC100504042M>
- [49] Merck KGaA, Darmstadt, Germany https://www.merckmillipore.com/INTL/en/product/Graphite,MDA_CHEM-104206 pristupljeno 11. 05. 2021.
- [50] Merck KGaA, Darmstadt, Germany https://www.merckmillipore.com/INTL/en/product/Paraffin,MDA_CHEM-107160 pristupljeno 11. 05. 2021.
- [51] Merck KGaA, Darmstadt, Germany https://www.merckmillipore.com/INTL/en/product/Tritolyl-phosphate,MDA_CHEM-814811 Pristupljeno 11. 05. 2021.
- [52] Xiongzhen Jiang, Maykel Manawan, Ting Feng, Ruiheng Qian, Ting Zhao, Guanda Zhou, Fantai Kong, Qing Wang, Songyuan Dai, Jia HongPan. Anatase and rutile in evonik aerioxide P25:Heterojunctioned or individual nanoparticles. *Catalysis Today.* 2017; 300: 12-17 <http://dx.doi.org/10.1016/j.cattod.2017.06.010>

SUMMARY

Development and characterization of electrochemical sensors based on carbon modified with TiO₂ nanoparticles

Saša Mićin¹, Borislav N. Malinović² and Tijana Đuričić²

¹Faculty of Security Sciences, University of Banja Luka, Banja Luka, Bosnia and Herzegovina

²Faculty of Technology, University of Banja Luka, Banja Luka, Bosnia and Herzegovina

(Original scientific paper)

The aim of this study is the development and characterization of a carbon-based electrochemical sensor, modified with TiO₂ nanoparticles for potential application in electroanalytical techniques. The influence of binder and modifier contents on morphological, physicochemical and electrochemical characteristics of the electrode material was investigated in order to determine the optimal ratio of the carbon material/binder/modifier. Carbon pastes were prepared from mixtures containing graphite powder, TiO₂ nanoparticles and liquid hydrocarbons. Scanning electron microscopy showed that the electrode material becomes more compact with the addition and the increase in the binder material content, while increasing the proportion of TiO₂ nanoparticles did not have any significant effect on the material morphology showing fairly homogeneous nanoparticle distribution in the graphite electrode material. The test results indicate that the modified carbon paste with 40 vol.% paraffin oil (PO) and 6-8 wt.% TiO₂ nanoparticles is characterized by the lowest value of specific resistance. By applying cyclic voltammetry, the most pronounced degree of reversibility was obtained in relation to the standard reversible redox system ([Fe(CN)]₃-/4-) for the electrode material with 30–40 vol.% PO and 8-10 wt.% TiO₂ nanoparticles. Characterization of the electrode material based on carbon modified with TiO₂ nanoparticles indicated that the optimal composition contains 40 vol.% PO and 6-8 wt.% TiO₂ nanoparticles, which is important for application in electroanalytical techniques.

Keywords: electroanalytical techniques, modified carbon electrodes, paraffin oil; tricresol phosphate; electrode material

Copper strip corrosion testing in hydrocracked base oil in the presence of different inhibitors

Borislav N. Malinović, Aleksandra Borković and Tijana Đuričić

University of Banja Luka, Faculty of Technology, Stepe Stepanovica 73, 78000 Banja Luka, Bosnia and Herzegovina

Abstract

In this paper, the corrosion test of copper in hydrocracked base oil HC-6 was performed in the presence of an additive for extremely high pressures (EP additive) in different concentrations. EP additives are used to reduce wear in industrial applications, under high load conditions. Since most of these additives are sulfur-based, whose compounds can be corrosive at high temperatures, their use leads to corrosion of some materials. To prevent corrosion in the base oil with the EP additive, three commercial corrosion inhibitors are added. By chemical composition, the inhibitor RC 8210 is a derivative of dimercaptothiadiazole, RC 4220 is a synthetic neutral calcium sulfonate, and IRGAMET 39 is a derivative of tolutriazole. Efficiency of the inhibitors was monitored by standard test methods for corrosiveness to copper arising from petroleum products by the copper strip test (ASTM D-130) and the gravimetric method, while oxidation stability of the base oil was monitored by peroxide number determination. Oxidation was performed at 100 ± 1 °C for 3 and 24 h. Results of these studies have shown that IRGAMET 39 is the most effective inhibitor in the presence of the EP additive at both examined oxidation times.

Keywords: ASTM D-130; copper coupons; lubricating oil; extreme pressure additive.

Available on-line at the Journal web address: <http://www.ache.org.rs/HI/>

TECHNICAL PAPER

UDC: 620.19:665.7.038.5

Hem. Ind. 76(3) 159-166 (2022)

1. INTRODUCTION

Corrosiveness of petroleum products indicates the product ability to cause metal corrosion. The main cause of corrosivity of lubricating oils is sulfur and its compounds, such as organosulfur molecules, thiophenes, disulfides, polysulfides, dialkyl sulfides (thioethers), and mercaptans (thiols). The origin of sulfur in lubricating oils can be from the base oil obtained by a basic oil production technology and refining process, or from various additives. Each compound exhibits its own unique reaction rate with copper, which ultimately forms copper sulfide species, as solid corrosion products or complexes, depending on the concentration of the compounds, copper surface condition, temperature, and aging time [1].

The use of extreme pressure (EP) additives leads to the formation of protective layers upon high loading in the friction process. These additives consist of chlorine, sulfur, and phosphorous compounds, which react tribochimically with the metal surface during the mechanical interaction and develop a well adhered and easy-to-shear protective layer [2]. Sulfur in EP additives reacts with the metal forming a tribofilm that improves the friction and wear behavior [3], but also causes corrosion of metals with which it comes into contact.

As copper is susceptible to corrosion, it is often used as an indicator of corrosiveness of petroleum products. There are a number of different standards to measure copper corrosion. The copper strip corrosion test is one of the most frequently used methods designed to assess the relative degree of corrosiveness of petroleum products [4,5].

Many studies on the issue of corrosion in lubricating oils are available in the literature, such as studies on transformer oils [6-11], as well as on the most commonly used inhibitors for these and other types of lubricating oils [12-14].

Corresponding authors: Tijana Đuričić, University of Banja Luka, Faculty of Technology, Stepe Stepanovica 73, 78000 Banja Luka, Bosnia and Herzegovina

E-mail: tijana.djuricic@tf.unibl.org

Paper received: 13 January 2022; Paper accepted: 4 June 2022; Paper published: 14 July 2022.

<https://doi.org/10.2298/HEMIND220113012M>



For efficient prevention of copper corrosion, metal passivators and deactivators can be used, which can be sulfur- and nitrogen-based. The most commonly applied are benzotriazole, toluylbenzotriazole, and aminomethyl-substituted toluylbenzotriazole (better known as Irgamet 39). In a study on the effect of Irgamet 39 on the copper strip oxidation after 4 h at 150 °C formation of a complex of impermeable film on the metal surface was found, which protected copper from corrosion and improved oxidative stability [9]. Also, effects of Irgamet 30 and Irgamet 39 on the oxidative stability of oil and copper corrosion were compared showing that Irgamet 30 inhibits oil oxidation but does not passivate the copper surface like Irgamet 39 [10].

In another study, corrosive sulfur in the form of dibenzyl disulfide (DBDS), dodecanethiol (DDM) or a combination of both and different concentrations of passivators Irgamet 39, 1-methylbenzotriazole (marked as T571) and *n,n*-Bis(2-ethylhexyl)-4-methyl-1h-benzotriazole-1-methanamine (marked as TTA) were added to the non-corrosive transformer oil [11]. All examined passivators have shown a protective effect against DBDS. Irgamet 39 at a concentration of 200 mg kg⁻¹ was shown to be the best choice for protection against DDM, while T571 proved to be the best passivator of copper in the presence of a combination of DBDS and DDM [11].

Ling and coworkers investigated the interaction mechanism of 2,5-dimercapto1,3,4-thiadiazole (DMTD) with copper and concluded that a reaction occurs at room temperature, building a Cu-DMTD complex. The adsorption nature of DMTD on copper surface is chemical. Sulfur atoms from DMTD molecules react with copper surface and polymerize into a polymer chain that covers the copper surface [12].

In addition to corrosion inhibitors, additives that improve the performance of EP additives, as well as provide antioxidant and dispersive and detergent properties, can be added to base oils. Synthetic calcium sulfonates have been shown to be the most effective for these purposes. In addition to cleaning, detergents also neutralize acidic combustion and oxidation products, thereby, minimizing corrosion, rust, and deposit formation in the engine [13,14].

The aim of this paper was to evaluate the influence of a sulfur-based EP additive on the corrosivity and oxidative stability of hydrocracked base oil HC-6. Since the tested additive causes corrosion of nonferrous metals, the protection efficiency of various inhibitors on the corrosion of copper was also examined.

2. EXPERIMENTAL

In the experimental part the corrosivity of copper strip in hydrocracked base oil HC-6 (Modriča Oil Refinery, Bosnia and Herzegovina) was tested in the presence of the EP additive and with the addition of three different (commercial) corrosion inhibitors. HC-6 base oil was obtained by the hydrocracking process at the Modriča Oil Refinery (Bosnia and Herzegovina). According to properties presented in Table 1, this oil has a high viscosity index, excellent oxidative stability, low sulfur and aromatic hydrocarbon contents and very low volatility.

Table 1. Characteristics of HC-6 [15]

Characteristic	Test method	Value
Viscosity at 40 °C, mm ² s ⁻¹	BAS ISO 3104	34.25
Viscosity at 100 °C mm ² s ⁻¹	BAS ISO 3104	5.96
Viscosity index	BAS ISO 2909	119
Flow point, °C	BAS ISO 3016	-8
Color (ASTM)	BAS ISO 2049	1.0
Flash point, °C	ISO 2592	260
Density at 15 °C, kg m ⁻³	ASTM D 5002	854.9
Sulfur content, ppm	BAS ISO 20846	30.0
Volatility (NOACK test), wt.%	DIN 51581	6.75

Used EP additive 7038 N (Additiv-Chemie Luers GmbH, Germany) contains sulfur based on vegetable ester and olefines [16], and three commercial inhibitors were used as corrosion inhibitors: IRGAMET 39, RC 4220 and RC 8210, whose chemical compositions and technical characteristics are given in the accompanying MSDS [17-19]. By chemical composition the inhibitor IRGAMET 39 (BASF Corporation GmbH, Germany) is based on the derivative tolutriazole,

RC 4220 (Rhein Chemie Rheinau GmbH, Germany) is synthetic neutral calcium sulfonate, and the inhibitor RC 8210 (Rhein Chemie Rheinau GmbH, Germany) is a dimercaptothiadiazole derivative. All these inhibitors are soluble in mineral and synthetic base oils, and compatibility with other additives needs to be determined experimentally.

Copper strip corrosion test was performed in accordance with the standard method ASTM D130 [20]. This standard contains a color chart for the copper strip corrosion test (Fig. 1). Oxidation of copper coupons (99.95 % Cu, Hemija Patenting d.o.o Lukavac, Bosnia and Herzegovina) in base oils, base oils with the EP additive and base oils with the EP additive and different concentrations of corrosion inhibitors was performed at 100 ± 1 °C for 3 and 24 h. After oxidation, copper strip tests are degreased and dried and their color is compared with the standard color chart.

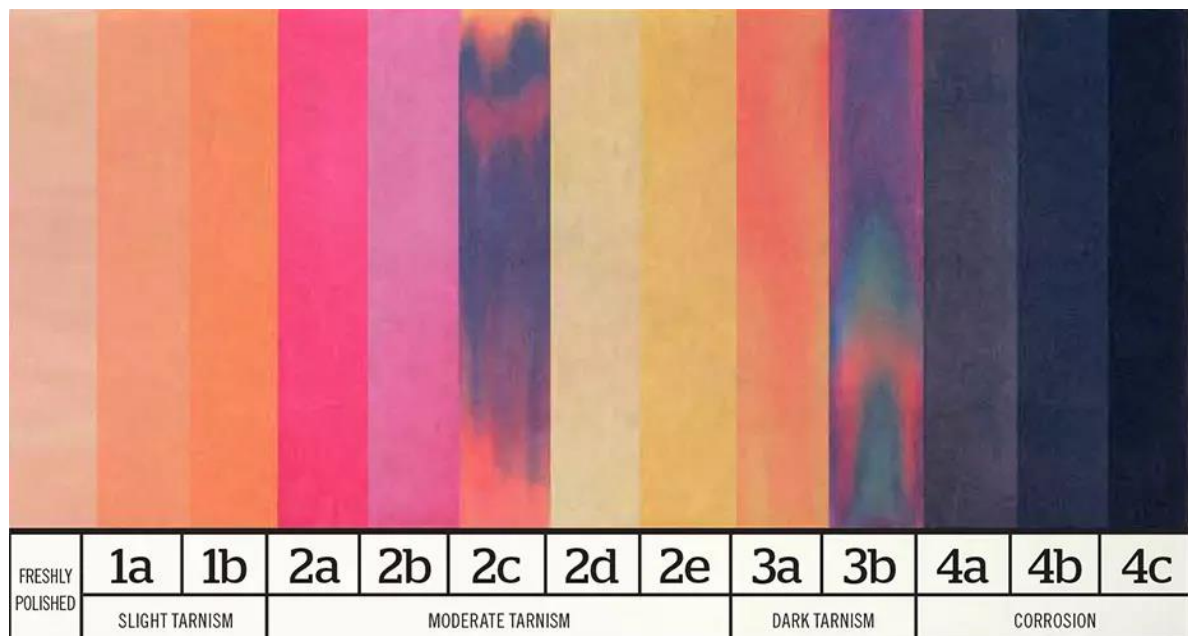


Figure 1. Color chart according ASTM D 130 copper strip corrosion standards

After 24 h of oxidation, change in the mass of copper coupons - weight growth, $\Delta m / g$ was determined as well as the positive mass corrosion index, $K_m^+ / g \text{ m}^{-2} \text{ h}^{-1}$. Based on the value of K_m^+ the negative mass corrosion index, $K_m^- / g \text{ m}^{-2} \text{ h}^{-1}$ was determined and the corrosion rate, $\pi / \text{mm year}^{-1}$ was thus determined by the gravimetric method and calculated by the following equations:

$$K_m^+ = \frac{\Delta m}{st} \quad (1)$$

$$K_m^- = K_m^+ \frac{nA_{\text{Me}}}{A_0} \quad (2)$$

$$\pi = K_m^- \frac{8.76}{d_{\text{Me}}} \quad (3)$$

where s is the copper coupon surface (m^2), t is the oxidation time (h), n is the valence of the metal, A_{Me} is the atomic mass of the metal (g mol^{-1}), A_0 is the atomic mass of the oxide (g mol^{-1}) and d_{Me} is the metal density (g cm^{-3}) [21].

Oxidation impact on the quality of base oil was monitored by peroxide number in accordance with the standard ASTM D 3703-99 [22]. During the process of oil oxidation, free radicals are formed first, followed by formation of peroxides and hydroperoxides, aldehydes, ketones, acids, esters, and finally resins and asphaltenes. The standard method is based on iodide oxidation to iodine by peroxide in an acidic medium, followed by the reaction with sodium thiosulfate until the blue color of starch indicator disappears and a colorless solution is obtained. The purpose of the oxidative stability determination is to assess the service life and behavior of the lubricating oil during exploitation [23].

3. RESULTS AND DISCUSSION

The first part of the research consisted of testing copper corrosivity in the base oil HC-6 alone and in the oil with addition of the EP additive at different concentrations, during 3 h at the temperature of 100 ± 1 °C. Due to the limited solubility of sulfur contained in EP additives in mineral oils [24], the tested range of the additive concentrations was 0.25 – 1 wt.%

At all tested EP additive concentrations, the color of the copper strip changed (different grades of tarnish) and copper corrosion started at the concentration of 0.25 wt.% (Table 2).

Table 2. Copper corrosion at different concentrations of EP additive (3 h at 100 ± 1 °C)

Concentration of the EP additive in base oil HC-6, wt.%	Copper strip corrosion according to the ASTM D 130
0.00	1a
0.25	3a
0.50	3b
0.75	4a
1.00	4a

In the further test, corrosion inhibitors were added at various concentrations, in the range of 25 - 200 ppm. The results are presented in Table 3, which indicates that IRGAMET and RC 8210 inhibitors were effective already at 25 ppm (1b). By applying the RC 4220 inhibitor at concentrations of 25 and 50 ppm, the corrosion degree is same as without the inhibitor, while at concentrations higher than 75 ppm the corrosion degree is even increased. This inhibitor is based on calcium sulfonate, so there is a possibility that by the increase in inhibitor concentration as more sulfur is introduced, the corrosion process is promoted with the formation of copper sulfide.

Table 3. Copper strip test in HC-6 oil with 0.25 % EP additive and various concentrations of corrosion inhibitors (3 h at 100 ± 1 °C)

Inhibitor concentration, ppm	Copper strip corrosion in according to ASTM D 130		
	IRGAMET 39	RC 4220	RC 8210
0	3a	3a	3a
25	1b	3a	1b
50	1b	3a	1b
75	1b	3b	1b
100	1b	3b	1b
200	1b	3b	1b

In this series of experiments the mass change of copper coupons was negligible, due to the short oxidation time. Since lubricating oils need to ensure good lubrication under extreme conditions and for several hours of operation, examined oxidation time has been extended and the results are presented in Table 4.

Table 4. Copper strip test in HC-6 oil with 0.25 % EP additive and various concentrations of corrosion inhibitors (24 h oxidation at 100 ± 1 °C)

Inhibitor concentration, ppm	Copper strip corrosion in according to ASTM D 130		
	IRGAMET 39	RC 4220	RC 8210
0	3b	3b	3b
25	1b	4a	2c
50	1b	4a	2b
75	1b	4a	2e
100	1b	4b	2a
200	1b	4b	1b

Due to the longer oxidation time, the change in mass was measurable, so the corrosion rate was calculated by the gravimetric method (Fig. 2).



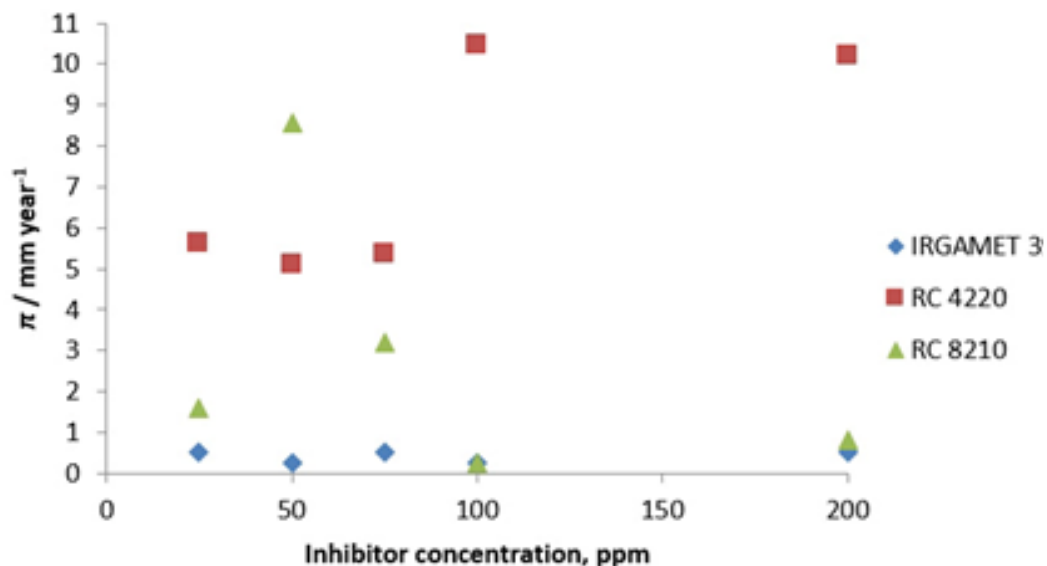


Figure 2. Copper corrosion rate in HC-6 oil with 0.25 % EP additive and various concentrations of corrosion inhibitors (24 h oxidation at $100 \pm 1^\circ\text{C}$)

In the case of IRGAMET 39, which is derivative of tolutriazole, the mass of coupons remained almost the same before and after 24 h of oxidation. This result indicates the protective effect of the inhibitor and prevention of corrosive sulfur action from the EP additive on the copper coupon. It can be concluded that even at prolonged oxidation this inhibitor is effective even at the lowest tested concentration of 25 ppm. Benzotriazoles and their derivatives have been shown to be effective inhibitors of copper corrosion and act as passivators. Passivators react by blocking the sites for corrosive sulfur compounds and are used as a remediation technique to protect copper against the corrosive sulfur attack and formation of copper sulfide [7,9,10].

By adding the RC 4220 inhibitor the coupon weight increased and thus the corrosion rate increased with increasing the inhibitor concentration. The ASTM D 130 method indicated that the increase in concentration of this inhibitor increases "tarnish" of the coupon, so that this inhibitor is not effective in the tested concentration range.

In the case of RC 8210 inhibitor (dimercaptothiadiazole derivative), the coupon weight increased with increasing the inhibitor concentration followed by the weight decrease. At concentrations of 100 and 200 ppm the change in coupon mass is negligible, with the lowest degree of coupon corrosion according to the ASTM D 130 method, leading to the conclusion that this inhibitor is effective at concentrations higher than 100 ppm.

The quality of lubricating oil and amounts of oxidation products formed were monitored by the peroxide number. The following table shows the values of peroxide numbers during 3 h in the HC-6 base oil and the oil with the EP additive and different concentrations of inhibitors.

Table 5. Peroxide number in HC-6 oil with 0.25 % EP additive and different concentrations of inhibitors (3 h at $100^\circ\text{C} \pm 1^\circ\text{C}$)

Inhibitor concentration, ppm	Peroxide number, mmol kg^{-1}		
	IRGAMET 39	RC 4220	RC 8210
0	0.22	0.22	0.22
25	0.20	0.23	0.45
50	0.21	0.21	0.51
75	0.15	0.26	0.68
100	0.17	0.32	0.82
200	0.23	0.27	0.98

By inspecting the peroxide number values of the oil with 0.25 % EP additive at 3 h (Table 5) and 24 h of oxidation (Figures 3 - 5) it can be seen that the oxidation time has a negative impact on the oxidative stability of the lubricant, since the peroxide number increased with time.

Inhibitors IRGAMET 39 and RC 4220 had negligible impacts on the HC-6 oil oxidative stability during 3 h of oxidation, based on statistically not different peroxide number values obtained in the systems with and without inhibitors. During 24 h of oxidation, in the systems with mentioned inhibitors the peroxide number was reduced, indicating that both inhibitors improve oxidative stability of the lubricant.

Addition of RC 8210 at increasing concentrations increases the tendency of the oil to form oxidation products, as the peroxide number increased at both 3 h and 24 h of oxidation.

Based on the following diagrams (Figures 3 - 5) it can be seen that the addition of inhibitors IRGAMET 39 and RC 4220 at a concentration of 50 ppm, the lowest values of peroxide number and corrosion rate, while with inhibitors RC 8210 these values are lowest at a concentration of 25 ppm.

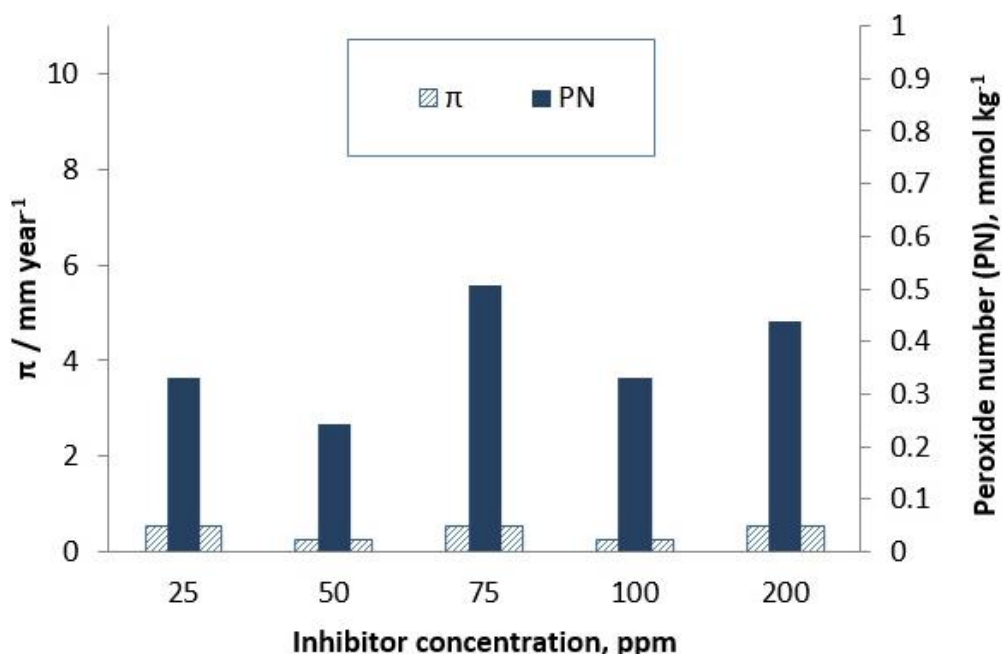


Figure 3. Corrosion rate and peroxide number in HC-6 with the addition of 0.25 % EP additive and various concentrations of IRGAMET 39 (24 h oxidation at $100 \pm 1^\circ\text{C}$)

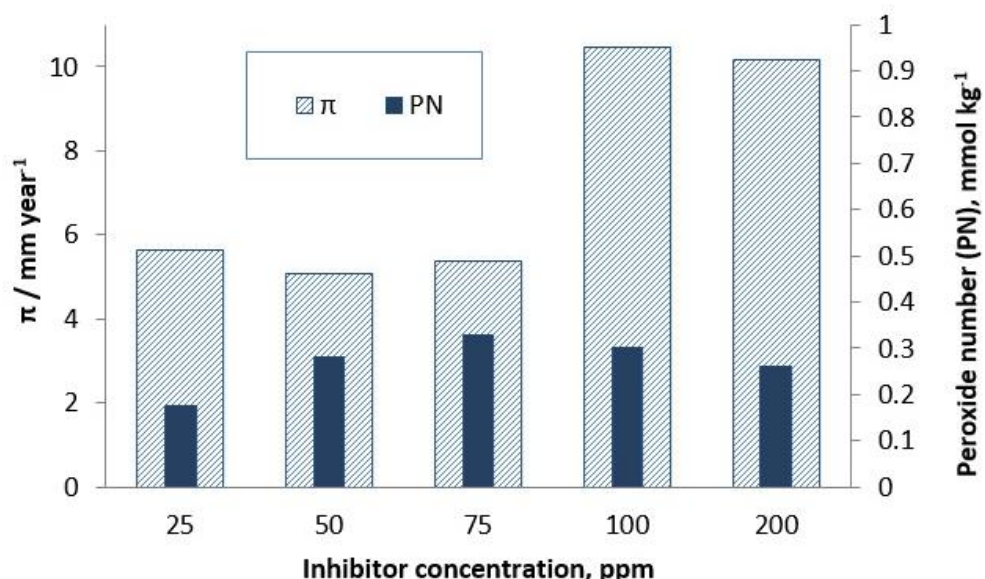


Figure 4. Corrosion rate and peroxide number in HC-6 with the addition of 0.25 % EP additive and various concentrations of RC 4220 (24 h oxidation at $100 \pm 1^\circ\text{C}$)

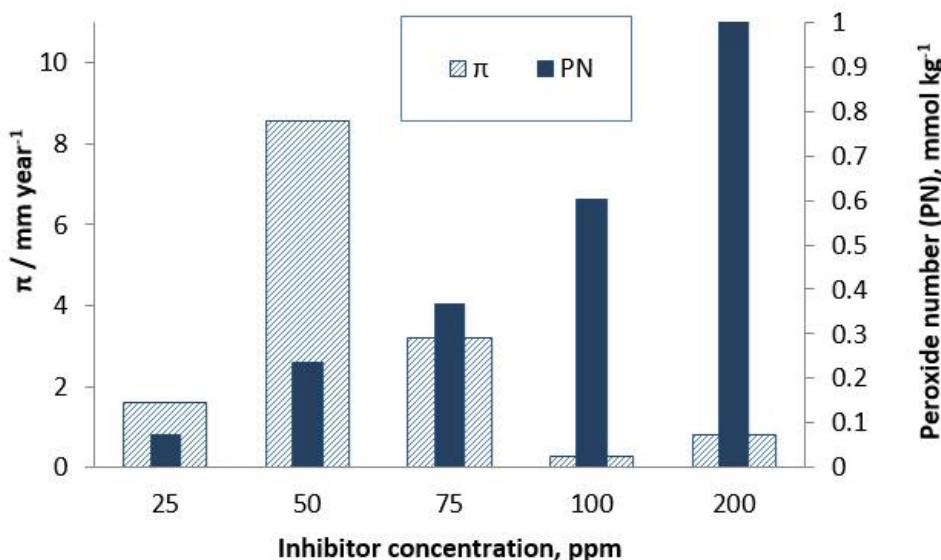


Figure 5. Corrosion rate and peroxide number in HC-6 with the addition of 0.25% EP additive and various concentrations of RC 8210 (24 h oxidation at $100 \pm 1^\circ\text{C}$)

4. CONCLUSION

The aim of this paper was to evaluate the influence of a sulfur-based EP additive on the corrosivity and oxidative stability of hydrocracked base oil HC-6 used to obtain lubricants and to determine which of the tested inhibitors is the most effective. Based on the obtained results the following conclusions can be made.

1. The tested EP additive has a negative impact on the corrosivity and oxidative stability of the lubricant.
2. The corrosion inhibitor IRGAMET 39 has shown the highest efficiency in protecting copper from corrosion, compared to the other examined inhibitors.
3. In terms of oxidative stability of the investigated lubricant, the RC 8210 inhibitor exhibited the worst results, showing the increase in peroxide number with the increase in concentration. The lubricant has shown the best oxidative stability in the presence of RC 4220, but this inhibitor is the worst in protecting copper from corrosion.

Overall, the inhibitor IRGAMET 39 is the most effective, because it has shown excellent protective properties against corrosion with minimal impact on the oxidative stability of the lubricant.

REFERENCES

- [1] Ahmad Khiara MS, Brown RCD, Lewin PL. Sacrificial Copper Strip Sensors for Sulfur Corrosion Detection in Transformer Oils. *Measurement*. 2019; 148: 1-6. <https://doi.org/10.1016/j.measurement.2019.106887>.
- [2] Alves SM, Schroeter RB, Bossardi JC dos S, Andrade CLF. Influence of EP additive on tool wear in drilling of compacted graphite iron. *J. Braz. Soc. Mech. Sci. & Eng.* 2011; 33: 197-202. <https://doi.org/10.1590/S1678-58782011000200011>.
- [3] Pawlak Z, Klamecki BE, Rauckyte T, Shpenkov GP, Kopkowski A. The tribocorrosion and micellar aspects of cutting fluids. *Tribol. Int.* 2005; 38: 1-4. <https://doi.org/10.1016/j.triboint.2004.04.004>.
- [4] Boshui C, Nan Z, Kai L, Jianhua F. Enhanced Biodegradability, Lubricity and Corrosiveness of Lubricating Oil by Oleic Acid Diethanolamide Phosphate. *Tribol. Ind.* 2012; 34: 152-157. <http://www.tribology.rs/journals/2012/2012-3/5.pdf>.
- [5] Crutcher E. Copper Corrosion in the Absence of Corrosive Sulfur. In: *Proceedings of TechCon US 2012 Conference*. Austin, Texas, United States, 2012, pp 1-11.
- [6] Xue J, Yang X, Hu J. The Differences in Potential Corrosive Effects of Sulfides and Disulfides in Insulating Oils. *IEEE T. Dielect. El.* In. 2015; 22(1): 366-371. <https://doi.org/10.1109/TDEI.2014.004210>.
- [7] Venkata Lakshmi RA, Murthy TSR. Investigation of Copper corrosion in transformer oil. *Int. J. Eng. Res.* 2012; 1: 2278-0181. <https://www.ijert.org/investigation-of-copper-corrosion-in-transformer-oil>.
- [8] Ahmad Khiar MS, Brown RCD, Lewin PL. Detection of Sulfur Corrosion in Transformer Insulation Oils Using an Interdigitated Capacitive Sensor Based on Printed Circuit Board Technology. In: *CEIDP 2017 - IEEE Conference on Electrical Insulation and Dielectric Phenomenon*. Fort Worth, Texas, United States, 2017, pp. 278-281.

- [9] Wan T, Qian H, Zhou Z, Gong SK, Hu X, Feng B. Suppressive Mechanism of the Passivator Irgamet 39 on the Corrosion of Copper Conductors in Transformers. *IEEE Trans. Dielectr. Electr. Insul.* 2012; 19(2): 454-459. <https://doi.org/10.1109/TDEI.2012.6180238>.
- [10] Schaut A, Autru S, De Rop A, Eeckhoudt S. Effects of Irgamet®30 as Additive in Transformer Oil. *IEEE Trans. Dielectr. Electr. Insul.* 2012; 19(1): 175-180. <https://doi.org/10.1109/TDEI.2012.6148516>.
- [11] Cong H, Zhang M, Shu X, Li Q. Protective Performance of Different Passivators on Oil-Paper Insulation Containing Multiple Corrosive Sulphides. *IEEE Access*. 2019; 7: 4083-4090. <https://doi.org/10.1109/ACCESS.2018.2888818>.
- [12] Ling H, Jian S, Jun R, Qingjin M, Tsing Y. The adsorption of 2,5-dimercapto-1,3,4-thiadiazole (DMTD) on copper surface and its binding behavior. *Chin. Sci. Bull.* 2001; 46: 387-389. <https://doi.org/10.1007/BF03183270>.
- [13] Nassar AM, Ahmed NS, El-shazly RI, Abd el menem YK. Preparation and evaluation of the mixtures of sulfonate and phenate as lube oil additives. *Int. J. Ind. Chem.* 2017; 8:383-395. <https://doi.org/10.1007/s40090-017-0128-x>.
- [14] Zhongyi H, Liping X, Sheng H, Aixi C, Jianwei Q, Xisheng F. Tribological and Antioxidation Synergistic Effect Study of Sulfonate-Modified Nano Calcium Carbonate. *PLOS ONE*. 2013; 8(5): e62050. <https://doi.org/10.1371/journal.pone.0062050>.
- [15] OPTIMA GRUPA. <https://optimagrupa.net/data/dokumenti/proizvodi/Tehni%C4%8Dki-list-HC-6.pdf>. Accessed May 21, 2021.
- [16] Safety Data Sheet - Additive EP 7038 N. Additiv-Chemie Luers GmbH, Brendelweg 164, D-27755 Delmenhorst, Germany. Printing date 24.05.2015.
- [17] Safety Data Sheet - Irgamet 39. Ir [https://vietducjsc.vn/upload/cdn/files/irgamet%2039%20msds\(1\).pdf](https://vietducjsc.vn/upload/cdn/files/irgamet%2039%20msds(1).pdf) Accessed May 21, 2021.
- [18] Safety Data Sheet - Additin RC 4220. <https://www.tri-iso.com/rhein-chemie-additin-rc-4220.html> Accessed May 21, 2021.
- [19] Safety Data Sheet - Additin RC 8210. <https://www.yumpu.com/en/document/view/30819948/rc-8210-webshop-rhein-chemie> Accessed May 21, 2021.
- [20] ASTM D 130 - 12: Standard Test Method for Corrosiveness to Copper from Petroleum Products by Copper Strip Test.
- [21] Stupišnek-Lisac E. *Korozija i zaštita konstrukcijskih materijala*. Zagreb, Fakultet kemijskog inženjerstva i tehnologije sveučilišta u zagrebu, 2007. ISBN: 978-953-6470-31-0
- [22] ASTM D 3703-99: Standard Test Method for Peroxide Number of Aviation Turbine Fuels.
- [23] Petrović ZR, Dugić PT, Aleksić VM, Botić TT, Kojić BN, Petrović RR. Uticaj kiselinom aktiviranog bentonita na oksidacionu stabilnost hidrokrekovanih baznih ulja. *Glasnik hemičara, tehnologa i ekologa Republike Srpske*. 2012; 7: 33-40. <https://doi.org/10.7251/GHTE1207033P>.
- [24] Zamberlin I. *Aditivi za maziva*. Maziva i podmazivanje. Zagreb: Savez Jugoslovenskih društava za primjenu goriva i maziva; 1986.

Ispitivanje korozije bakarne trake u hidrokrekovanim baznim ulju u prisustvu različitih inhibitora

Borislav N. Malinović, Aleksandra Borković i Tijana Đuričić

Tehnološki fakultet, Univerzitet u Banjoj Luci, Stepe Stepanovića 73, 78000 Banja Luka, Bosna i Hercegovina

(Stručni rad)

Izvod

U ovom radu ispitivana je korozija bakra u hidrokrekovanim baznim ulju HC-6 u prisustvu različitih koncentracija aditiva za ekstremno visoke pritiske (EP aditiv). EP aditiv se koriste za smanjenje habanja u industrijskim primenama, pod uslovima velikog opterećenja. Budući da je većina ovih aditiva na bazi sumpora čija jedinjenja mogu biti korozivna na visokim temperaturama, njihova upotreba dovodi do korozije nekih materijala. Da bi se sprečila korozija bakra u baznom ulju sa EP aditivom dodana su tri komercijalna inhibitora korozije. Po hemijskom sastavu inhibitor RC 8210 je derivat dimerkaptotiadiazola, RC 4220 sintetički neutralan kalcijum sulfonat, a IRGAMET 39 je derivat tolutriazola. Efikasnost inhibitora praćena je u skladu sa standardnom ASTM D-130 metodom, gravimetrijskom metodom, a oksidaciona stabilnost baznog ulja praćena je određivanjem vrednosti peroksidnog broja. Oksidacija je trajala 3 i 24 časa na $100^{\circ}\text{C} \pm 1^{\circ}\text{C}$. Ispitivanje je pokazalo da je IRGAMET 39 najefikasniji inhibitor u prisustvu EP aditiva u oba ispitivana vremena oksidacije.

Ključne reči: ASTM D-130; bakarni kuponi; maziva ulja; EP aditiv



Corrosion effects on structural integrity and life of oil rig drill pipes

Aleksandar Sedmak¹, Radzeya Zaidi¹, Borivoje Vujičić², Živče Šarkočević⁴, Snežana Kirin³, Zoran Stamenić¹, Miloš Đukić¹ and Gordana Bakić¹

¹University of Belgrade, Faculty of Mechanical Engineering, Serbia

²Electric Power Industry of the Republic of Srpska, Trebinje, Bosnia and Herzegovina

³Innovation center of the Faculty of Mechanical Engineering, Belgrade, Serbia

⁴Faculty of Technical Sciences, University of Priština with seat in Kosovska Mitrovica, Serbia

Abstract

Corrosion effects on structural integrity and life of oil rig welded pipes are analysed by experimental, analytical, and numerical methods. Experiments were performed using standard tensile specimens and CT specimens for static loading, Charpy specimens for impact loading, and 3 Point Bending specimens for fatigue crack growth with amplitude loading. In each case new and old pipes were used to evaluate corrosion effects. Results indicated negligible corrosion effects in the case of tensile properties and impact toughness, and strong effects in the case of fracture toughness and especially fatigue crack growth rates, increasing the risk of static failure and reducing significantly structural life. Analytical expressions are used for oil rig pipe structural integrity and life assessment to quantify these effects. Recently introduced risk-based approach is applied to analyse oil rig drill pipe with a corrosion defect treated as a surface crack.

Keywords: risk-based assessment; failure analysis diagram; fatigue; risk matrix.

Available on-line at the Journal web address: <http://www.ache.org.rs/HI/>

ORIGINAL SCIENTIFIC PAPER

UDC: 622.24.053:67.019:539.388.1

Hem. Ind. 76(3) 167-177 (2022)

1. INTRODUCTION

Casing steel pipes used in oil drilling rigs are subjected to a corrosive atmosphere making them susceptible to material degradation, sometimes in combination with errors in design and manufacturing. The main concern is the influence of CO₂ and H₂S in the oil and gas exploitation facilities because these gases, especially under high pressures and temperatures, create a corrosive environment [1,2]. Therefore, besides common reasons for failures of the pipelines, such as insufficient resistance to crack initiation and propagation and especially occasional inadequate quality of welded joints, corrosion defects often reduce strength and crack resistances, causing static or fatigue failure [3,4]. In this context it is necessary to analyse material resistance to cracking not only for new material, but also for material after certain period of exploitation, referred in the following text as used material. To fully comprehend the complex mechanism of corrosive action of fluids from oil and gas wells, all the factors caused by the presence of carbon dioxide, hydrogen sulfide, chloride, and mercury, affecting the initiation and development of corrosion should be taken into consideration [5,6].

Presence of flaws in the basic material or in welded joints of protective welded pipes in oil wells does not necessarily cause the loss of their integrity, [7-8]. Assessment which refers to the tolerability of some kinds of flaws depends on possible interactions of the following factors: geometry of protective welded pipes, stress states (operational and residual), type, size and location of the flaw, mechanical properties of welded joints, conditions of exploitation, etc [9-10]. On the basis of accurate determination of the flaw type and size and calculation of the operational ability of the welded joint, the decision regarding its use or rejection can be reached. Structural integrity is a relatively new scientific and engineering discipline, which in a broader sense comprises the state analysis and diagnostics of behaviour, lifetime evaluation and structure refurbishment. This means that, besides the common task of assessing the integrity of

Corresponding authors: Aleksandar S. Sedmak, University of Belgrade, Faculty of Mechanical Engineering, Kraljice Marije 16, 11120 Belgrade 35, Serbia; E-mail: aleksandarsedmak@gmail.com

Paper received: 25 February 2022; Paper accepted: 27 June 2022; Paper published: 18 July 2022.

<https://doi.org/10.2298/HEMIND220222014S>



structure when the flaw is detected using non-destructive inspection (NDI) methods, this discipline also comprises the analysis of the stress state of the structure with and without a crack.

Numerous papers have been published on pipe failures due to cracks and other defects, including corrosion, [11-16], and some of them focused on welded joints, [17]. Nevertheless, all of them lack a comprehensive approach, which would include experimental, numerical, and analytical approaches to the problem of corroded pipes and the remaining pipe strength. Toward this aim, several papers were published in the last decade by the authors of the present study, [18-22], including previous experimental investigation on the pipe taken from exploitation in an oil drilling rig after 70,000 hours (8 years) of service [23,24]. In the present paper, the new method, recently introduced and applied for pressure vessels, [25-29], is applied to assess structural integrity of API J55 steel pipes, damaged by corrosion, using risk-based approach. In respect to welded joints, focus here is on the base metal, since it was shown that it is more sensitive to cracking than the weld metal [23, 24].

2. EXPERIMENTAL METHODS

API J55 steel, with the chemical composition shown in Table 1, and metallographic examination shown in Figure 1, indicating typical rolled ferrite-pearlite microstructure, is used here for testing as a common material for oil rig drilling pipes. Specimens were cut from the casing pipe manufactured by high frequency (HF) welding - producer US Steel, Serbia). The pipe was withdrawn from a drilling rig during a reparation procedure after about 70000 hours (8 years) of operation. At the same time, new pipe was used for testing both the material properties and pipe behaviour under pressure [23]. Testing of tensile properties, impact toughness, fracture toughness and fatigue crack growth rate is presented in the following text. Specimens were cut out from both new and used pipes and machined to standard dimensions for each testing.

Table 1. Chemical composition of API J55 steel [23]

Element	C	Si	Mn	P	S	Cr	Ni	Mo	V	Cu	Al
Content, wt.%	0.29	0.23	0.96	0.013	0.022	0.1	0.058	0.012	0.003	0.13	0.025

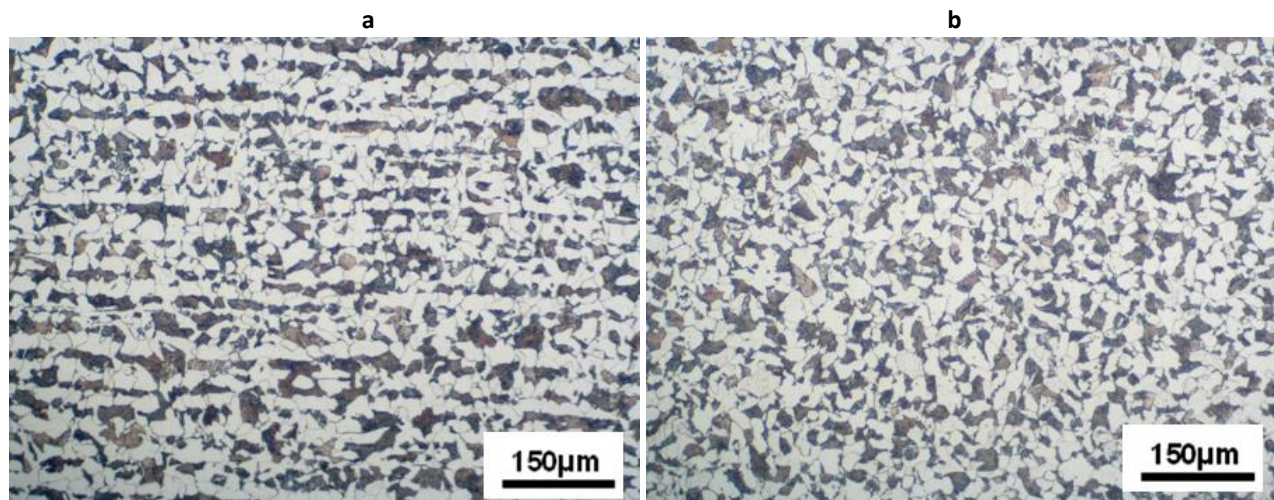


Fig. 1. Microstructure of API J55 steel: a) rolling direction; b) transverse direction [23]

2. 1. Tensile properties

Tensile properties were tested in accordance with the standard ASTM E8-08, [30], using specimens of the base metal prepared according to the standard ASTM A370, Fig. 2, [31], as shown in [21,23]. Testing was done by using the electromechanical testing machine, SCHENCK-TREBEL RM 100 (SCHENCK - Germany), in displacement control, with the rate 5 mm/min.

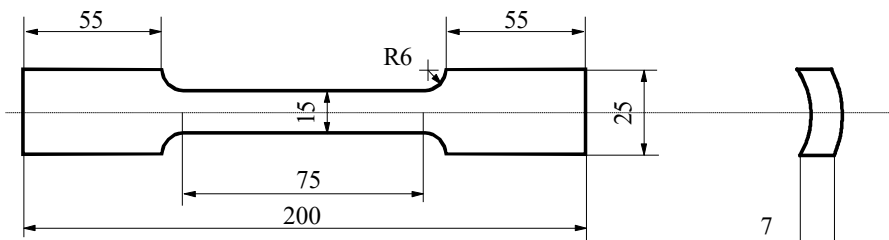


Fig. 2. Specimens for tensile testing [23]

2. 2. Impact toughness

Impact toughness was tested by using the instrumented Charpy pendulum SCHENCK TREBELL 150/300 and Charpy specimens, Fig. 3, according to the standard ASTM E23-01 [32], as shown in more details in [23]. Instrumented pendulum enables separation of energies for crack initiation and propagation, which are equally important indicators of material behaviour under impact loading, as the total energy.

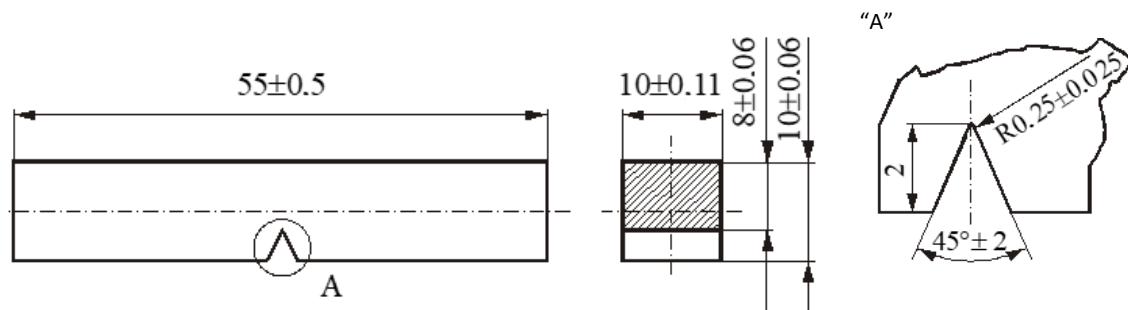


Figure 3. Charpy specimen for impact toughness testing

2. 3. Fracture toughness

Keeping in mind that the material tested here is not a brittle one, it was necessary to use elastic-plastic fracture mechanics parameter, such as J integral, to estimate fracture toughness [33]. Toward this aim, so-called crack resistance curves, *i.e.* J - R curves, are used to get the critical J_{lc} value, which is then used to calculate K_{lc} , *i.e.* the fracture toughness, according to the standard ASTM E1820, [33]. To obtain J - R curves and J_{lc} values, relevant for real pipes, standard compact tension (CT) specimens were used and modified, since they were directly cut out from new and used pipes, with curvature and thickness as shown in Fig. 4, [14,19,23]. Testing was done by using the electromechanical testing machine, SCHENCK-TREBEL RM 100, using special grips for CT specimens.

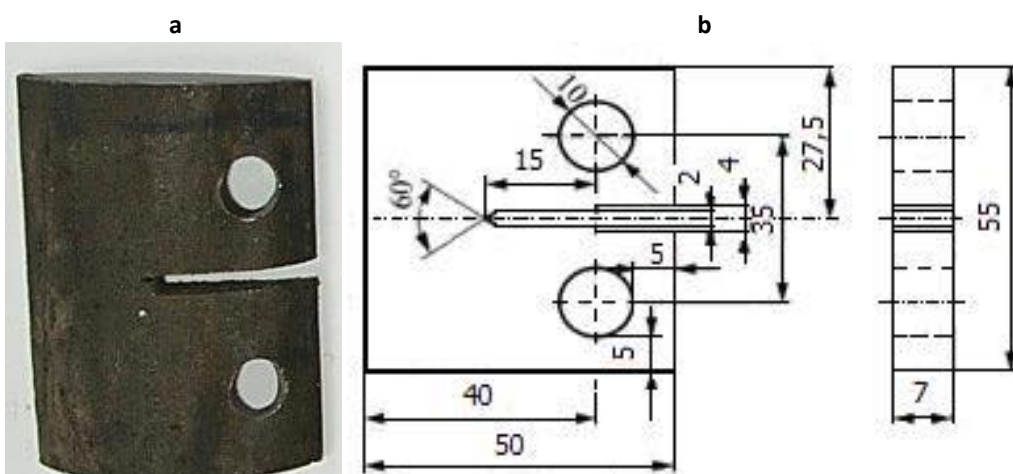


Figure 4. CT specimen: a) photograph, b) dimensions

2. 4. Fatigue Crack Growth testing

Fatigue crack growth (FCG) was tested at room temperature, in accordance with ASTM E647, [34] using Three Point Bending (3PB) specimen on a Fractomat device (Rumul, Switzerland), as shown in Fig. 5, and explained in more details in [23].

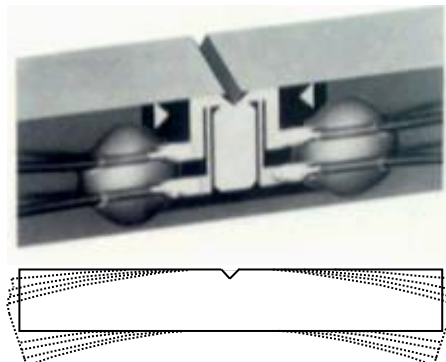


Fig. 5. Fatigue crack growth testing: 3PB specimen with foil for measuring the crack length assembly

2. 5. Prototype testing

Testing of prototype was conducted on a pressure vessel with defects of the circular shape. The vessel was made from a part of the casing pipe made by HF welding of API J55 steel, closed at both ends with nominal dimensions: diameter $\phi 139.7$ mm, wall thickness 6.98 mm, Fig. 6a. In the experiment performed [23], strain gages and rosettes were used to evaluate J integral by so-called the direct measurement technique. Different artificially made surface defects with lengths $D = 26, 28$, and 30 mm and depths $a = 1.75, 3.5$, and 5.25 mm (Fig. 6b) were monitored to assess their effects on structural integrity [21,23].

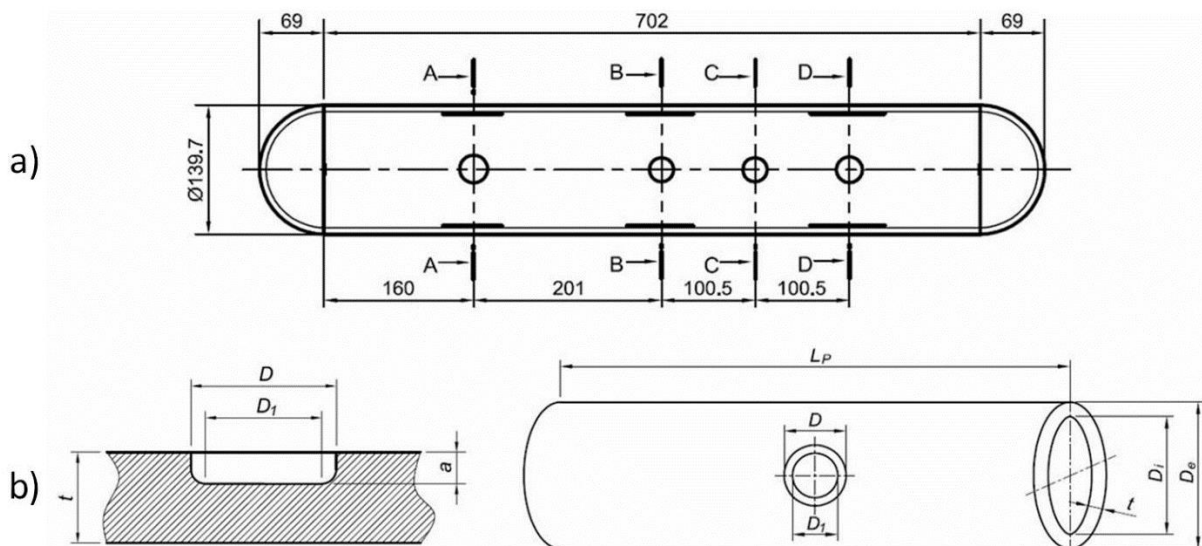


Fig. 6. a) Prototype with artificial defects, b) defect details

3. RESULTS

3. 1. Tensile testing

Results of tensile testing are shown in Table 2 for the new and used material, respectively. As one can see, yield stress (R_e) is significantly reduced due to damage in used material, while tensile strength (R_m) and elongation (A_5) are not significantly affected. One possible explanation of such a behaviour could be that damage has reversed the

mechanism used to obtain unusually high R_e of the new material, but this phenomenon is yet to be investigated. Anyhow, it is considered here as a fact indicating the corrosion effect on tensile properties. It should be also noticed that the hardness values were almost the same, 195 ± 10 in both cases [23].

Table 2. Tensile properties for new and used material [23]

$R_e \pm SD / MPa$		$R_m \pm SD / MPa$		$A_5 \pm SD / \%$	
New material	Used material	New material	Used material	New material	Used material
547.7 ± 7.6	379.7 ± 3.3	586.7 ± 6.2	562.3 ± 2.9	28.7 ± 1.3	33.0 ± 1.2

3. 2. Impact toughness

Impact toughness values determined for the new and used material are shown for different testing temperatures in Table 3, indicating weak influence of corrosion damage. All other details and results are shown in [30], including the effect of different microstructures in the base metal (BM), weld metal (WM) and heat-affected-zone (HAZ), which turned out to be insignificant.

Table 3. Impact toughness for new / used material

Mean value \pm standard deviation

Testing temperature, °C	$E_{uk} \pm SD / J$	
	New material	Used material
-40	26.3 ± 3.1	26.7 ± 3.7
-20	52.3 ± 0.9	54.3 ± 2.5
+20	99.0 ± 0.0	102.3 ± 6.1

3. 3. Fracture toughness

Fracture toughness values are shown in Table 4, indicating stronger influence of corrosion damage than in the case of tensile properties and impact toughness. Of special interest are minimum K_{ic} values, $121.4 \text{ MPa}\cdot\text{m}^{0.5}$ for the new material, and $91.4 \text{ MPa}\cdot\text{m}^{0.5}$ for the used one, in both cases for the base metal, as the most sensitive to cracking.

Table 4. Fracture toughness K_{ic} , new / used material

Crack location	$K_{ic} / \text{MPa}\cdot\text{m}^{0.5}$	
	New material	Used material
Base metal	121.4	91.4

3. 4. Fatigue crack growth testing

Results for the threshold values, ΔK_{th} , and Paris law coefficients C and m , are shown in Table 5 for new and used material, tested with amplitude loading corresponding to the stress intensity factor range $\Delta K=15 \text{ MPa}\cdot\text{m}^{0.5}$. More detailed results, including relation between the FCG rate, da/dN , and stress intensity factor range, ΔK , are presented in form of a diagram in [14,23]. Here, the FCG rate is presented for the stress intensity factor range $\Delta K=15 \text{ MPa}\cdot\text{m}^{0.5}$, indicating a strong effect of corrosion damage, since the FCG rate is almost 6-fold higher for the used material.

Table 5. Fatigue crack growth parameters, [23]

	$\Delta K_{th} / \text{MPa}\cdot\text{m}^{0.5}$	C	m	$(da/dN) / (\text{m} / \text{cyc}) (\Delta K=15 \text{ MPa}\cdot\text{m}^{0.5})$
New material	9.5	$1.23\cdot10^{-13}$	3.931	$5.17\cdot10^{-9}$
Used material	9.2	$2.11\cdot10^{-15}$	6.166	$3.75\cdot10^{-8}$

To summarize, there is insignificant influence of corrosion on tensile properties and impact toughness, but both fracture toughness and especially FCG rate are strongly affected, indicating potential large differences in structural integrity and life assessment.

3. 5. Prototype testing

Experimental results of prototype testing are shown in Figure 7 in the form of J integral vs. pressure, and explained in more details in [20], including comparison with FEM, indicating safe operation at the design pressure of 10 MPa. One can note that failure did not occur for testing pressure as high as 22 MPa.

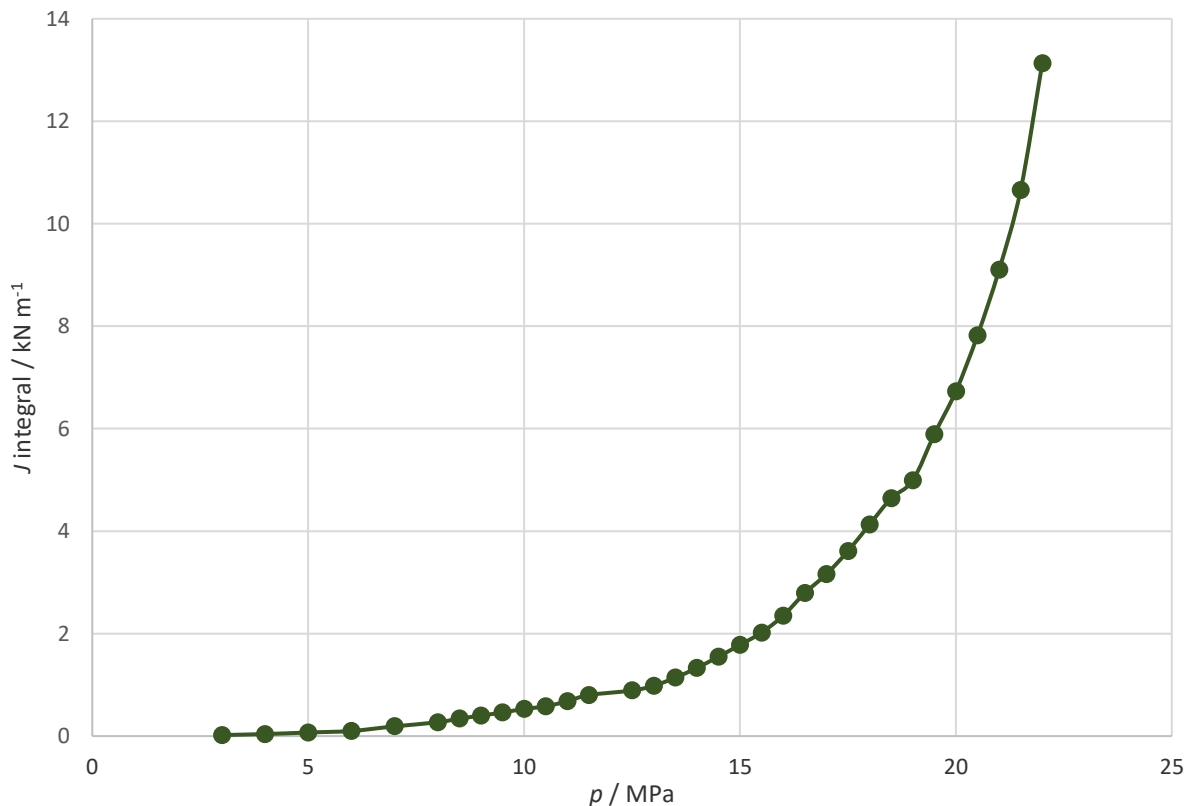


Figure 7. Prototype testing results - J integral vs. pressure

4. STRUCTURAL INTEGRITY ASSESSMENT

Analytical assessment of structural integrity is based on calculation of the stress intensity factor and stress ratio, with an aim to define the corresponding point in the Failure Analysis Diagram (FAD) [35]. Basic concept of the FAD, shown in Figure 8, is that a point below the limit line is safe, while a point outside the limit line is not safe. The limit line is defined by equation (1):

$$K_r = S_r \left[\frac{8}{\pi^2} \ln \sec \left(\frac{\pi}{2} \cdot S_r \right) \right]^{0.5} \quad (1)$$

where K_r is the ratio between the stress intensity factor K_I and its critical value K_{Ic} , while S_r is the ratio between the net stress S_{net} and the stress critical value S_c .

To evaluate points in the case analysed here, the stress intensity factor K_I is calculated according to the following equation (2):

$$K_I = Y S \sqrt{\pi a} \quad (2)$$

where Y is the geometry factor, depending on the crack type and size, [24], $S = p \cdot r/t$ is the circumferential stress in a thin cylindrical vessel, p is the pressure, r radius, and t thickness. The net stress is calculated in the same way as S , but for the reduced cross-section, where the crack is located.

The critical value of K_I , i.e. fracture toughness K_{Ic} , is already defined in Table 4, whereas the critical value of stress, S_c , is commonly defined as the mid-value of yield and tensile strengths, equation (3)[23]:

$$S_c = \frac{R_e + R_m}{2} \quad (3)$$

For calculation of the above parameters a crack with the depth $a = 3.5$ mm and length $2c = 28$ mm was considered. The cross section reduction is then $(3.5 \times 28) / (6.98 \times 702) = 0.0200$, and net stress $S_{\text{net}} = 100 / 0.9800 = 102.0$ MPa. According to the data given in Table 2, the critical stress is $S_c = (547.7 + 586.7) / 2 = 567.2$ MPa for the new material, and $S_c = (379.7 + 562.3) / 2 = 471$ MPa for the used one. Now, one can calculate the X coordinate as by equation (4):

$$X = \frac{S_{\text{net}}}{S_c} \quad (4)$$

These values are 0.19 and 0.23 for the new and used material at the pressure of 10 MPa, respectively. Corresponding values for the pressure of 22 MPa are 0.42 and 0.51, respectively.

To get the Y coordinate, the stress intensity factor for a surface edge crack in a cylinder is needed. It can be obtained by using different methods for geometry factors, depending on the crack size [36]. According to the procedure explained in [24], the geometry factor for the crack 3.5 mm in depth and 28 mm in length is $Y_{\text{total}} = 2.538$, and the corresponding stress intensity factor is $K_I = 32.6 \text{ MPa} \cdot \text{m}^{0.5}$ for the pressure of 10 MPa and $71.7 \text{ MPa} \cdot \text{m}^{0.5}$ for the pressure of 22 MPa. Taking into account the critical values of stress intensity factor from Table 4 ($K_{Ic} = 91.4 \text{ MPa} \cdot \text{m}^{0.5}$ for the used material, and $121.4 \text{ MPa} \cdot \text{m}^{0.5}$ for the new one), the Y coordinate becomes 0.35 for the used material and 0.27 for the new one (pressure 10 MPa), and 0.77 for the used material and 0.59 for the new one (pressure 22 MPa). All four points are in the safe region, as shown in Figure 8, indicating also good agreement with the experimental results.

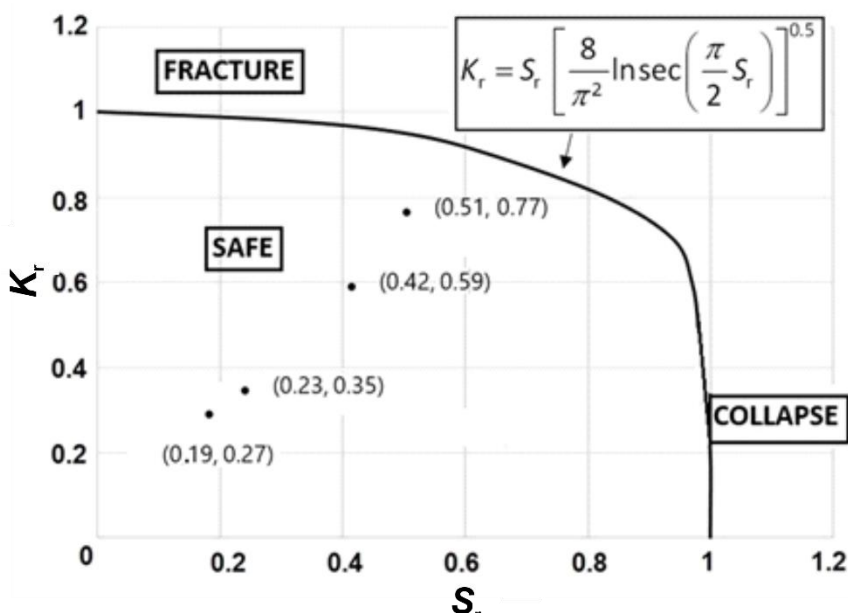


Fig. 8. Failure analysis diagram: pressure 10 MPa: new (0.19, 0.27) and used (0.23, 0.35) material; pressure 22 MPa: new (0.42, 0.59) and used material (0.51, 0.77)

Probability of failure can be now estimated according to the position of these 4 points. Using the novel procedure, one obtains 0.28 and 0.37 for the pressure of 10 MPa, new and used material, respectively, as well as 0.62 and 0.82 for the pressure of 22 MPa, also for the new and used material, respectively. Having in mind the medium consequence, as explained in [22], one obtains the risk matrix, Table 6, indicating high risk level for the pressure of 22 MPa and used material.

This is the crucial point in the analysis performed here. One should notice that the risk-based analysis shows in a simple way that material aging increases the risk for one category, whereas testing over-pressure does it for two categories! Obviously, material aging cannot be avoided, but over-pressure has to be reduced as much as possible. According to this analysis, 30 % should be the maximum value to keep all points at the medium risk level.

Table 6. Position of assessment points in the risk matrix

Probability category	Consequence category					Risk legend
	1 - very low	2 - low	3 - medium	4 - high	5 - very high	
≤0.2 very low						Very low
0.2-0.4 low			$p=10, \text{ MPa}$ new 0.33			Low
0.4-0.6 medium			$p=10, \text{ MPa}$ used 0.42			Medium
0.6-0.8 high			$p=22, \text{ MPa}$ new 0.73			High
0.8-1.0 very high			$p=22, \text{ MPa}$ used 0.92			Very High

3.3. Structural life assessment

According to the results of FCG rates, presented in Table 5, one should expect significant reduction of fatigue life of corrosion damaged material. To evaluate this detrimental effect, the Paris law was used for both analytical and numerical calculations in the following equation, as shown in equation (5) [24]:

$$\frac{da}{dN} = C(\Delta K)^m = C \left(Y \left(\frac{a}{W} \right) \Delta \sigma \sqrt{\pi a} \right)^m \quad (5)$$

where $Y(a/W)$ is the geometry factor depending on the crack geometry. The Paris law can be integrated directly if one neglects dependency of the geometry parameter Y on crack geometry, or numerically if dependency is taken into account, as was done here by dividing the range of crack depth growth as follows: 3.5; 4.19; 4.88; 5.57; 6.26; 6.9; 7 mm. Coefficients C and m are used for the new and used BM, as given in Table 5. The geometry coefficient $Y(a/W)$ was in the range from 2.39 to 4.29, also affected by different crack lengths. Amplitude loading is defined as $R=0.79$ (in ABAQUS input data file) for 21 MPa (maximum stress 100 MPa, minimum stress 79 MPa, [23]). Calculation is based on the Raju-Newman solution for a surface crack in a thin-walled cylindrical shell, equation (6)[36]:

$$K_I = \left[M_f + \left(E_k \sqrt{\frac{c}{a}} - M_T \right) \left(\frac{a}{t} \right)^s \right] \frac{\sigma \sqrt{\pi \cdot a}}{E_k} \cdot M_{tm} \quad (6)$$

where: M_f is a function depending on the crack geometry (on the ratio a/c); s is the function depending on the crack geometry (on the ratio a/c) and on the relative crack depth (on the ratio a/t); M_{tm} (M_s) is the surface correction factor for a surface crack and M_T is the Folias correction factor.

To fit the Raju and Newman results for the deepest point $\theta = \pi/2$, the parameter (s) is given by equation (7):

$$s = 1.6 + 3(a/c)^3 + 8(a/c)(a/t)^5 + 0.008(a/c) \quad (7)$$

Results obtained in this way are presented in Table 7. The presented data indicate cca 17 % reduction of fatigue life for the used material as compared to the new one.

Table 7. Data for crack length $2C = 28$ mm, using parameters M_f , E_k , s , M_T , M_{tm} and F_{total} as defined in [24]

a / mm	c/a	a/t	a/c	M_f	E_k	$S(\theta = \pi/2)$	M_T	M_{tm}	Y_{total}	$K_I / \text{MPa} \cdot \text{m}^{0.5}$	a_c / m		$N(\theta = \pi/2)$	
											old	new	old	new
3.5	4.000	0.501	0.250	1.105	1.149	1.742	1.022	1.016	2.448	25.69	0.200	0.353	0	0
4.19	3.341	0.600	0.299	1.100	1.200	1.894	1.032	1.032	2.483	28.51	0.191	0.337	7029810	6254403
4.88	2.869	0.699	0.349	1.095	1.257	2.216	1.043	1.060	2.557	31.69	0.173	0.305	10536232	10520849
5.57	2.513	0.798	0.398	1.090	1.320	2.839	1.055	1.110	2.716	35.96	0.145	0.255	12092670	13392910
6.26	2.236	0.897	0.447	1.085	1.388	3.962	1.069	1.207	3.074	43.14	0.108	0.190	12586914	15166127
6.9	2.029	0.989	0.493	1.081	1.456	5.697	1.083	1.405	3.910	57.60	0.069	0.121	12661710	15985600
7	2.000	1.003	0.500	1.080	1.466	6.049	1.086	1.456	4.144	61.50	0.062	0.110	12668570	16030191



4. DISCUSSION

In order to verify the approach applied in this research, results are now compared with the experimental and numerical ones, presented in [21]. To do so, the maximum allowed pressure has been calculated according to the critical value taken from the failure analysis diagram (FAD) for the used material, leading to $p=26.8$ MPa (22/0.82), since the probability level for the pressure 22 MPa is 0.82, and for the allowed (critical) pressure it is 1. Maximum allowed pressures, as given in [21] for 3 analytical and FEM values obtained for 3 different reference stresses (0.8, 0.85, and 0.9 of the ultimate tensile strength - UTS), are in the range 37.1 to 48.2 MPa. The maximum allowed pressure calculated based on FAD is clearly lower than any of them. Taking into account the fact that these values are obtained for the real geometry of defect, it is easy to conclude that the significantly smaller value obtained here is in accordance with the fact that the defect is considered as a surface crack, whereas in analytical and numerical calculations it was treated as a geometry imperfection. In this way, our approach is verified as a conservative and reliable, and also as a simple one.

Results for remaining life, *i.e* the number of cycles needed for crack growth from the initial depth (3.5 mm) to 6.26 mm, for crack length 28 mm, Table 7, are also given in Table 8 for the used and new material to show more clearly the effect of material aging. One can see that this effect is important, but not significant, since the reduction in the remaining life is 17 %, from about 2.8 years for the new material to about 2.3 years for the used material. One can notice that the effect is much more pronounced for a longer crack, as presented [22], and also shown here in Table 8.

Table 8. Number of cycles N and remaining life for crack growth in depth from 3.5 to 6.26 mm

Crack length	N		Time, year*	
	Used material	New material	Used material	New material
2c=28 mm	12,586,914	15,166,127	2.328	2.805
2c=200 mm **	464,212	2,433,641	0.092	0.482

*1 year=5,046,009 cycles, **data taken from [22]

One issue remains critical in the approach presented here. Namely, as shown in [24], analytical expressions do not exist for evaluation of surface crack stress intensity factors, which would be the best approach for crack analysis regardless the crack type and size. In this research, the Raju-Newman expression is used, but its validity for very deep cracks is questionable. Anyhow, analytical expressions used here are useful and present a practical engineering tool to assess structural integrity and life of a cracked corroded component in a simple way.

5. CONCLUSIONS

According to the presented analysis of oil rig welded pipes, following conclusions can be drawn.

- Fracture toughness and FCG rate are strongly affected by corrosion damage, although tensile properties and impact toughness are not. This is probably valid for ferritic steels in general, but not austenitic ones.
- The most pronounced effect of corrosion damage is in the case of amplitude loading, since it increases the FCG rate up to 6 times, which in turn significantly reduces structural life. Anyhow, this result should not be generalized, since it is specific for the case studied here.
- Corrosion damage increases the failure risk for one category (low to medium - working pressure, high to very high – test pressure), whereas the increase from working to testing pressure increases the failure risk for two categories (from low to high – new material, medium to very high – used material).
- Testing pressure has to be reduced as much as possible. According to this analysis, 30 % should be the maximum value to keep the risk at medium level. The optimal value should be 10 %.
- Failures due to relatively short cracks can be prevented by timely intervention, what might not be the case for relatively long cracks.

Acknowledgement: This research was supported by the Ministry of Education, Science and Technological Development of the Republic of Serbia (contracts 451-03-9/2021-14/200105 and 451-03-9/2021 -14/200213).



REFERENCES

- [1] Popoola LT, Grema AS, Latinwo GK, Gutti B, Balogun AS. Corrosion problems during oil and gas production and its mitigation, *Int J Ind Chem.* 2013; 4(1); 35; <http://dx.doi.org/10.1186/2228-5547-4-35>
- [2] Wasim M, Djukic M. External corrosion of oil and gas pipelines: A review of failure mechanisms, *J Nat Gas Sci Eng.* 2022; 100: 104467, <https://doi.org/10.1016/j.jngse.2022.104467>
- [3] Perez TE. Corrosion in the oil and gas industry: an increasing challenge for materials, *JOM* 2013; 65(8): 1033-1042; <https://doi.org/10.1007/s11837-013-0812-z>
- [4] Sharma SK, Maheshwari S. A review on welding of high strength oil and gas pipeline steels. *J Nat Gas Sci Eng* 2017; 38: 203-217; ISSN: 1875-5100
- [5] Askari M, Aliofkazraei M, Afroukhteh, S. A comprehensive review on internal corrosion and cracking of oil and gas pipelines, *J Nat Gas Sci Eng.* 2019; 71: 102971; <https://doi.org/10.1016/j.jngse.2019.102971>
- [6] <http://earth.uni-muenster.de/earth/d/dokumente/schlumberger/English/Corrosion/>, 05.1999
- [7] Šarkočević Ž, Arsić M, Medjo B, Kozak D, Rakin M, Buržić Z, Sedmak A. Damage level estimate of API J55 steel for welded seam casing pipes. *Strojarstvo: J Theory Appl Mech Eng* 2009; 51: 303-311; <https://doi.org/10.1016/j.mspro.2014.06.155>
- [8] Lazić Vulićević Lj, Arsić M, Šarkočević Ž, Sedmak A, Rakin M. Structural life assessment of oil rig pipes made of API J55 steel by high frequency welding, *Technical gazette* 2013; 20(6): 1091-1094; ISSN: 1330-3651
- [9] Medjo B, Rakin M, Gubeljak N, Matvienko Y, Arsic M, Sarkocevic Z, Sedmak A. Failure resistance of drilling rig casing pipes with an axial crack, *Eng Fail Anal.* 2015; 58: 429-440; <https://doi.org/10.1016/j.engfailanal.2015.05.015>
- [10] Rakin M, Medjo B, Arsić M, Šarkočević Ž, Sedmak A. Effect of exploitation conditions and flaw geometry on the load carrying capacity of casing pipes for oil drilling rigs, *Key Eng Mat.* 2012; 488-489: 577-580; <https://doi.org/10.1016/j.mspro.2014.06.155>
- [11] Azevedo CRF, Sinatra A. Failure analysis of a gas pipelines, Instituto de Pesquisas Tecnologicas do Estado de São Paulo, *Eng Fail Anal.* 2004; 11: 387-400; <https://doi.org/10.1016/j.engfailanal.2003.06.004>
- [12] Assanelli AP, Toscano RG, Johnson DH, Dvorkin EN. Experimental/numerical analysis of the collapse behavior of steel pipes. *Eng Computat.* 2000; 17: 459 - 86.
- [13] Fu B, Batte AD. Advanced Methods for the Assessment of Corrosion in Linepipe, Health and Safety Executive Summary Report, OTO 1999-051, HSE Books, 1999; <https://www.hse.gov.uk/research/otopdf/1999/oto99051.pdf>
- [14] Kiefner J, Vieth PA. Modified criterion for evaluating the strength of corroded pipe, Final Report for PR 3-805 project to the Pipeline Supervisory Committee of the American Gas Association, Battelle, Ohio, 1989.; <https://www.worldcat.org/title/final-report-on-project-pr-3-805-a-modified-criterion-for-evaluating-the-remaining-strength-of-corroded-pipe/oclc/43015134>
- [15] Kiefner J, Vieth P. Evaluating pipe - 1 new method corrects criterion for evaluating corroded pipe, *Oil & Gas J.* 1990; 6: 56-9
- [16] Fu B, Kirkwood M. Predicting failure pressure of internally corroded linepipe using the finite element method, OMAE95, *Pipeline Technology*, international conference on offshore mechanics & arctic engineering, 1995; V: 175-85.; ISBN 0-7918-1311-8; TRN: IM9615%245
- [17] Lee J-S, Ju J-B, Jang J, Kim W-S, Kwon D. Weld crack assessments in API X65 pipeline: failure assessment diagrams with variations in representative mechanical properties, *Mat Sci Eng.* 2004; 373: 122-30; <https://doi.org/10.1016/j.msea.2003.12.039>
- [18] Rakin M, Medjo B, Arsić M, Šarkočević Ž, Ivanović I, Sedmak A. API J55 steel casing pipe with an initial surface crack under internal pressure - Determination of fracture parameters, *Key Eng Mat.* 2014; 601: 65-70; [10.4028/www.scientific.net/KEM.488-489.577](http://www.scientific.net/KEM.488-489.577)
- [19] Rakin M, Arsić M, Medjo B, Šarkočević Ž, Sedmak A. Structural integrity assurance of casing pipes in the oil and gas industry, *WIT Trans Built Environ.* 2013; 134: 401-410; <https://doi.org/10.2495/SAFE130361>
- [20] Kirin S, Sedmak A, Zaidi R, Grbović A, Šarkočević Ž, Comparison of experimental, numerical and analytical risk assessment of oil drilling rig welded pipe based on fracture mechanics parameters, *Eng Fail Anal.* 2020; 114(4); <https://doi.org/10.1016/j.engfailanal.2020.104600>
- [21] Sedmak A, Arsić M, Šarkočević Ž, Medjo B, Rakin M, Arsić D, Lazić M. Remaining strength of API J55 steel casing pipes damaged by corrosion, *Int J Press Vess Piping.* 2020; 188; <https://doi.org/10.1016/j.ijpvp.2020.104230>
- [22] Zaidi R, Kozak D, Sedmak A, Kirin S, Franulovic M. Risk assessment based on analytical evaluation of structural integrity and life of drilling rig pipe, *Procedia Struct. Integr.* 2021; 33: 1181-1186; <https://doi.org/10.1016/j.prostr.2021.10.132>
- [23] Šarkočević Ž. Resistance to Damage and Fracture of Protective Welded Pipes in Oil Wells, Ph.D. Dissertation (in Serbian), University of Belgrade, 2010.
- [24] Zaidi R. Application of fracture mechanics parameters to residual life assessment of welded pipes exploitation under fatigue loading, Ph.D. Dissertation, University of Belgrade, 2021.
- [25] Golubović T, Sedmak A, Spasojević Brkić V, Kirin S, Rakonjac I. Novel risk based assessment of pressure vessels integrity. *Technical Gazette* 2018; 25: 803-807; <https://doi.org/10.17559/tv-20170829144636>
- [26] Zaidi R, Sedmak A, Kirin S, Martić I, Šarkočević Z. Structural integrity and life assessment of oil drilling rig pipes using analytical method, *Struct Integ Life.* 2022; 22: 63-68



- [27] Sedmak A, Algool M, Kirin S, Rakicevic B, Bakic R. Industrial safety of pressure vessels - Structural integrity point of view, *Hem. Ind* 2016; 70: 685-694; <https://doi.org/10.2298/HEMIND150423005>
- [28] Golubović T, Sedmak A, Spasojević Brkić V, Kirin S, Veg E. Welded joints as critical regions in pressure vessels – case study of vinyl-chloride monomer storage tank, *Hem Ind*. 2018; 72(4): 177-182; <https://doi.org/10.2298/HEMIND171009006G>
- [29] Zaidi R, Sedmak A, Kirin S, Grbovic A, Li W, Lazic Vulicevic L, Sarkocevic Z. Risk assessment of oil drilling rig welded pipe based on structural integrity and life estimation, *Eng. Fail Analysis*. 2020; 112: 104508; <https://doi.org/10.1016/j.engfailanal.2020.104508>
- [30] ASTM E8/E8M-08, Standard Test Methods for Tension Testing of Metallic Materials
- [31] ASTM A370-20, Standard Test Methods and Definitions for Mechanical Testing of Steel Products
- [32] ASTM E23-01, Standard Test Methods for Notched Bar Impact Testing of Metallic Materials
- [33] ASTM E1820-20, Standard Test Method for Measurement of Fracture Toughness
- [34] ASTM E647 - 15e1 Standard Test Method for Measurement of Fatigue Crack Growth Rates
- [35] BS 7910:2005 Guide to methods for assessing the acceptability of flaws in metallic structures, vol. 3, 2005
- [36] FITNET Fitness-for-service (FFS) Annex, (2008), Volume 2, ISBN 978-3-940923-01-1

Efekti korozije na integritet konstrukcije i životni vek cevi za bušenje izvora nafte

Aleksandar Sedmak¹, Radzeya Zaidi¹, Borivoje Vujičić², Živče Šarkočević⁴, Snežana Kirin³, Zoran Stamenić¹, Miloš Đukić¹ i Gordana Bakić¹

¹Univerzitet u Beogradu, Mašinski fakultet, Beograd, Srbija

²Direkcija za proizvodnju električne energije, Trebinje, Bosna i Hercegovina

³Inovacioni centar Mašinskog fakulteta, Beograd, Srbija

⁴Fakultet tehničkih nauka, Univerzitet u Prištini sa sedištem u Kosovskoj Mitrovici, Srbija

(Naučni rad)

Izvod

Uticaj korozije na integritet i vek naftnih bušećih cevi je analiziran eksperimentalnim, analitičkim i numeričkim metodama. Eksperimenti su rađeni na standardnim zateznim i "CT" epruvetama, ispitnim statičkim opterećenjem, Šarpi epruvetama ispitanim na udarno opterećenje i epruvtama na savijanje u 3 tačke, ispitanim na amplitudno opterećenje. U svakom slučaju je ispitani novi i korišćeni materijala da bi se odredio uticaj korozije. Rezultati su ukazali na mali uticaj korozije u slučaju zateznih svojstava i žilavosti, a relativno veliku uticaj u slučaju žilavosti loma i brzine rasta zamorne prsline, što značajno povećava rizik od loma i smanjuje preostali vek cevi. Kvantifikacija ovog uticaja je određena pomoću analitičkih izraza za faktor integrleta napona. Nedavno uvedeni pristup analizi rizika je primenjen da se odredio nivo rizika u novim i korišćenim cevima, pri proračunskom i ispitnom pritisku.

Ključne reči: procena rizika; dijagram analize loma; zamor; matrica rizika



Overview of the conference COIN2022 - Contemporary batteries and Supercapacitors, International Symposium, Belgrade 2022

Slavko Mentus^{1,2} and Milica Vujković²

¹Serbian Academy of Sciences and Arts, Knez Mihajlova 35, Belgrade, Serbia

²University of Belgrade, Faculty of Physical Chemistry, Studentski trg 12, 11000 Belgrade, Serbia

The Serbian Academy of Sciences and Arts hosted the participants of the symposium titled: "COIN2022 - Contemporary batteries and Supercapacitors – International Symposium Belgrade 2022", 1-2 June 2022. The symposium was organized by the University of Belgrade – Faculty of Physical Chemistry, Belgrade, Serbia, the National Institute of Chemistry, Ljubljana, Slovenia, the University of Montenegro, Faculty of Metallurgy and Technology, Podgorica, Montenegro and the Serbian Academy of Sciences and Arts, Belgrade, Serbia. The world-renowned leaders of large European projects and their coworkers, with the local and regional project leaders, coworkers and students, shared the activities and achievements in the field of energy storage and conversion. In addition, Alumni of the University of Belgrade presented the results of their ongoing research. The conference covered different research and industrial perspectives in Europe and also educational activities within the prestigious MESC+ study program. Local project leaders and students were acquainted with possibilities of upgrading their skills and knowledge through postgraduate studies in the best European and world institutions.

Keywords: energy conversion, European project leaders, advanced studies

Available on-line at the Journal web address: <http://www.ache.org.rs/HI/>

BOOK AND EVENT REVIEW

UDC: 005.745:621.355

Hem. Ind. 76(3) 179-182 (2022)

After commercialization in the 1990s, thanks to its high practical energy density, Li-ion battery became the influencing factor of everyday life. This battery is now the heart of countless number of portable electronic devices (mobile phones, tablets, laptops etc.), being today a common property of almost every man (in 2020, 45 GWh of energy was stored in Li-ion batteries in portable devices). From 2010., it is used as the propellant of electric cars, with the intention to replace all oil powered cars in the next few decades. The production rate of battery powered cars increased progressively and reached one million/year in 2017 and exceeded 6 million/year in 2021. Furthermore, in the near future, huge stationary battery packs should serve to buffer the oscillating energy output of solar and wind power plants. The inclusion of nanomaterials in the process of Li-ion battery production shifted its characteristics toward supercapacitor ones, and consequently, the supercapacitors are now the subjects of investigation as a fast-charging chemical power sources, alternative or supplement to batteries. However, the scarcity of raw materials for Li-ion batteries in the Earth's crust impels electrochemists to search for other types of batteries of similar usability and not limited by raw materials.

A group of distinguished European and domestic project leaders contributing significantly to the recent development of Li-ion batteries and supercapacitors and to their potential substitutes, met at the symposium entitled "COIN2022 - Contemporary batteries and Supercapacitors – International Symposium Belgrade 2022", held 1-2 June this year in the Serbian Academy of Sciences and Arts. The institutional organizers were the University of Belgrade – Faculty of Physical Chemistry, Belgrade, Serbia, the National Institute of Chemistry, Ljubljana, Slovenia, the University of Montenegro, Faculty of Metallurgy and Technology, Podgorica, Montenegro, and the Serbian Academy of Sciences and Arts, Belgrade, Serbia. Among distinguished invited speakers, we may mention French academician Prof. Patrice Simon, Université Paul Sabatier, Toulouse, France, Prof. Cristian Masquelier, Université de Picardie Jules Verne, Amiens, France, Prof. Robert Dominko, National Institute of Chemistry, Ljubljana, Slovenia, and Kristina Edström, Uppsala University, Uppsala, Sweden. These world-renowned leaders of large European projects and their coworkers shared their activities and achievements in the field of energy storage and conversion. In addition, professors and researchers from the region presented the results of their ongoing research, and the particular attention was drawn to the presentation of the

Corresponding author: Slavko Mentus, Serbian Academy of Sciences and Arts, Knez Mihajlova 35, Belgrade, Serbia
E-mail slavko@ffh.bg.ac.rs



project regarding the construction of the first Gigafactory for Li-ion batteries production in Europe, (ElevenEs, www.elevenes.com) located in Subotica. The conference program, including 14 invited lectures and 28 posters, covered different research and industrial perspectives in Europe and also educational activities within the prestigious MESC+ (Materials for Energy Storage and Conversion +) study program. This symposium was an excellent opportunity for local project leaders, their coworkers and students to learn about both actual and future European actions in the field of electrochemical energy storage, and to be acquainted with possibilities of upgrading their skills and knowledge through postgraduate studies in the best European and world institutions.

The Program and Book of Abstracts is available in printed form (ISBN 978-86-82139-86-7).



Fig.1. The members of the Organizing Committee of the conference COIN2022 - Contemporary batteries and Supercapacitors- International Symposium Belgrade 2022 (from left to right): Prof. Robert Dominko, academician Slavko Mentus, Prof. Veselinka Grudić, Dr Milica Vujković

Sl. 1. Članovi organizacionog odbora konferencije COIN2022 – Savremene baterije i superkondenzatori – Međunarodni simpozijum Beograd 2022 (s leva na desno): prof. Robert Dominko, akademik Slavko Mentus, prof. Veselinka Grudić, dr Milica Vujković

Osvrt na simpozijum COIN2022 – Savremene baterije i superkondenzatori, međunarodni simpozijum, Beograd 2022

Slavko Mentus^{1,2} i Milica Vujković²

¹Srpska akademija nauka i umetnosti, Knez Mihajlova 35, Beograd, Srbija

²Univerzitet u Beogradu, Fakultet za fizičku hemiju, Studentski trg 12, 11000 Beograd, Srbija

Izvod

Srpska akademija nauka i umetnosti ugostila je 1-2. juna 2022. učesnike simpozijuma pod nazivom: COIN2022 – Savremene baterije i superkondenzatori – Međunarodni simpozijum Beograd 2022. Simpozijum su organizovali Univerzitet u Beogradu – Fakultet za fizičku hemiju, Beograd, Srbija, Nacionalni hemijski institut, Ljubljana, Slovenija, Univerzitet Crne Gore, Metalurško-tehnološki fakultet, Podgorica, Crna Gora i Srpska akademija nauka i umetnosti, Beograd, Srbija. Svetski priznati rukovodioци velikih evropskih projekata i njihovi saradnici, sa lokalnim i regionalnim vođama projekata, saradnicima i studentima, razmenili su aktivnosti i dostignuća u oblasti skladištenja i konverzije energije. Pored toga, alumni Univerziteta u Beogradu predstavili su rezultate svog tekućeg istraživanja. Konferencija je obuhvatila različite istraživačke i industrijske perspektive u Evropi, kao i obrazovne aktivnosti u okviru prestižnog studijskog programa MESC+. Domaći rukovodioци projekata i studenti upoznati su sa mogućnostima unapređenja svojih veština i znanja kroz postdiplomske studije u najboljim evropskim i svetskim institucijama.

Ključne reči: konverzija energije, rukovodioци evropskih projekata, napredne studije

PRIKAZ KNJIGA I DOGAĐAJA

UDK: 005.745:621.355

Hem. Ind. 76(3) 179-182 (2022)

Nakon komercijalizacije Li-jonske baterije 1990. godine, zahvaljujući svojoj visokoj praktičnoj gustini energije, ova baterija postala je faktor koji utiče na svakodnevni život. Ona je sada izvor energije bezbrojnih prenosivih elektronskih uređaja (mobilnih telefona, tableta, laptopova itd.), koji su danas u vlasništvu gotovo svakog čoveka (U Li-ion baterijama prenosivih uređaja 2020. godine uskladišteno je 45 GWh energije). Od 2010. godine koristi se kao pogonsko sredstvo električnih automobila, sa namerom da u narednih nekoliko decenija zameni sve automobile sa pogonom na tečna fosilna goriva. Godišnja proizvodnja automobila sa pogonom na baterije progresivno je rasla i dostigla više od milion u 2017., a premašila 6 miliona u 2021. Štaviše, u bliskoj budućnosti, predviđa se da će ogromni stacionarni baterijski paketi da služe za ublažavanje oscilirajuće izlazne energije solarnih i vetroelektrana. Uključivanje nanomaterijala u proces proizvodnje Li-jonskih baterija pomerilo je njene karakteristike ka superkondenzatorima, pa su superkondenzatori sada predmet istraživanja kao brzo punjivi hemijski izvori električne energije, kao alternativa ili dopuna baterijama. Međutim, nedostatak sirovina za Li-jonske baterije u Zemljinoj kori postavlja pred elektrohemicičare urgentan zadatak da traže druge tipove baterija slične upotrebljive vrednosti, čija proizvodnja neće biti ograničena dostupnošću sirovina.

Na simpozijumu COIN2022 – Savremene baterije i superkondenzatori – Međunarodni simpozijum Beograd 2022”, održanom 1-2. juna 2022. u Srpskoj akademiji nauka i umetnosti, sastala se grupa uglednih evropskih i domaćih rukovodilaca projekata koji su značajno doprineli novijem razvoju Li-ion baterija i superkondenzatora i njihovim potencijalnim zamenama. Institucionalni organizatori su bili: Univerzitet u Beogradu – Fakultet za fizičku hemiju, Beograd, Srbija, Nacionalni hemijski institut, Ljubljana, Slovenija, Univerzitet Crne Gore, Metalurško-tehnološki fakultet, Podgorica, Crna Gora i Srpska akademija nauka i umetnosti, Beograd Srbija. Među istaknutim pozvanim predavačima možemo pomenuti francuskog akademika prof. Patrice Simon, Université Paul Sabatier, Toulouse, Francuska, Prof. Cristian Maskuelier, Université de Picardie Jules Verne, Amiens, Francuska, Prof. Robert Dominko, Nacionalni institut za hemiju, Ljubljana, Slovenija i Kristina Edstrom, Uppsala University, Uppsala, Švedska.

Ovi i drugi svetski poznati rukovodioци velikih evropskih projekata i njihovi saradnici, govorili su o svojim aktivnostima i dostignućima u oblasti skladištenja i konverzije energije. Pored toga, profesori i istraživači iz regiona predstavili su rezultate svojih tekućih istraživanja, a posebnu pažnju privukla je prezentacija projekta izgradnje prve gigafabrike za proizvodnju Li-jonskih baterija u Evropi (ElevenEs, www.elevenes.com), locirane u Subotici.



Program konferencije, kroz 16 pozvanih predavača i 28 posterskih prezentacija, obuhvatio je različite istraživačke i industrijske perspektive u Evropi, kao i obrazovne aktivnosti u okviru prestižnog studijskog programa MESC+ (Materiali za skladištenje i konverziju energije +). Ovaj simpozijum je bio odlična prilika da domaći rukovodioci projekata, njihovi saradnici i studenti slušaju o aktuelnim i budućim evropskim akcijama u oblasti elektrohemijskog skladištenja energije, te da se upoznaju sa mogućnostima unapređenja svojih veština i znanja kroz postdiplomske studije u najboljim evropskim i svetskim institucijama.

Program i Knjiga sažetaka dostupni su u štampanom obliku (ISBN 978-86-82139-86-7).



Sl. 2 Svečana sala Srpske akademije nauka i umetnosti. Otvaranje konferencije COIN2022 – Savremene baterije i superkondenzatori, Međunarodni simpozijum Beograd 2022

Fig. 2. Main Hall of Serbian Academy of Sciences and Arts. The opening section of the conference COIN2022 - Contemporary batteries and Supercapacitors, International Symposium Belgrade 2022